Soils, Salts, and Water: Geochemical and Astrobiological Investigations of Briny Martian Regolith

Andrew O'Brien Shumway

A dissertation

submitted in partial fulfillment of the

requirements for the degree of

Doctor of Philosophy

University of Washington

2025

Reading Committee:

David C. Catling, Chair

Jonathan D. Toner

Baptiste Journaux

Program Authorized to Offer Degree:

Earth and Space Sciences

University of Washington

Abstract

Soils, Salts, and Water: Geochemical and Astrobiological Investigations of Briny Martian Regolith

Andrew O'Brien Shumway

Chair of Supervisory Committee:

David C. Catling

Department of Earth & Space Sciences

Despite its present cold and dry surface, Mars may once have been able to support life—and perhaps still could. Liquid water is essential for life as we know it, and there is ample physical and chemical evidence proving that water flowed in Mars' distant past. Today, what H_2O remains exists primarily as ice or vapor, but some liquid water may form on the surface through interactions with salts and regolith (i.e., soil). This dissertation explores how salt, soil, and water shape the chemistry, mechanical properties, and astrobiological potential of Mars' surface.

The first part of this thesis investigates modern surface processes through laboratory analog experiments with Martian regolith simulant. Mars' soil is rich in salts (such as perchlorates) that can form liquid brine, but prior investigations of the formation, stability, and habitability

of these brines frequently neglected the soil component. Experimental results presented here demonstrate that regolith has a strong effect on brine properties, increasing the water content and stabilizing perchlorate brine at Mars-relevant conditions. Specifically, we find that regolith can inhibit salt and ice crystallization in brines, which likely also improves the habitability of those brines. These results greatly expand the geographic and temporal extent where potentially habitable brines could exist on Mars.

Related experiments test a hypothesized formation mechanism for mysterious seasonal features dubbed Recurring Slope Lineae (RSL). RSL are apparently linked to water because of their appearance during warm seasons, yet simultaneously exhibit characteristics of dry granular flows. This work reconciles these seemingly contradictory observations by testing a semi-dry model of RSL formation, in which seasonal humidity cycles alternatively stabilize and destabilize slopes, periodically triggering mass wasting. Experimental results illustrate a correlation between relative humidity, soil hydration, and slope stability, which supports the hypothesis that RSL are desorption-triggered granular flows. Findings demonstrate that neither liquid water nor high abundances of salt are required to explain RSL, which raises questions about their protected status and presumed astrobiological potential.

This thesis also reports novel geochemical measurements of salty Martian regolith made *in situ* using the Planetary Instrument for X-ray Lithochemistry (PIXL) on NASA's *Perseverance* rover. PIXL's investigations map the elemental chemistry of regolith at a higher spatial resolution than any previous measurement on Mars. We interpret the results to infer the mineralogy and provenance of various regolith components that appear to be contributed from local, regional, and global sources. Abundances of S and Cl, which may form soluble species, deviate from the global trend for Martian soils, which suggests a unique local aqueous history. The results provide compelling new motivation for a future mission to return a sample of Martian regolith—two of which have been cached by *Perseverance*.

As a whole, this dissertation elucidates how water interacts with salty soil, which improves our understanding of the various roles of water on Mars, the potential habitability of the surface, and possible resources and/or hazards for future human explorers.

Table of Contents

List of Figures iv

List of Tables..viii

Acknowledgements.. ix

1. Introduction..1

1.1 Motivation & Background 1

1.2 Thesis outline 3

2. Regolith Inhibits Salt and Ice Crystallization in $Mg(ClO_4)_2$ Brine, Implying More Persistent and Potentially Habitable Brines on Mars 5

2.1 Introduction...7

2.2 Materials and Methods 10

2.2.1 Salt and Regolith Materials..10

2.2.2 Measuring Water Content and Water Activity in Briny Regolith 11

2.2.3 Measuring the Melting Point of Briny Regolith 12

2.3 Results...13

2.3.1 Water Content and Water Activity at 25°C: 13

2.3.2 Depressed Melting Point in Briny Regolith..19

2.3.3 Inferring Water Activity at Lower Temperature 21

2.4 Discussion and Implications for Mars 23

2.4.1 Regolith Inhibits Salt Precipitation 23

2.4.2 Regolith Inhibits Ice Crystallization 24

2.4.3 Structure of Brines in Regolith 26

2.4.4 Implications for Habitability, Planetary Protection, and Exploration of Mars 27

2.5 Conclusion...29

2.6 Acknowledgements..30

3. Seasonal Loss of Adsorbed Water as a Formation Mechanism for Recurring Slope Lineae on Mars 31

3.1 Introduction...32

3.1.1 Background 32
3.1.2 Summary of Wet and Dry RSL Models 33
3.1.3 Dehydrating Slopes as a Trigger for RSL 34
3.2 Methods 35
3.3 Results 38
3.3.1 Soil Hydration and Relative Humidity 38
3.3.2 Angle of Repose and Relative Humidity 40
3.4 Discussion 43
3.4.1 Support for the Water Desorption Model 43
3.4.2 Comparison to Spacecraft Data 46
3.4.3 Significance for Astrobiology and Planetary Protection 47
3.5 Conclusion 48
4. Mineralogically Diverse and Salt-rich Regolith in Jezero Crater Characterized using X-ray Spectroscopy 50
4.1 Introduction 51
4.1.1 Previous Analyses of Martian Regolith 52
4.1.2 Mars 2020 Mission 54
4.2 Methods 56
4.2.1 Overview of PIXL 56
4.2.2 Geologic Context 58
4.2.3 PIXL Regolith Scans 60
4.3 Results 65
4.3.1 Micro Context Image (MCC) Images 65
4.3.2 Elemental and Diffraction Results 66
4.3.3 Fines and Dust 75
4.3.4 Chlorine and Sulfur 79
4.4 Discussion: 81
4.4.1 Potential source regions of regolith components 81
4.4.2 Evidence of Aqueous Activity and Alteration 88
4.4.3 Regolith Hydration and Brine-Forming Salts 88

4.4.4 Relevance for Mars Sample Return 91
4.5 Conclusion 94
4.6 Acknowledgements 95
4.7 Data Availability Statement 95
5. Conclusion 96
5.1 Chapter Summaries 96
5.2 Future work 97
References 100
Appendix A. Supplementary Information for Chapter 4 143
A.1 Dust Layer Model 143
A.2 K-means Clustering Algorithm 143
A.3 Chlorine Quantification 144
A.4 Pyroxene 145
Appendix B. Curriculum Vitae 151

List of Figures

Figure 2-1 Adsorption isotherms show the minor extent of a wetting-drying hysteresis effect in regolith and brine-regolith mixtures. At any given relative humidity, samples that are drying from a prior wet state retain more water than identical samples that are wetting from a prior dry state (Hillel, 1971). Datasets for 0.6 and 1.0 wt. % $Mg(ClO_4)_2$ in MMS are excluded here because only drying curves were measured for those samples. The regolith used was Mojave Mars Simulant (MMS) and all experiments were conducted at 25°C. 14

Figure 2-2 The water content in regolith varies based on the RH and the amount of salt in the regolith across several systems: modeled pure brine (dashed curves), regolith without salt (black circles and dotted curves), an ideal mixture of brine and regolith (solid curves), and experimental brine-regolith mixtures (colored circles). The curves for the ideal brine-regolith mixtures sum the behavior of pure brine and salt-free regolith, assuming each component behaves independently. However, experimental brine-regolith mixtures deviate greatly from ideal behavior for 0.6 to 5.8 wt.% salt (A–D). The step changes that occur in some systems at ~40.4% RH are the result of salt precipitation. Notably, salt phase transitions are absent in the experimental datasets for 0.6 to 5.8 wt.% salt (A–D). For comparison, a positive example of salt crystallization in regolith is shown (panel E). All data represent samples at 25°C that have lost water from a prior wet state (i.e., "drying curve" in Fig. 2-1). 15

Figure 2-3 At any specified relative humidity, experimental brine-regolith mixtures (circles) are less concentrated than pure brine (black curve). The trend of pure $Mg(ClO_4)_2$ brine (black curve) was calculated using a revised Pitzer model for perchlorates described in Toner et al. (2015a), and terminates at the saturation point (4.44 molal, RH = 40.4%). Also shown is the known lower a_w limit for life on Earth (a_w = 0.585, dashed red line; Stevenson et al., 2017). All data represent samples at 25°C that have lost water from a prior wet state (i.e., "drying curve" in Fig. 2-1). 18

Figure 2-4 Measured melting points of brine-regolith samples (squares) are depressed compared to pure brine (black line) at a given salt concentration (mol kg_w^{-1}). The freezing point of pure $Mg(ClO_4)_2$ brine was calculated using a revised Pitzer model described in Toner et al. (2015a). At all wt. % salt measured, some relatively high-concentration samples showed no signs of freezing, melting, or forming glass whatsoever, over the full range of temperatures (-150°C to 20°C). The concentrations of these unfrozen samples are shown in the lower panel. All data represent samples that have lost water from a prior wet state (i.e., "drying curve" in Fig. 2-1). 20

Figure 2-5. To probe how the a_w of briny regolith changes with temperature, we predicted the a_w at each sample's melting temperature (squares) via equation (2-1), then compared to the measured a_w of the same sample at 25°C (circles). Note that the melting temperature varies for each sample (see Fig. 2-4), but for all samples $T_{melt} < T_{ref} = 25°C$. All data represent samples that have lost water from a prior wet state (i.e., "drying curve" in Fig. 2-1). 22

Figure 3-1. Schematic (left) and still images (right) showing the tumbler apparatus that was used to measure angle of repose as a function of relative humidity (RH). Within, Mars regolith simulant (dark brown) was equilibrated at a known RH and the water content was measured. Driven by a motor, the tumbler slowly rotates counterclockwise, gradually increasing the profile of the sediment within, until the slope fails. Still images from the experimental video show examples of the maximum slope reached before a failure event (top right) and the slope relaxed to after failure (bottom right). In the images shown, RH = 36% and H_2O content = 1.85 wt. %. Red arrows indicate direction of rotation. 38

Figure 3-2. Adsorption isotherm for fine-grained (<500 μm) regolith analog Mojave Mars Simulant (MMS), showing the adsorbed water content at various relative humidity (RH). Hysteresis in wetting vs. drying regolith results in different water content at any given RH, dependent on whether the sample is gaining or losing water (i.e., wetting and drying curves, black and white circles, respectively). Measured RH and water content of tumbler chamber (magenta squares) generally agree with the wetting curve data (i.e., the larger mass of sediment in the tumbler reached equilibrium with the water vapor in the headspace). 39

Figure 3-3. Histograms show the distribution of slope angles measured immediately before (static) and after (dynamic) slope failure events. The mean angle of repose is represented by a solid circle, with a standard error of the mean smaller than the point plotted. See Table 3-1 for more statistical information about these distributions. 41

Figure 3-4. Mean static (blue) and dynamic (orange) angles of repose measured in simulated Martian regolith equilibrated at RH = 0%, 28%, 36%, 74%, and 96%. Angle of repose increases at higher RH. Error bars show the standard error of the mean. Linear regressions are also shown.. 43

Figure 4-1. Orbital context images of Jezero crater taken by the High Resolution Imaging Science Experiment (HiRISE; McEwen et al., 2007). The white line represents the path travelled by the *Perseverance* rover. Approximate boundaries for the Séítah (green), Máaz (purple), and Shenandoah (yellow) formations are shown, adapted from Royer et al. (2025) and Stack et al. (2024). Informal names for features and outcrops are also shown in white text. Stars and corresponding labels indicate PIXL scans that are relevant to this work: unabraded rock targets *Naltsos* and *Beaujeu*, abraded bedrock *Uganik Island*; and regolith targets *Ursus Cove*, *Topographers Peak*, and *Marmot Bay*. (B) shows a zoomed-in view of the Cape Nukshak section of the Shenandoah formation on the fan front, where PIXL's regolith scans took place. Image credits: NASA/JPL/University of Arizona. 56

Figure 4-2: Context images for the PIXL scans at the *Amalik* workspace. Yellow arrows point to the approximate locations of the *Ursus* Cove PIXL target on the bedform. A) Front Hazcam image showing PIXL deployed over the *Ursus Cove* target. B) MastCam-Z Left image of the

Ursus Cove target. C) Close-up WATSON image of *Ursus Cove*, with approximate footprints of the two PIXL scans. All image files are listed in Table A-2. 62
Figure 4-3: Context images for the PIXL targets at *Observation Mountain*. Blue arrows point to the approximate locations of the PIXL scans. *Topographers Peak* (TP) is comprised of regolith that was excavated by a wheel scuff maneuver, while *Marmot Bay* (MB) is undisturbed surface regolith. A) Front Hazcam image of PIXL deployed over *Topographers Peak*. B) Front Hazcam image of the scuff. The locations from which the two regolith samples were later collected are indicated with stars. C) Mastcam-Z Right image of the *Topographers Peak* target. The line of small depressions near the bottom of this image are LIBS pits created by SuperCam analyses of this target (see Cousin et al., 2025). D) WATSON image of *Topographers Peak,* with the approximate footprint of the PIXL scan shown as a blue box. E) WATSON image of *Marmot Bay* with the approximate footprints of the PIXL grid (large square) and map (rectangle) scan footprints. F) Close-up WATSON image of *Marmot Bay*, with the approximate footprints of the PIXL scans. All image files are listed in Table A-2. 65
Figure 4-4. PIXL Micro Context Camera (MCC) images of the three regolith targets. (A-C) False color images of each target in the near-infrared (NIR; 735 nm), green (G; 530 nm), and blue (B; 450 nm) channels, flat-fielded and enhanced. (D-E) MCC ratio image of NIR/G reflectance values. Note that distinct populations of grains with similar spectral signatures are distinguishable within and between scans. The black, white, and orange arrows point to examples of the dark-, light-, and intermediate-toned grains, respectively. Rectangles show the extents of PIXL's XRF measurements. 66
Figure 4-5. Visualizations of abundances of key oxides, as well as diffraction results, for *Ursus Cove* (left), *Topographers Peak* (center), and *Marmot Bay* (right). A) WATSON images with the approximate PIXL footprints (aligned manually). B) Red, green, blue (RGB) map illustrating abundances of FeO_T, MgO, and SiO_2, respectively. C) RGB map showing FeO_T, Al_2O_3, and CaO abundances, D) RGB map showing Cl, SO_3, and Al_2O_3 abundances. SO_3 (green) is scaled to the maximum value from *Marmot Bay* (11.9 wt. %) for visual clarity, but note several points in *Ursus Cove* contain up to ~40 wt.% SO_3 (see section 4.3.2.5). E) Map showing diffraction results. Blue illustrates regions where multiple contiguous points exhibit identical diffraction peaks (i.e., larger monocrystalline domains), while red indicates points that diffract, but are not related to a larger crystal. Transparent regions exhibited no detectable diffraction peaks (white arrows indicate examples of non-diffracting grains). 1 mm white scale bars are shown throughout. 69
Figure 4-6: (Top row) Maps illustrating locations of identified components within three PIXL scans. (Bottom row) SiO_2 vs. FeO_T + MgO vs. CaO + K_2O + Na_2O ternary diagrams visualizing the compositions of the corresponding regolith components displayed above. 70
Figure 4-7. A) Composition of finer-grained regolith measured by PIXL (black) normalized to Average Basaltic Soil (gray; O'Connell-Cooper et al., 2017). B) PIXL fines (black) normalized

to Martian dust (gray; Berger et al., 2016). P_2O_5 and Cr_2O_3 not shown in B) because they were not detected and not reported by APXS, respectively (Berger et al., 2016). 1σ uncertainties are shown for PIXL data (Heirwegh et al., 2022; Schmidt et al., 2025); accuracy errors are shown for APXS data (Gellert et al., 2015).. 77
Figure 4-8. Cl vs. SO_3 (molar) for fine-grained regolith across three targets (*Marmot Bay*, *Topographers Peak*, and *Ursus Cove*). Individual measurements (circles) and the bulk sum value (square) are shown. Gray histogram plots on either axis show the distribution of the overlapping PIXL measurements. An orthogonal regression (black line) fit through the data has a slope of S/Cl = 2.43 ± 0.06 and an intercept of -0.13. 80
Figure 4-9. Forsterite number (Fo#) of olivine regolith grains (dark gray; this work) compared to olivine identified by PIXL in the fan top and Séítah regions (Moreland et al., submitted) and the Máaz formation (Schmidt et al., 2025). Squares show the Fo#s for two instances where PIXL scanned similar olivine sand on top of bedrock at *Naltsos* (Hausrath et al., 2023) and *Beaujeu* (Schmidt et al., 2025). The Mg:Fe molar ratio of dust is indicated with a triangle (Berger et al., 2016). Circles represent individual PIXL points identified as olivine. Diamonds show the bulk sum value across a target or formation. 86

List of Tables

Table 3-1. Relevant data and statistical parameters from each slope angle experiment. RH is relative humidity, and N is the number of slopes measured. 42

Table 4-1. Details of PIXL's regolith scans on the fan front. "Sol" refers to a Martian solar day, with sol 1 indicating the start of the landed mission. Scan size describes the approximate footprint of the XRF map. Step size refers to the average distance between consecutive measurements in a scan. Duplicate regolith samples were collected from Observation Mountain and cached for potential return by a future mission. 61

Table 4-2. Abundances of major oxides measured in each regolith component. 1σ uncertainties are derived from PIQUANT (Heirwegh et al., 2022). Additional trace element abundances are reported in Table A-3. 75

Table 4-3. Summary of identified regolith components, notable reflectance, chemistry, and diffraction properties, where they were detected, and potential sources. MB = *Marmot Bay*, TP = *Topographers Peak*, UC = *Ursus Cove*. [a]O'Connell-Cooper et al. (2017), [b]Schmidt et al. (2024), [c]Knight et al. (2024). 88

Table 4-4. Summary of several key PIXL observations about the sampled regolith, which raise questions that could be answered through analysis of a Martian regolith sample in terrestrial labs using instrumentation not available on spacecraft hardware. 92

Acknowledgements

This dissertation represents a colossal undertaking that was only possible thanks to immense support from many mentors, colleagues, friends, and family.

I must begin by thanking my advisor, David Catling, for his deep knowledge, limitless patience, and unwavering support over these years as I grew into a proper scientist. I thank Jon Toner for introducing me to the wonderful world of aqueous geochemistry, and for continuing to advise and support my work from afar. Special thanks to Baptiste Journaux for insightful discussions, helpful advice, and astronomical adventures over the years. I thank Brook Nunn for always reminding me that we can't spell "astrobiology" without "biology," and for her inspiring work simulating life-detection missions. I am deeply grateful to Michael Gomez and David Shean, who shared their expertise during critical milestones in my academic journey.

In addition to my committee, I owe a deep debt of gratitude to several mentors who have shaped my career at inflection points. I credit Luju Ojha and George MacDonald for starting me on this interplanetary journey when I was an undergraduate researcher, and I am thrilled to still get to work with them from time to time all these years later. Tim Elam I cannot thank enough for giving me the opportunity of a lifetime to explore another world by recruiting me for the *Perseverance* team. I am deeply grateful for Tanya Kizovski's boundless optimism, encouragement, and mentorship while we deeply pondered a few grains of sand on another planet.

I am honored to have been surrounded by so many brilliant and kind colleagues at UW who have become close friends: my academic twin, Lucas Fifer; Taryn Black, who taught me how to talk about science real good; my fellow PIXLites, Lauren O'Neil, Kimberly Sinclair, and An Li; and the entire UW ESS and Astrobiology communities including Yuk Chun Chen, Pete Wynn, Rudy Garcia, Nick Wogan, Zach Cohen, Ardith Bravenec, Trent Thomas, Ping-Chun Lin, Sarah King, Michael Wong, Joshua Krissansen-Totton, and Haskelle Trigue White-Gianella.

Throughout all the twists and turns of graduate school, I have also been supported by a rag-tag team of physicists I met at Georgia Tech, who forged a community so strong that we became lifelong friends, and who continue to inspire me to be curious about the universe: Jared, Grace, Evan, Ed, Alex, Darian, James, Mel, Casey, Steve, Silas, and Thomas.

I need to thank my family for their unconditional love and support: my father, Jud Shumway, who first inspired my love of space by taking me stargazing; my mother, Karen Shumway, who taught me to trust my heart and keeps me grounded on Earth; my siblings, Emma and Geoff, who I would follow to the ends of the universe; and my many grandparents, aunts, uncles, and cousins who helped forge me into the person I am today.

Finally, I offer profound thanks to Amber Torell, who has been with me through all the ups and downs of graduate school, constantly fills my life with joy, and always reminds me not to sell myself short.

“One thing seems clear. Having landed on Mars we shall have to go back to explore it, to learn from it, to cherish it and perhaps to transform it.”

– Carl Sagan, 1979

Per Aspera Ad Astra

1. Introduction

1.1 Motivation & Background

Life as we know it requires liquid water to survive. In science fiction, Mars is frequently imagined as a place where life once flourished—or perhaps still does—but the modern reality of a planet without oceans, rivers, or precipitation instead seems to point to a dry and lifeless world. However, Mars' arid exterior is a façade that obscures the planet's rich history as a wet and potentially once-habitable world. Just like Earth, Mars has been profoundly shaped and reshaped by water over eons (Squyres, 1984; Wordsworth, 2016). The present oxidized, salt-rich, dust-covered surface preserves clues about these past aqueous eras, which can be revealed through chemical, mineralogical, and morphological investigations (e.g., Ehlmann & Edwards, 2014; Grotzinger & Milliken, 2012; Kite & Conway, 2024).

Today, whatever liquid water once flowed on Mars is largely absent, as much of it was lost to photolysis and hydrogen escape to space (e.g., Hunten & McElroy, 1970; Jakosky, 2021). Pure liquid water is generally unstable on the modern surface due to low temperatures and pressures (on average, -58 °C and 6 mbar, respectively; Catling & Kasting, 2017; Ingersoll, 1970). Instead, what H_2O remains on Mars exists mostly as ice (e.g., in polar caps, permafrost, and water-ice clouds) or as water vapor (Byrne, 2009; Wray, 2021). Despite extreme conditions, small amounts of liquid water may yet exist in Mars' salty soil. Note that the terms "soil" and "regolith" are used interchangeably throughout to refer to the loose, unconsolidated, rocky material that overlies bedrock (van Es, 2017)

Hygroscopic salts litter Mars' surface, likely originating from past aqueous and/or volcanic activity (e.g., Clark & Kounaves, 2016). Presently, these salts play a major role in the hydrological cycle, mediating water exchange between the surface and atmosphere, and storing water in their hydrated forms (e.g., David et al., 2022). Most important to this work, perchlorate (ClO_4^-) salts are ubiquitous across Mars and can absorb water vapor to dissolve into brine (i.e., deliquesce) under present surface conditions (Clark & Kounaves, 2016; Gough et al., 2011, 2023; Nuding et al., 2014; Sutter et al., 2017). Once formed, liquid perchlorate brines can persist to extremely low temperatures because they strongly depress the freezing point (e.g., -74°C for Ca-perchlorate; Stillman & Grimm, 2011).

Water can also exist on the surface in adsorbed phases—which form when atmospheric water vapor adheres to surfaces via van der Waals forces, forming thin films of H_2O, sometimes just a few molecules thick (Boxe et al., 2012; Pommerol et al., 2009). Adsorbed water is distinct from liquid water, but it shares many of the same properties, including hypothetically supporting life (Möhlmann, 2005). The Martian surface adsorbs large quantities of water each night, then releases it back to the atmosphere the following morning (e.g., Beck et al., 2010; Fanale & Cannon, 1971; Jakosky et al., 1997; Savijärvi & Harri, 2021). Important to this work is the often-overlooked fact that deliquescence and adsorption can occur simultaneously in salty regolith, creating thin brine films in the pore space between grains, which behave uniquely from either the brine or regolith endmembers.

In addition to astrobiological motivations, geochemical investigations of salts and regolith are useful as a window into understanding the geologic history of Mars (e.g., Berger et al., 2020; Clark et al., 1982; O'Connell-Cooper et al., 2017; Squyres et al., 2006; Yen et al., 2005). Absent plate tectonics or recent volcanism, Mars' ancient surface preserves clues about an era that is largely missing from Earth's own rock record—a time when life on Earth was nascent and water flowed on Mars (Nimmo & Tanaka, 2005). Salts deposited during these aqueous eras can offer clues about the Martian paleoclimate and the role water has played in altering the surface (e.g., Ehlmann & Edwards, 2014). Similarly, regolith may represent the average composition of Mars' crust, weathered and mixed to homogeneity (Berger et al., 2020; Clark et al., 1982; McSween & Keil, 2000; O'Connell-Cooper et al., 2017). Therefore, geochemical investigations of regolith composition can reveal information about chemical and physical processes on a global scale. Additionally, the finest-grained fraction of regolith (i.e., dust) merits study because it is easily suspended in Mars' thin atmosphere, where it plays a major role in Martian weather (e.g., dust devils, storms) and climate (i.e., by absorbing radiation; Newman et al., 2002).

This dissertation addresses fundamental questions at the intersection of planetary science and astrobiology: How has water shaped Mars' surface through time? What evidence of past (potentially habitable) environments are preserved in Mars' rocks and regolith? Can liquid water still exist on Mars today? To tackle these questions, this work leverages laboratory experiments (Chapters 2 and 3) and analysis of spacecraft data (Chapter 4) to explore how water, salts, and regolith interact with one another to transform the geochemistry and habitability of Mars' surface. Each chapter investigates past or present liquid water and the implications for habitability, which is relevant to astrobiology.

1.2 Thesis outline

Chapter 2 challenges a prevailing narrative in the literature by demonstrating that Martian regolith allows thin films of perchlorate brine to persist under colder and drier conditions than previously thought possible. Prior research in this realm has focused almost exclusively on the properties of pure brines, frequently neglecting any effect that regolith has on the freezing point, solubility, or habitability of those solutions. This chapter experimentally studies realistic analog mixtures of brine *and* regolith across a wide range of Mars-relevant temperatures, relative humidities (RH), and salt concentrations. Results demonstrate that mixtures of brine and regolith mixtures can hold more water and resist crystallization better than either component individually. These findings greatly expand the physical and temporal extent where water might exist on Mars today. Brines formed in this way can chemically react with minerals, increase the cohesivity of regolith (e.g., by forming omnipresent soil crusts; Hausrath et al., 2023), and potentially form modern habitable niches.

Chapter 3 reconciles multiple competing hypotheses to better explain mysterious slope features known as Recurring Slope Lineae (RSL). RSL are strongly linked to water, but their precise formation mechanisms remain a mystery (McEwen et al., 2011). Many hypotheses attribute RSL to some form of liquid water (usually brines), while competing hypotheses claim they no more than dry granular flows (e.g., Dundas, 2020; Stillman et al., 2020). In this chapter, these seemingly contradictory hypotheses are united through experiments that demonstrate how soil hydration and slope stability follow seasonal trends in humidity, which can seasonally destabilize slopes and trigger granular flows. Unlike other mechanisms, this model explains RSL physical appearance and seasonality while requiring only soil and atmospheric water vapor, which is most consistent with the modern Martian climate. Determining how much water (if any) water is present in RSL is crucial for assessing their astrobiological potential, since RSL are currently off-limits to all but the cleanest spacecraft out of concerns about contamination of potentially habitable sites. In the hypothesis tested, RSL are unlikely to contain enough water to support life, which calls into question their presumed habitability.

Chapter 4 leaves the laboratory and embarks on a field trip to Mars, through the eyes of NASA's *Perseverance* rover. This chapter presents first-of-their-kind geochemical maps of Martian regolith constructed using the Planetary Instrument for X-ray Lithochemistry (PIXL)—a micro-scale X-ray fluorescence (XRF) spectrometer (Allwood et al., 2020). Wind-mixed regolith has a nearly uniform composition across Mars (O'Connell-Cooper et al., 2017), so these novel high-resolution (< 1 mm) results provide insights about planet-scale geochemistry. At the same time, PIXL detects deviations from the global regolith composition (i.e., high levels of Cl, potentially in the form of perchlorate), which provide a window into past aqueous conditions local to Jezero crater. These results also present a crucial first look at the chemistry and mineralogy of two regolith samples collected and cached by *Perseverance*, which may one day be returned to Earth for future study (Hausrath et al., 2025). PIXL's insights provide exciting new justification for the return of a regolith sample, and lay the groundwork for future researchers to understand the *in situ* context of these samples once they are returned.

Finally, **Chapter 5** summarizes key findings, then looks forward to future research efforts that could address the fascinating science questions raised by this work.

2. Regolith Inhibits Salt and Ice Crystallization in $Mg(ClO_4)_2$ Brine, Implying More Persistent and Potentially Habitable Brines on Mars

This chapter was originally published as: Shumway, A. O., Catling, D. C., & Toner, J. D. (2023). Regolith Inhibits Salt and Ice Crystallization in $Mg(ClO_4)_2$ Brine, Implying More Persistent and Potentially Habitable Brines on Mars. *The Planetary Science Journal, 4*(8), 143. https://doi.org/10.3847/PSJ/ace891.

Abstract

On Mars, liquid water may form in regolith when perchlorate salts absorb water vapor and dissolve into brine, or when ice-salt mixtures reach their melting temperature and thaw. Brines created in this way can chemically react with minerals, alter the mechanical properties of regolith, mobilize ions in the soil, and potentially create habitable environments. Although any Martian brines would exist in contact with regolith, few studies have investigated how regolith alters the formation and stability of brines at Mars-relevant conditions. To fill this gap, we studied magnesium perchlorate brine in a Martian regolith simulant at salt concentrations up to 5.8 wt. %. We measured the water mass fraction and water activity between 3 and 98 % relative humidity at 25°C using the isopiestic method and monitored salt and ice crystallization at temperatures between -150°C and 20°C with differential scanning calorimetry. The results show that regolith inhibits salt and ice crystallization, allowing water to form and persist at much colder and drier conditions than pure brine. Remarkably, in several samples, neither salt nor ice crystallized at any conditions. These results suggest that brines could exist in regolith for longer periods of the Martian year than previously thought and could persist indefinitely under certain conditions. By retaining water, inhibiting salt and ice crystallization, and maintaining habitable water activity, briny regolith may be a more favorable environment for life than pure brine alone.

These findings indicate the critical importance of brine-regolith interactions for understanding the properties, evolution, and potential habitability of Mars' surface.

2.1 Introduction

Water affects geochemistry, regolith properties, and habitability, and is a central focus for the exploration of Mars. NASA's *Curiosity* and *Perseverance* rovers are searching for signs of life where surface water once flowed, while avoiding "Special Regions" that are protected for the presence of potentially habitable liquid water (Rummel et al., 2014). Although it is difficult for liquid water to exist on present-day Mars due to low temperatures and atmospheric pressures, liquid water may form via deliquescence (Gough et al., 2011), adsorption (Möhlmann, 2005), and/or eutectic ice melting (Stillman & Grimm, 2011). Deliquescence occurs when salts adsorb atmospheric water vapor, dissolve, and form brine. In contrast, adsorption occurs when water vapor adheres directly to regolith surfaces and forms thin films. Eutectic ice melting occurs when solid salt-ice mixtures melt to form brine at a temperature below 0°C. Deliquescence, adsorption, and eutectic melting could also all occur simultaneously to create adsorbed brines in Martian regolith. Prior experiments have shown that salty regolith uptakes water at twice as fast as regolith alone, and found evidence of both deliquescence and adsorption occurring (Slank et al., 2022). Once formed, brines are more stable than pure water because salts reduce the freezing point and evaporation rate of the solution (Chevrier et al., 2009; Gough et al., 2011).

Of the many salts detected on Mars' surface, perchlorates are notable for their abundance and widespread distribution in the regolith, as well as their low eutectic temperatures and extreme hygroscopicity. Perchlorates were first discovered on Mars by the *Phoenix* lander's Wet Chemistry Laboratory (WCL), which found 0.4 to 0.6 wt. % perchlorate in the regolith (Hecht et al., 2009). Subsequent geochemical modeling of WCL data suggests that $Mg(ClO_4)_2$ was the dominant salt in that regolith (Toner et al., 2014a), although other studies suggest that calcium (Kounaves, Chaniotakis, et al., 2014) or sodium (Stillman & Grimm, 2011) were the dominant cations. The discovery of perchlorate by *Phoenix* spurred a reanalysis of Viking lander data, which concluded that perchlorates in the regolith could explain the anomalous detection of chlorinated methane, a result initially attributed to terrestrial contamination (Navarro-González et al., 2010). Evidence of perchlorates has also been found in Gale Crater, where the Sample Analysis at Mars instrument on the *Curiosity* rover measured evolved O_2 and HCl at a temperature that suggests they were likely produced by thermal decomposition of perchlorate and/or chlorate in the regolith (Archer et al., 2014; Ming et al., 2014; Sutter et al., 2017). Most recently, multiple instruments on the *Perseverance* rover have independently detected perchlorates in aqueously altered rocks in Jezero Crater (Farley et al., 2020; Scheller et al., 2022; Tice et al., 2022; Wiens et al., 2022). Trace perchlorate has even been detected in Martian meteorites at ~ppm-ppb levels (Jaramillo et al., 2019; Kounaves, Carrier, et al., 2014). The confirmed and probable detections of perchlorates at several sites on Mars and in Martian meteorites suggests that perchlorate is likely ubiquitous across the Martian surface (Sutter et al., 2017), and is potentially produced in the atmosphere and deposited across the globe (Catling et al., 2010).

Perchlorate detections are significant because some perchlorate salts may deliquesce and form brine at Martian surface conditions (Chevrier et al., 2009; Gough et al., 2011; Toner et al., 2014b). Once formed, perchlorate brines can remain liquid far below the freezing point of pure water. For example, magnesium perchlorate solution remains a stable liquid down to the eutectic temperature, ~209 K according to (Toner et al., 2014a), although the precise value for the eutectic temperature is debated (see also Chevrier et al., 2009; appendix A of Stillman and Grimm, 2011). Perchlorate brines can also form metastable liquids at temperatures as low as 150 K due to supercooling (Toner et al., 2014b). The potential existence of perchlorate brines on Mars' surface has motivated extensive research on the properties of pure perchlorate brines at Mars-relevant conditions (Chevrier et al., 2009; Fischer et al., 2016, 2016; Gough et al., 2011, 2023; Hecht et al., 2009; Nikolakakos & Whiteway, 2015; Nuding et al., 2014, 2015; Toner et al., 2015a; Toner & Catling, 2016).

In the absence of salts, thin films of water can exist in regolith as adsorbed and/or unfrozen water (Anderson, 1967; Möhlmann, 2004). Adsorbed water forms when water vapor adheres to regolith surfaces and forms thin films, typically just a few monolayers thick. Adsorbed water is distinct from bulk liquid water, yet is interesting because it can enable photo redox reactions of minerals and could hypothetically support life (Möhlmann, 2005). Unfrozen water is a similar physiosorbed state where thin films of water persist in frozen soils at the interface between substrate and ice. The amount of unfrozen water is a function of the soil's temperature, mineralogy, and specific surface area (Anderson, 1967). Unfrozen water is also a distinct phase from liquid water, yet is inhabited in terrestrial environments and could also be habitable on Mars (Gilichinsky, 2002).

Despite extensive research on pure perchlorate brines (salt + water) and on adsorbed and unfrozen water in regolith (water + regolith), systems of brines in Martian regolith (salt + regolith + water) are relatively poorly studied. Numerous terrestrial studies have found that brines freeze at colder temperatures when they exist in the pore space of clays and soils (Banin & Anderson, 1974; Bing & Ma, 2011; L. Wang et al., 2021). We might expect Martian regolith to similarly depress the freezing point of $Mg(ClO_4)_2$ brine, yet numerous previous studies treat regolith as inert and neglect any effect it may have on brine properties. Some experimental work has explored how Mars-like regolith affects the phase transitions of perchlorate brine, but the salt concentrations were much higher than what has been measured on Mars. Primm et al. (2018) found that regolith does not affect the freezing temperature, deliquescent RH, or efflorescent RH when mixed at a 1:1 wt. % ratio with $Mg(ClO_4)_2$ salt. Meanwhile, Toner et al. (2014b) found that ice crystals formed in briny regolith at conditions where the pure brine would remain a supercooled liquid. Understanding how ice and salt form in briny regolith is crucial for assessing the astrobiological potential of putative Martian brines because crystallization damages cells and locks away H_2O in a form that is inaccessible to life.

In this work, we show that a Martian regolith simulant dramatically influences the properties of $Mg(ClO_4)_2$ brine across a wide range of Mars-relevant temperatures, relative humidities (RH), and salt concentrations. By comparing experimental brine-regolith mixtures with the modelled behavior of pure brine and ideal brine-regolith mixtures, we explore how regolith affects the water content, water activity, solubility, and phase transitions of $Mg(ClO_4)_2$ solutions. Then, we interpret our experimental results to assess how briny regolith would influence the geochemistry and potential habitability of Mars' surface.

2.2 Materials and Methods

2.2.1 Salt and Regolith Materials

In these experiments, we studied mixtures of magnesium perchlorate brine in Mars Mojave Simulant (MMS) regolith. We chose $Mg(ClO_4)_2$ because magnesium and perchlorate are major components of the water-soluble fraction of Martian regolith (Hecht et al., 2009; Toner et al., 2014a), and such salts may form brine at Mars-relevant conditions (Gough et al., 2011; Toner et al., 2014b, 2015b). Additionally, the properties of pure aqueous $Mg(ClO_4)_2$ solutions have been extensively studied (Chevrier et al., 2009; Gough et al., 2011; Toner et al., 2014b), which provides important points of reference to compare with our new data on brine-regolith mixtures.

For regolith, we used MMS because it physically and chemically resembles actual Martian regolith (Peters et al., 2008). MMS is composed of weathered basalt crushed to a grain size of 0.5 to 1.27 mm. It was originally developed to test the *Phoenix* and *Curiosity* spacecraft (Peters et al., 2008), and has been used previously to investigate mixtures of $Mg(ClO_4)_2$ and regolith (Primm et al., 2018; Toner et al., 2014b). While MMS best suits our experimental needs, there are a variety of other Martian regolith simulants with different elemental composition, minerology, and grain sizes, which may exhibit different properties. We considered and tested Mars Global Simulant (MGS), a simulant created to match the spectral properties of Martian regolith (Cannon et al., 2019). MGS was ruled out for this work because some of the component minerals (e.g., anhydrite, silica, and anhydrous $MgSO_4$) are extremely hygroscopic agents that created a strong hysteresis effect during adsorption/desorption. Although such active components may occur in Martian regolith, for this study, we chose to focus on $Mg(ClO_4)_2$ as the main active hygroscopic component.

One potential interaction between regolith and brine is that cations in the regolith can exchange with dissolved salts, altering the composition of the brine (Appelo & Postma, 2004). To focus this study on physical interactions, we chose to control brine composition by replacing any exchangeable cations in the regolith with Mg^{2+} prior to the experiments. First, we saturated the MMS with $Mg(ClO_4)_2$ over three sequential extractions, then repeatedly rinsed the regolith with deionized water to remove any soluble species, draining excess water using filter paper over a vacuum. Finally, we dried the regolith in a vacuum overnight at 60°C to dehydrate it.

We then created the regolith-brine samples by pipetting the desired amount of $Mg(ClO_4)_2$ solution into ~0.5 g of MMS. Then, we added deionized water in excess (~0.05 mL), which wetted the entire sample. Upon addition of deionized water, we assume the salt is evenly distributed throughout the sample. We created samples of MMS mixed with $Mg(ClO_4)_2$ at 0% (no salt), 0.6%, 1.0%, 2.2%, and 5.8% by weight.

2.2.2 Measuring Water Content and Water Activity in Briny Regolith

Water activity (a_w) quantifies the availability of water in solution, and is useful for describing habitability because all known life requires $a_w \geq 0.585$ to grow (Stevenson et al., 2017). We measured water content and a_w of briny regolith at 3-98% RH and 25°C using the isopiestic method, which equilibrates samples at a specified RH using a reference solution with a known vapor pressure (Rard & Platford, 1991). We prepared the reference solution from a 99.999% pure Sigma Aldrich H_2SO_4 solution, and the concentration was measured in triplicate by neutralizing the solution with NH_3, evaporating to dryness, and weighing the residue. In the experiments, samples of briny regolith and RH reference solutions were placed into an apparatus, which is described in detail by (Toner & Catling, 2018). The apparatus was then evacuated using a vacuum pump, sealed with a Teflon stopcock, and submerged in a 25°C bath for 2-3 days. Though temperatures on Mars' surface are frequently much colder, 25°C is a standard reference temperature and allows us to compare results with data from the literature. In the bath, water vapor exchanged between the sample and the reference solution until the system reached equilibrium. Because the H_2SO_4 reference solution has a well-defined vapor pressure as a function of concentration, we precisely know the RH of the system. Consequently, the RH also gives the water activity of the sample because the entire system is in equilibrium ($RH_{eq} = a_w$). By taking the masses of sample and reference both before and after equilibration, we measured the water content, salt concentration, and a_w of the brine-regolith mixture. For the isopiestic experiments, we used

MMS mixed with $Mg(ClO_4)_2$ in the following amounts: 0 wt. % (no salt), 0.57 ± 0.0037 wt. % , 1.0 ± 0.012 wt. %, 2.2 ± 0.027 wt. %, and 5.8 ± 0.062 wt. % (the variations reported here and throughout are the sample standard deviation).

To interpret the experimental results, it is useful to compare the measured behavior of brine-regolith mixtures to the modelled behavior for pure brine. We model the water content, water activity, and freezing point depression of pure $Mg(ClO_4)_2$ brine by adapting the revised Pitzer model described in Toner et al. (2015a). It is additionally useful to compare the experimental results to the null hypothesis that brine and regolith act independently from each other. We model the water content of such "ideal" brine-regolith mixtures by summing the water content modelled for pure brine and the water content measured in salt-free regolith.

2.2.3 Measuring the Melting Point of Briny Regolith

At Martian surface conditions, aqueous $Mg(ClO_4)_2$ solutions could transition between phases of liquid brine, crystalline ice and/or salt, and glass–which forms when crystallization is kinetically inhibited in the transition from a viscous liquid to a rigid, amorphous solid (Chevrier et al., 2009; Toner et al., 2014b). These phase transitions are well-characterized for pure $Mg(ClO_4)_2$ brine, but are complicated by the presence of regolith, which binds water molecules to mineral surfaces and could provide nucleation sites for ice or solid salt to crystallize.

We probed phase transitions in brine-regolith mixtures at low temperatures (-150°C to 20°C) using a TA Instruments Q2000 Differential Scanning Calorimeter (DSC). A DSC detects phase transitions by measuring heat flow through a sample as temperature changes. When a sample changes phase (e.g., melts, freezes, or forms glass), it will release or absorb heat in a manner characteristic of that specific phase transition. By inspecting the heat flow through the sample as a function of temperature, we identified the various phase transitions and the temperatures at which they occurred.

However, it is particularly difficult to measure the freezing temperature in $Mg(ClO_4)_2$ brine because perchlorates are prone to supercooling, a metastable state where solutions remain liquid below their eutectic temperature (Toner et al., 2014b). Supercooling may be responsible for the differing eutectic temperatures of $Mg(ClO_4)_2$ reported in the literature (Stillman & Grimm, 2011; Toner et al., 2015b). To avoid supercooling, we instead probed each sample for its melting temperature, which is theoretically equivalent to the freezing temperature at thermodynamic equilibrium. However, hysteresis in freezing and thawing soils may cause the melting temperature to be higher (Devoie et al., 2022). First, we rapidly cooled the brine-regolith sample down to -150°C, held that temperature for 5 minutes, then warmed to 20°C at a rate of 10°C/min. As the sample warmed, we identified melting points at the peak of endothermic dips in the heat flow curve. For this analysis we used TA Instruments Universal Analysis software. We note that the DSC measures the external temperature of the hermetically sealed pan that contains the sample. We assume any difference in temperature between the pan and sample is negligible due to the small sample size (~30-40mg), high thermal conductivity of the aluminum pan, and duration that the sample is held at low temperature. In the calorimetry experiments, we used MMS mixed with $Mg(ClO_4)_2$ in the following amounts: 0.57 ± 0.0042 wt. %, 1.0 ± 0.0064 wt. %, 2.2 ± 0.029 wt. %, and 5.5 ± 0.14 wt. %.

2.3 Results

2.3.1 Water Content and Water Activity at 25°C:

The 25°C isopiestic experiments measured water content (Figs. 2-1 & 2-2) and brine concentration (Fig. 2-3) as a function of RH in mixtures of $Mg(ClO_4)_2$ brine and MMS regolith. These results address a key knowledge gap in the literature about how much water could exist in perchlorate-rich Martian regolith at various RH and salt abundances.

When soils adsorb or desorb water, they experience a hysteresis effect where the water content depends on the soil's hydration history (Hillel, 1971). At identical temperature and RH conditions, soils drying from a wet state will retain more water than soils wetting from a dry state (Hillel, 1971). To measure this hysteresis effect, we collected data for the wetting and drying curves for regolith and some brine-regolith samples (Fig. 2-1). We measure that the hysteresis effect in our experiments is relatively small (at most, 0.4 wt. % difference between the two curves), so for simplicity, we will focus on the drying curves for the remainder of this paper.

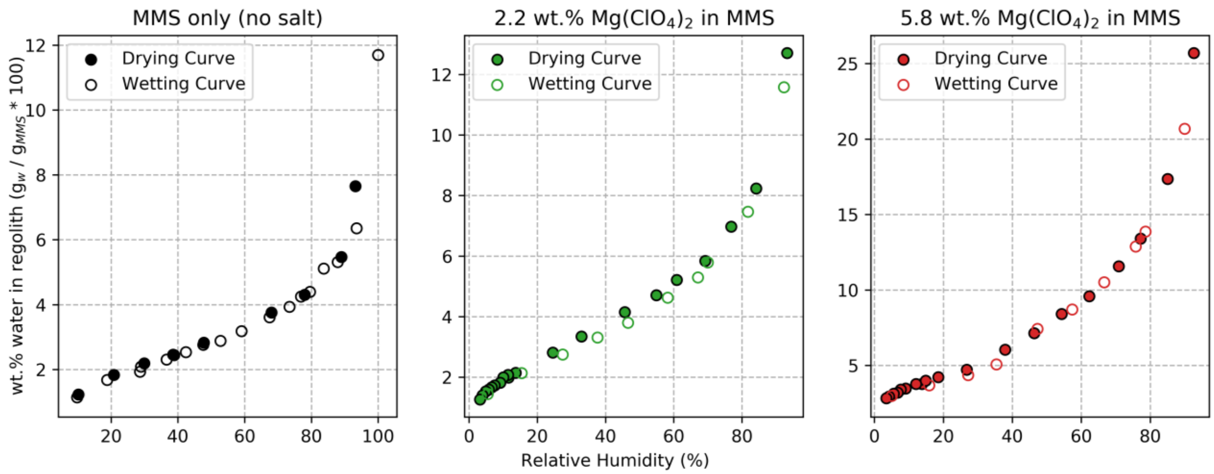

Figure 2-1 Adsorption isotherms show the minor extent of a wetting-drying hysteresis effect in regolith and brine-regolith mixtures. At any given relative humidity, samples that are drying from a prior wet state retain more water than identical samples that are wetting from a prior dry state (Hillel, 1971). Datasets for 0.6 and 1.0 wt. % $Mg(ClO_4)_2$ in MMS are excluded here because only drying curves were measured for those samples. The regolith used was Mojave Mars Simulant (MMS) and all experiments were conducted at 25°C.

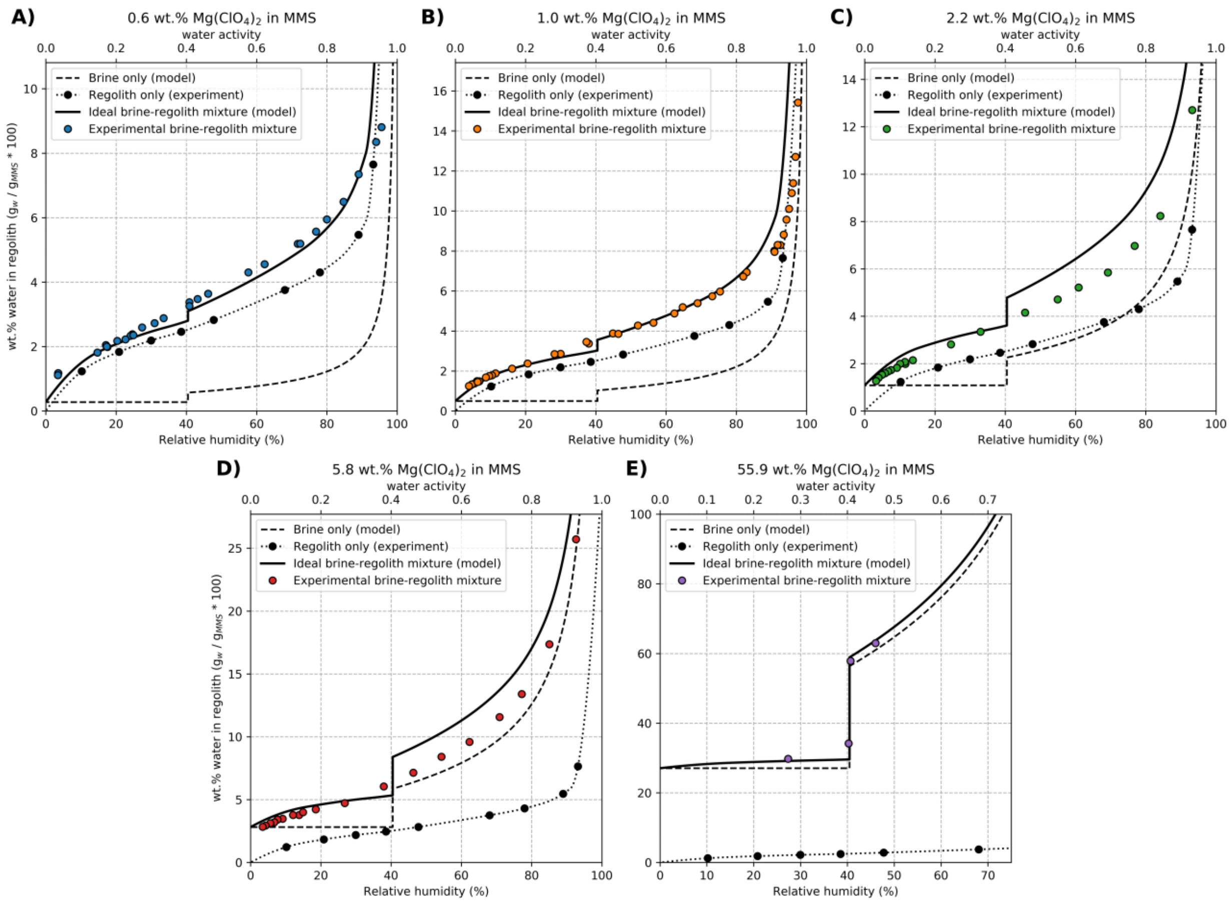

Figure 2-2 The water content in regolith varies based on the RH and the amount of salt in the regolith across several systems: modeled pure brine (dashed curves), regolith without salt (black circles and dotted curves), an ideal mixture of brine and regolith (solid curves), and experimental brine-regolith mixtures (colored circles). The curves for the ideal brine-regolith mixtures sum the behavior of pure brine and salt-free regolith, assuming each component behaves independently. However, experimental brine-regolith mixtures deviate greatly from ideal behavior for 0.6 to 5.8 wt.% salt (A–D). The step changes that occur in some systems at ~40.4% RH are the result of salt precipitation. Notably, salt phase transitions are absent in the experimental datasets for 0.6 to 5.8 wt.% salt (A–D). For comparison, a positive example of salt crystallization in regolith is shown (panel E). All data represent samples at 25°C that have lost water from a prior wet state (i.e., “drying curve” in Fig. 2-1).

Our experiments reveal that brine-regolith mixtures do not behave like ideal mixtures of the brine and regolith endmembers, but instead exhibit unique properties (Fig. 2-2). To model the pure brine component (dashed curves in Fig. 2-2), we adapted the revised Pitzer model described in Toner et al. (2015a) and assumed a fixed amount of salt that exists within, but behaves independently from, the regolith. Note that this is an implicit assumption made by any study that neglects the effect of regolith on brine properties. For salt-free regolith systems, we experimentally measured adsorbed water content using the isopiestic method (black circles in Fig. 2-2), then interpolated between experimental datapoints with a spline curve (dotted curve in Fig. 2-2). Mixtures of brine and regolith have water associated with both salt and mineral phases, and so retain more water than the pure brine or regolith-only endmembers. We predicted the behavior of an ideal brine-regolith mixture (solid curves in Fig. 2-2) by summing the water contents of the pure brine model and regolith-only experiments at every RH. However, the measured behavior of experimental brine-regolith mixtures (colored circles in Fig. 2-2) deviates greatly from ideal predictions. For samples with 0.6 wt. % salt in regolith, the actual mixture tended to be wetter than the ideal case, except when RH exceeded ~90% (Fig. 2-2A). Meanwhile, samples with 1 wt. % salt closely matched the ideal case for RH 0-80 %, but contained less water than predicted for RH > 80% (Fig. 2-2B). Samples with 2.2 and 5.8 wt. % salt tended to be drier than the ideal mixture over all RH (Figs. 2-2 C & D). Potential explanations for these results are discussed in section 2.4.3.

One major deviation from ideal behavior is that salt crystallization is not observed in experimental brine-regolith mixtures with low wt.% salt (Fig. 2-2 A-D). Salt can precipitate from a pure brine when it is saturated, which occurs at RH = 40.4% for $Mg(ClO_4)_2$ at 25°C (Toner et al., 2015a). If water evaporates from the saturated solution, RH and brine concentration remain constant while any excess salt precipitates out of solution. Eventually, only solid $Mg(ClO_4)_2$ hexahydrate would remain at 0.021 % RH (Besley & Bottomley, 1969), with 6 moles of water per mole of salt. We note that $Mg(ClO_4)_2$ solution effloresces at 19% RH (Gough et al., 2011), but in this work, salt forms according to the phase diagram (i.e., at 40.4% RH) because the experiment strongly promotes equilibrium conditions.

In Fig. 2-2, salt crystallization appears as a sharp transition at RH = 40.4 % in the pure brine and ideal brine-regolith mixture models (dashed and solid lines, respectively), as well as in the experimental data for 56 wt. % salt in regolith (Fig. 2-2E). However, this salt crystallization phase change is notably absent from all other experimental brine-regolith data, even at RH well below 40.4 % (Fig. 2-2 A-D). There is similarly no evidence of salt crystallization in the wetting curves (Fig. 2-1). The smooth trend of the data suggests that salt never precipitated in the experiments with 0 to 5.8 wt.% salt in regolith (Fig. 2-2 A-D). This conclusion is further supported by visual evidence, as salt crystals were not observed in any samples with 0.6 to 5.8 wt. % salt (Fig. 2-2 A-D), but were seen in samples with an arbitrarily high salt fraction (56 wt. %) at RH ≤ 40.4 % (Fig. 2-2E).

While we observe no evidence of salt formation in samples with <5.8 wt. % salt, it is possible that crystallization could have occurred undetected in the 0.6 and 1.0 wt. % samples (Fig. 2-2 A-B). In these samples, salt crystallization would be indicated by a relatively small loss of water (0.30 and 0.54 wt. % H_2O, respectively), which might be hidden in the gaps between measured data. By comparison, any salt crystallization in the 2.2 and 5.8 wt. % samples would have been detected because the relatively large loss of water (1.2 and 3.1 wt. % H_2O, respectively) would be apparent in the experimental data (Fig. 2-2 C-D). Because salt crystallization was plainly observed in the 56 wt. % samples (Fig. 2-2E), but did not occur in the 5.8 or 2.2 wt. % samples, we infer that salt also did not crystallize in the 1.0 and 0.6 wt. % samples.

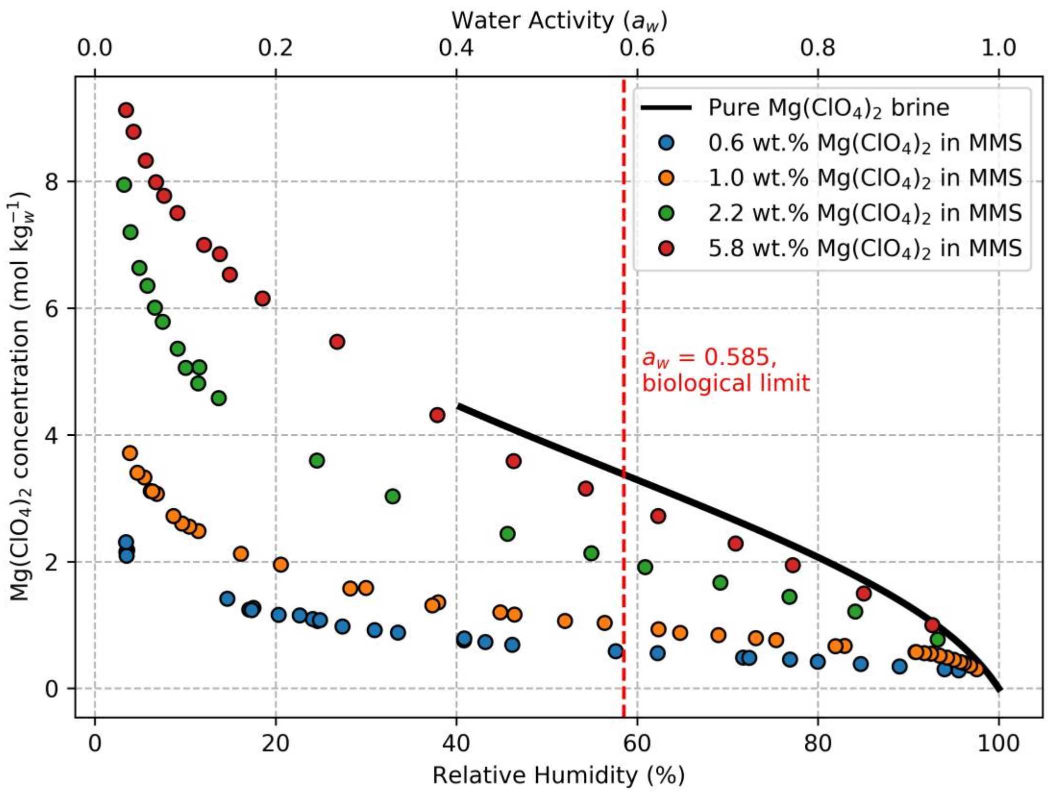

Figure 2-3 At any specified relative humidity, experimental brine-regolith mixtures (circles) are less concentrated than pure brine (black curve). The trend of pure $Mg(ClO_4)_2$ brine (black curve) was calculated using a revised Pitzer model for perchlorates described in Toner et al. (2015a), and terminates at the saturation point (4.44 molal, RH = 40.4%). Also shown is the known lower a_w limit for life on Earth (a_w = 0.585, dashed red line; Stevenson et al., 2017). All data represent samples at 25°C that have lost water from a prior wet state (i.e., "drying curve" in Fig. 2-1).

We find that brines in regolith are less concentrated than pure brine at the same RH and temperature (Fig. 2-3). The magnitude of the drop in salt concentration varies based on the wt. % salt in regolith, with low wt. % salt samples (e.g., blue circles) deviating most from the behavior of the pure brine (black curve). Meanwhile, samples with a higher wt. % salt (e.g., red circles) behaved more like a pure brine.

Although brines on Mars will change concentration in response to environmental RH and temperature conditions, it is informative to consider the inverse relationship to interpret how regolith affects brines in laboratory studies on Earth. In Fig. 2-3, we see that for a given salt concentration in solution, water activity is greatly reduced in brine-regolith mixtures (circles) compared to the pure brine (black line). Regolith reduces a_w in brine because mineral surfaces bind water molecules, which lowers the availability of water in solution (see section 2.4).

2.3.2 Depressed Melting Point in Briny Regolith

The depressed a_w we measure in regolith-brine mixtures (Fig. 2-3) implies a corresponding depression in the freezing point relative to the pure brine (Marion & Kargel, 2007; Toner et al., 2015a). However, freezing points of perchlorate brines are notoriously difficult to measure due to supercooling; instead, we measured the melting point, which is theoretically equivalent at thermodynamic equilibrium. However, it is likely that the measured melting points are higher than the samples' freezing points, because soils experience hysteresis and thaw at warmer temperatures than they freeze at (Devoie et al., 2022).

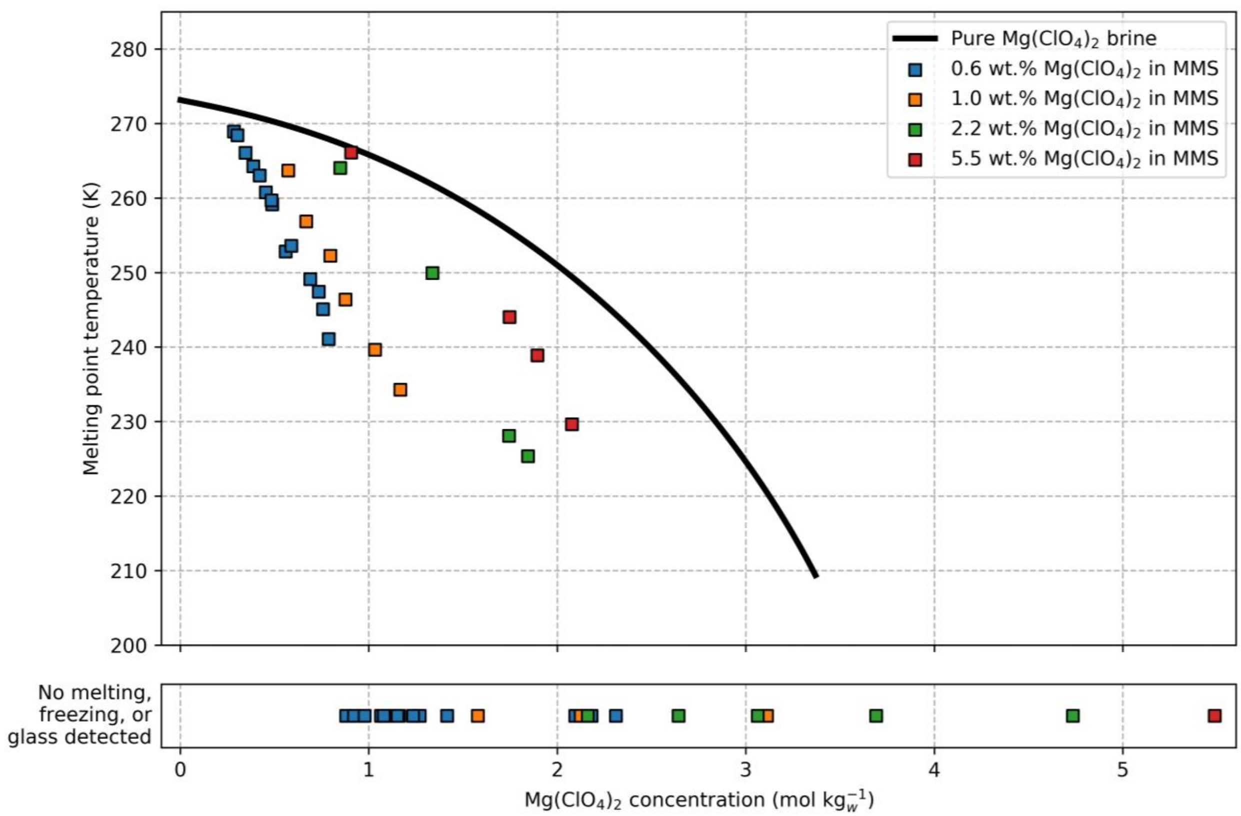

Figure 2-4 Measured melting points of brine-regolith samples (squares) are depressed compared to pure brine (black line) at a given salt concentration (mol kg_w^{-1}). The freezing point of pure $Mg(ClO_4)_2$ brine was calculated using a revised Pitzer model described in Toner et al. (2015a). At all wt. % salt measured, some relatively high-concentration samples showed no signs of freezing, melting, or forming glass whatsoever, over the full range of temperatures (-150°C to 20°C). The concentrations of these unfrozen samples are shown in the lower panel. All data represent samples that have lost water from a prior wet state (i.e., "drying curve" in Fig. 2-1).

Calorimetry measurements show that melting points in regolith-brine samples are depressed relative to pure brine at all salt concentrations (Fig. 2-4). The most significant melting point depressions occurred in samples with the lowest wt. % of salt in regolith (blue squares, upper panel); meanwhile, samples with higher weight % salt behaved more like the pure brine (red squares, upper panel). We did not measure any melting points lower than the eutectic temperature of $Mg(ClO_4)_2$, which is the coldest temperature that a stable liquid brine can reach (209.3K, according to Toner et al., 2015a).

However, not all samples had their melting point depressed by regolith. Instead, many samples showed no signs of melting, freezing, or forming glass whatsoever (Fig. 2-4, lower panel). The brine in these samples remained unfrozen, despite being held at -150°C for 5 minutes, then warmed by 10°C per minute to 20°C. This behavior was observed in samples at each wt.% salt, but only occurred in samples with very low water content.

2.3.3 Inferring Water Activity at Lower Temperature

Melting point measurements can also be used to determine the water activity at very low temperatures. During melting, ice fixes the vapor pressure and therefore the water activity of the system according to equation 2-1 (Marion & Kargel, 2007):

(2-1) $$a_w = 1.906354 - (1.880285 \times 10^{-2})T + (6.603001 \times 10^{-5})T^2 - (3.419967 \times 10^{-8})T^3$$

We used equation (2-1) to calculate the a_w of each sample at its measured melting temperature (T_{melt}), then compared to the measured a_w at 25°C (T_{ref}) (Fig. 2-5). We note that equation (2-1) has previously been shown to provide reliable predictions for the water activity of perchlorate brines at their melting points (Toner et al., 2015a; Toner & Catling, 2016). Even for a brine in regolith, equation (2-1) remains a reliable method for inferring a_w whenever ice is present, because ice controls the vapor pressure of the system.

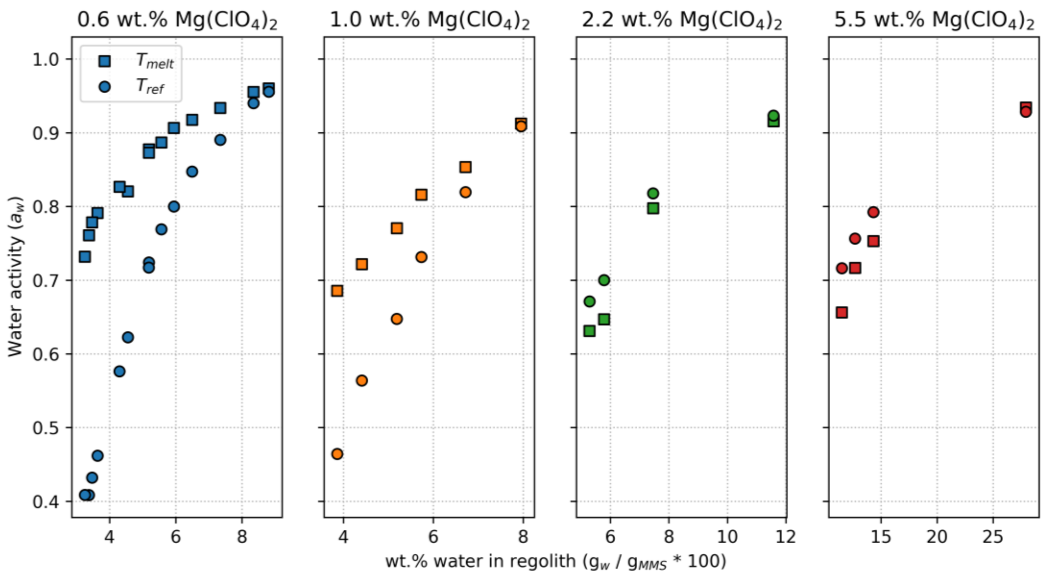

Figure 2-5. To probe how the a_w of briny regolith changes with temperature, we predicted the a_w at each sample's melting temperature (squares) via equation (2-1), then compared to the measured a_w of the same sample at 25°C (circles). Note that the melting temperature varies for each sample (see Fig. 2-4), but for all samples $T_{melt} < T_{ref}$ = 25°C. All data represent samples that have lost water from a prior wet state (i.e., "drying curve" in Fig. 2-1).

The sign and magnitude of the change in a_w with temperature depends on the amount of salt and water with respect to regolith (Fig. 2-5). All samples with 2.2 wt. % salt and all but one sample with 5.5 wt. % salt were projected to have lower a_w at the melting temperature than at 25°C, i.e. water in solution was less available at colder temperatures. Conversely, samples with more Mars-like salt abundance (0.6 and 1.0 wt. % salt) had a much higher a_w at the melting temperature, suggesting water was more available at the colder temperature. Notably, we project that every sample had a_w exceeding the lower limit for habitability (a_w > 0.585) at the melting temperature.

The extreme changes in a_w with temperature predicted here are atypical for most materials and are likely due to hysteresis in the freezing and thawing process. Previous work shows that wet soils thaw at a higher temperature than they freeze at (Devoie et al., 2022). This hysteresis occurs because freezing concentrates water in ice grains and within larger pore spaces, which reduces the melting point depression caused by interactions with the regolith surface (known as the Gibbs-Thomson effect).

2.4 Discussion and Implications for Mars

2.4.1 Regolith Inhibits Salt Precipitation

Our results demonstrate that salt formation is suppressed in Mars-like brine-regolith mixtures, which indicates that water can persist in regolith at drier conditions than in pure brine. In Fig. 2-2, salt formation appears as an abrupt transition at RH = 40.4%, where the saturated brine begins precipitating salt while RH and dissolved ion concentration remain constant. This phase change is apparent in the models for pure brine and the ideal brine-regolith mixtures, as well as the experimental data for 56 wt. % salt (Fig. 2-2E). However, it is absent from all other experimental brine-regolith data (Fig. 2-2 A-D). In fact, we see no evidence of salt formation at any RH for samples with 0.6 – 5.8 wt. % salt, which suggests that regolith completely suppresses salt formation in these samples. At lower temperatures, salt formation was similarly suppressed, and we never observed salt crystallization while probing phase transitions with the DSC between -150°C and 20°C.

Salt formation may have been suppressed because brines in regolith are more dilute than pure brine at a given RH (Fig. 2-3). Salt precipitates from pure $Mg(ClO_4)_2$ brine at the saturation concentration (4.44 molal at 25°C). At lower concentrations, all ions remain dissolved in solution. Brines in regolith are more dilute and remain under the saturation concentration, even at RH < 40.4%, where a pure brine would precipitate salt. Notably, the samples with the most Mars-like salt contents (0.6 and 1 wt. %) maintained a concentration below 4.44 molal at every RH measured (3%-98%), which could explain why no salt formed in these samples. Meanwhile, saltier samples (2.2 and 5.8 wt. %) exceeded the saturation concentration at low RH, yet still showed no signs of precipitating salt.

The equations that describe the precipitation of $Mg(ClO_4)_2$ hexahydrate provide another plausible explanation for why salt crystallization was suppressed in brine-regolith mixtures:

(2-2) $\mathrm{Mg^{2+} + 2\,ClO_4^- + 6\,H_2O \rightleftharpoons Mg(ClO_4)_2 \cdot\ 6\,H_2O}$

(2-3) $K_{sp} = a_{Mg} \cdot {a_{ClO_4}}^2 \cdot {a_w}^6\ =\ \gamma_{Mg}\, {\gamma_{ClO_4}}^2\, (4m^3)\, {a_w}^6$

Here, K_{sp} is the solubility constant that describes salt precipitation, a_i is the activity of each ion or water, γ_i is the ion activity coefficient, and m is the molal saturation concentration of brine. In our experiments, we find that a_w tends to be lower in brine-regolith mixtures than in a pure brine at the same concentration (Fig. 2-3). Because K_{sp} remains constant regardless of whether the reaction occurs in regolith or not, if regolith reduces the a_w of brine, then it must proportionally increase the saturation concentration (m) and/or activity coefficient (γ). Considering the respective powers of each term in equation (2-3), even a small decrease in a_w could cause an exponential increase in the concentration required to precipitate salt (m), which may explain the observed increase in solubility.

Another explanation for the lack of salt formation is that brines in regolith may become supersaturated. Supersaturation is a metastable state where the concentration of dissolved ions exceeds what could ordinarily be dissolved at equilibrium conditions. Perchlorates are particularly prone to the similar metastable state of supercooling. Similar mechanisms could allow metastable states where both salt and ice formation are inhibited for perchlorate brines in regolith. Although regolith may be expected to decrease supercooling by providing additional nucleation sites, prior work that added regolith to Mg- and Ca-perchlorate brine did not observe a decrease in supercooling (Toner et al., 2014a). Further experiments probing the phase transitions during supercooling and supersaturation are needed to understand the mechanisms responsible for both processes.

2.4.2 Regolith Inhibits Ice Crystallization

We similarly found that regolith also inhibits ice crystallization in $Mg(ClO_4)_2$ brine. These results indicate that brines can persist at lower temperatures when in regolith. Previously, the phase boundary between liquid and ice in $Mg(ClO_4)_2$ solution was only well-understood for pure brine (Chevrier et al., 2009; Toner et al., 2015a). The ice line for pure $Mg(ClO_4)_2$ brine is shown as a solid black line in Fig. 2-4. However, when brine is in regolith, the melting temperature is much lower than pure brine, or is eliminated completely (Fig. 2-4). These findings greatly expand the potential physical extent and the annual duration of unfrozen water on Mars' surface.

The magnitude of the melting point depression decreases with increasing wt. % of salt in regolith (Fig. 2-4). We hypothesize this trend exists because high salt content absorbs more water, increasing the overall water content of the brine-regolith mixture (Fig. 2-2). Since the regolith only strongly interacts with the solution that is closest to the brine-regolith interface, the overall effect of regolith is diminished when more brine is present. Consequently, saltier, wetter samples behave more like pure brine. These results are consistent with previous studies, which found that 1:1 mixtures by weight of $Mg(ClO_4)_2$ salt in MMS had a similar freezing temperature to pure $Mg(ClO_4)_2$ brine (Primm et al., 2018). However, measured perchlorate content in Martian regolith are lower (~0.4 - 0.6 wt. %) (Hecht et al., 2009; Toner et al., 2014a). We find that at Mars-relevant salt abundances, regolith does strongly depress the melting point of $Mg(ClO_4)_2$ brine. These results are also consistent with numerous terrestrial studies, which demonstrate that soils reduce the freezing point of various salt solutions (Banin & Anderson, 1974; Bing & Ma, 2011; L. Wang et al., 2021).

Some relatively dry samples showed no signs of melting or freezing whatsoever, despite being cooled to -150°C. When wet soils freeze, a layer of unfrozen water can persist as thin, mobile films between soil surfaces and ice (Anderson, 1967; L. Wang et al., 2021). In our experiments, the samples that remained entirely unfrozen had very low water content and high salt concentration. We hypothesize that all the water in these samples existed as unfrozen brine, tightly bound to regolith surfaces and charged salts. The strong bonds to regolith and salt then inhibit freezing completely, allowing unfrozen water to persist to at least -150°C, which is colder than the lowest temperatures on Mars' surface. These results suggest that at Mars-relevant salt concentrations, thin films of highly-concentrated, adsorbed brines could persist throughout diurnal and seasonal cycles, potentially persisting over multiple Mars years.

2.4.3 Structure of Brines in Regolith

Brine-regolith mixtures exist in a phase between two endmembers: adsorbed water (water + regolith) and pure brine (water + salt). The behavior of the mixture as a whole is highly dependent on the relative abundance of salt in the regolith. Samples with low wt. % salt absorb less water, so the limited water adheres tightly to regolith surfaces. As a result, the system as a whole behaves more like adsorbed fluid. Conversely, samples with high wt. % salt absorb more water, so proportionally more water exists away from the regolith-solution interface. As a result, the regolith has a lesser effect on the brine's properties, and the system approaches the behavior of a pure brine. Brines in regolith follow this trend in terms of water content (Fig. 2-2), water activity and brine concentration (Fig. 2-3), and melting point (Fig. 2-4).

One peculiar observation is that saltier brine-regolith samples tended to contain less water than the sum of the brine-only and regolith-only endmember states (i.e., experimental data vs. ideal model in Fig. 2-2 C-D). We hypothesize that this may be due to large, weakly-charged ClO_4^- anions, which are attracted to the cations in the regolith and subsequently block H_2O molecules from adhering to regolith surfaces. As a result, saltier samples (Fig. 2-2 C-D) contain less water in the adsorbed phase compared to regolith samples with little salt (Fig. 2-2 A-B) or no salt (Fig 2-2, black circles). Future work would be needed to test this hypothesis and explore the effect in more detail.

Regolith disrupts crystallization via the Gibbs-Thomson effect, where the interfacial tension of a fluid on a curved surface increases the energy required to form crystals (Devoie et al., 2022). This effect is strongest very near regolith surfaces and diminishes farther from the interface. When briny regolith freezes, thin films of unfrozen brine can persist tightly bound to regolith surfaces. We hypothesize that some samples in this study contain so little water that the entirety of the brine remains in an unfrozen state at the regolith-solution interface (Fig. 2-4, lower panel). It is unclear from these experiments how thick the unfrozen layer is, or at what water content the free brine regime begins, though we anticipate a region of transition between the two. Prior investigations of unfrozen water found between 1-25 layers of unfrozen water in salt-free clays, depending on temperature (Anderson, 1967). We hypothesize that the addition of salts would further disrupt crystallization and increase the thickness of the unfrozen layer, but future work would be needed to quantify the thickness of this physiosorbed layer for various surface areas and ion concentrations. Future studies could also employ other Martian regolith simulants to explore how brine properties vary in regolith of differing elemental composition, mineralogy, grain size, and specific surface area.

Although adsorbed and unfrozen brines are distinct phases from liquid water, they have several key properties relevant to geochemistry and astrobiology. Adsorbed water can enable geochemical weathering of the surface, and could hypothetically support life (Möhlmann, 2005). Meanwhile, unfrozen water in soil is mobile and can transport ions throughout the matrix (Anderson, 1967; Hoekstra & Miller, 1967; Stillman et al., 2010). On Earth, unfrozen brines support diverse populations of microbes in the permafrost (Gilichinsky et al., 1993), and could feasibly also support life and/or preserve biosignatures on Mars (Gilichinsky, 2002). Future experiments with live microbes would lead to a more robust understanding of the habitability of this unique phase of water in briny Martian regolith.

2.4.4 Implications for Habitability, Planetary Protection, and Exploration of Mars

By inhibiting salt and ice formation, regolith stabilizes brines and may improve their habitability. Crystallization damages cells and locks away H_2O molecules in forms inaccessible to life (i.e., ice or hydrated salt), but our experiments reveal that regolith prevents crystallization over a wide range of Mars-relevant conditions (between 25°C and -150°C and at RH values as low as 3%). Accounting for the salt- and ice-inhibiting effects of regolith, potential brines on Mars could contain more bioavailable water and have fewer hazards for life than previously thought. These effects are astrobiologically significant because they expand the range of conditions where we could search for life in possible Martian brines. They are also relevant for planetary protection because they expand the regions where terrestrial microbes delivered by spacecraft may be able to survive.

A crucial parameter for assessing habitability is water activity, which measures the biological availability of water in a brine and sets a lower limit for life (life requires $a_w \geq 0.585$ to grow) (Stevenson et al., 2017). Planetary protection also relies on a_w to designate "Special Regions," which are areas that merit additional safeguards due to their potential habitability (Rummel et al., 2014). Previously, habitability of potential Martian brines has been assessed using the well-documented a_w of pure brine, while neglecting any effect of regolith. Our results demonstrate that regolith strongly reduces the a_w of a brine at a given concentration at 25°C, and frequently even lowers a_w below the limits for habitability and Special Region status (Fig. 2-3). In Fig. 2-3, any point that falls to the left of the red dashed line is not habitable. However, regolith itself does not necessarily make brines less habitable, because any actual brines on Mars would adjust a_w according to environmental conditions (i.e., temperature and RH), while molal salt concentration varies as water is exchanged with the atmosphere. Nevertheless, these findings demonstrate that predicting habitability on Mars based on the a_w of pure brines is not a sufficient approach, and future studies should account for how strongly regolith depresses a_w.

Despite having lower a_w at 25°C, brines in regolith may–perhaps counter-intuitively–have more habitable a_w at the colder melting temperature. We calculate that every sample in our study had a_w permissible for life ($a_w > 0.585$) at its melting temperature (Fig. 2-5). However, the a_w at the freezing temperature is likely lower because hysteresis causes freezing to occur at a lower temperature than thawing in soils (Devoie et al., 2022). Regardless of whether a_w is permissible for life, low temperatures remain a barrier for habitability. The measured melting temperatures were frequently below the known limits for cell division (-18°C) and metabolism (-33°C; Rummel et al., 2014). Future experiments measuring a_w below 0°C are necessary to better understand the low-temperature habitability of perchlorate brines in regolith.

While low a_w brines like we measure at 25°C are generally less habitable, low a_w itself is not necessarily biocidal (Hallsworth, 2021). Some terrestrial organisms can survive wet-dry cycles, even when a_w drops below their minimum required value for metabolism or reproduction (Meisner et al., 2021). Brines that experience changing a_w conditions could still support life that is dormant during low-a_w periods, then active when a_w conditions permit (Möhlmann, 2005). On the other hand, chaotropicity (i.e., the disruption of intermolecular bonding and structure) may be the most limiting factor for habitability in potential Martian brines, regardless of whether a_w is permissible (Hallsworth, 2021).

In addition to the implications for geochemistry and habitability, these results are also important for understanding ion mobilization and the mechanical properties of Martian regolith. The *Phoenix* lander observed perchlorate ions distributed throughout the soil and locally concentrated in patches, which suggests mobilization and could be evidence of recent thin brine films (Cull et al., 2010). Our results help explain how perchlorate could migrate in the cold and dry polar conditions: regolith could keep brines mobile by inhibiting salt and ice crystallization. *Phoenix* and several other missions also encountered unusually cohesive regolith (Arvidson et al., 2004a; Arvidson et al., 2004b; Arvidson et al., 2009; Minitti et al., 2013; Moore et al., 1999). In the example of the *Phoenix* lander, the regolith was so unexpectedly cohesive that mission planners had to improvise a "sprinkle" delivery method to collect a sample (Arvidson et al., 2009). Perchlorate brine films in the regolith could explain the strong cohesion observed. Our results are also relevant to the ongoing *Perseverance* mission, which is equipped to sample regolith in Jezero Crater (Moeller et al., 2020), where perchlorate salts have been detected (Farley et al., 2022; Scheller et al., 2022; Tice et al., 2022; Wiens et al., 2022).

2.5 Conclusion

Interactions with regolith are critical for assessing the abundance, persistence, and habitability of putative brines on Mars. Experiments show that regolith can inhibit freezing and salt precipitation, allowing water to persist at much colder and drier conditions than are possible for pure brine. Regolith may also make potential surface brines more habitable by inhibiting crystallization of salt and ice, which damage cellular structures. Some relatively dry samples never crystallized over the full range of Martian surface temperatures, suggesting that thin films of unfrozen brine could persist in regolith over diurnal and seasonal cycles. The persistence of brines in regolith greatly expands the spatial and temporal extent of potentially habitable conditions on Mars.

Overall, we demonstrate a novel approach for investigating brines as they would likely exist on Mars' surface, i.e., adsorbed to and in the pore space of regolith. Brines in regolith do not behave like ideal mixtures of pure brine and adsorbed water, but are instead a unique system complicated by interactions between all three components (water, salt, and regolith). Therefore, the distinct properties of briny regolith systems must be considered to accurately explore how brines would affect the geochemistry, habitability, and mechanical properties of Mars' surface. This new approach to studying brine-regolith systems holistically will improve astrobiological and geochemical investigations, mission planning, and planetary protection on Mars.

2.6 Acknowledgements

This work was supported by NASA Solar Systems Workings Grant #80NSSC21K0149.

3. Seasonal Loss of Adsorbed Water as a Formation Mechanism for Recurring Slope Lineae on Mars

At time of writing, this chapter is in preparation to be submitted for publication. Co-authors include Sarah King, David C. Catling, and Jonathan D. Toner.

Abstract

Recurring slope lineae (RSL) are seasonally recurring dark streaks that incrementally propagate down warm Martian slopes. RSL are strongly linked to water because of their activity during warm seasons and gradual fading during colder seasons, but their precise formation mechanisms remain a mystery. Whether RSL are wet, and how much water they contain, are fascinating questions because water shapes the morphology, geochemistry, and habitability of Mars' surface, and is a valuable resource for future human exploration. Several competing hypotheses have proposed RSL as either wet (brine) flows or dry granular flows, though neither wet nor dry models alone sufficiently explain all RSL morphology and seasonality. In this work, we test a hypothesis that reconciles the wet and dry flow models by describing RSL as granular flows triggered by a loss of adsorbed water during low relative humidity (RH) seasons. In this model, seasonal dehydration lowers cohesion between grains, destabilizing slopes and initiating mass wasting. We tested this "water desorption hypothesis" through analog experiments that measured water adsorption and angle of repose in a Mars regolith simulant between 0-96% RH. The results demonstrate how regolith hydration and angle of repose positively correlate with RH, which supports the hypothesis that RSL are granular flows triggered by seasonal slope dehydration. Unlike other mechanisms, the desorption model explains RSL seasonality while requiring only soil and atmospheric water vapor, which is more consistent with Mars' arid surface conditions. These results have implications for astrobiology and planetary protection, since—contrary the prevailing narrative—RSL in this model are unlikely to contain enough water to sustain life,

which informs future astrobiological investigations and planetary protection considerations for future missions.

3.1 Introduction

3.1.1 Background

Recurring Slope Lineae (RSL) have captured the interest of planetary scientists and astrobiologists due to their putative connection to liquid water—an anomaly on Mars' otherwise arid, frozen surface. They have been observed at many locations across the midlatitude and equatorial regions of Mars (e.g., Chojnacki et al., 2016; McEwen et al., 2011, 2014; Ojha et al., 2014; Stillman et al., 2014, 2017, 2020; Stillman & Grimm, 2018). RSL appear in high resolution satellite images as narrow (~0.5 - 5 m wide) dark streaks that extend up to hundreds of meters downslope (McEwen et al., 2011). RSL are unique because of their seasonal activity and recurrence—appearing and incrementally propagating downslope during periods of warm temperatures and/or high insolation, then gradually fading until they are indistinguishable from their surroundings (McEwen et al., 2014; Stillman et al., 2020). This seasonal recurrence on warm and sun-facing slopes strongly suggests a role for some volatile (i.e., water) in their formation, but the precise mechanisms behind RSL have so far eluded explanation.

Understanding how RSL form is hugely important because—if they contain sufficient liquid water—they may be able to support life, either native Martian organisms and/or terrestrial biological contamination (Rummel et al., 2014; Stillman et al., 2017). Despite uncertainty about the amount and availability of water involved, RSL sites have been proactively assigned a protected status that requires any spacecraft planning to visit them to adhere to the strictest sterilization protocols (Rummel et al., 2014). Constraining the quantity and role of water in RSL is therefore critical for assessing the habitability of Mars today and for informing planetary protection measures for future missions. Alternatively, wet-but-uninhabitable RSL could serve as a reservoir of water to sustain future crewed missions. Describing RSL is also important to understand how water exchanges between the atmosphere and surface, and to constrain the global water inventory.

Many models have been proposed to explain RSL, but presently there is no consensus on how RSL form, nor how much (if any) water is involved. Below, we briefly summarize several proposed wet and dry mechanisms for RSL formation, then build on past models by uniting several hypotheses to explain RSL using only seasonally variable amounts of water vapor in the atmosphere.

3.1.2 Summary of Wet and Dry RSL Models

The seasonal activity of RSL during warm conditions is suggestive of flowing or seeping water, potentially as brines that form when temperatures exceed the melting point of ice or eutectic temperature of an ice-salt mixture (McEwen et al., 2011; Stillman et al., 2014, 2016). In this model, their dark color is explained as wetting of (salty) soils (Heinz et al., 2016), and brine flow and evaporation models might explain their gradual growth downslope and fading, respectively (Huber et al., 2020).

However, wet models face several major challenges, most crucially explaining a source of liquid water capable of resupplying RSL each year that is consistent with the present Martian climate. Subsurface aquifers are one proposed source of such water (e.g., Abotalib & Heggy, 2019; Stillman et al., 2014, 2016). Water may also be sourced from deliquescent salts, which are able to form liquid brines under certain Martian surface conditions (Gough et al., 2016; A. Wang et al., 2019). Another limitation on wet models is that thermal measurements place an upper limit on the amount of water present at ~0.5 to 3 wt. % (Edwards & Piqueux, 2016). Finally, wet hypotheses are challenged by a terrestrial analog study that observed inconsistencies between the surface expression and dynamics of RSL compared to salty wet streaks in the McMurdo Dry Valleys of Antarctica (Toner et al., 2022).

An alternative hypothesis that is consistent with the modern Martian climate is that RSL are dry granular flows. Dry flow hypotheses are supported by morphological evidence that RSL frequently exist on slopes near the angle of repose observed for Martian dunes (e.g., Dundas et al., 2017; Stillman et al., 2020; Tebolt et al., 2020). In planetary literature, the stable angle of repose refers to the maximum stable angle a granular slope can reach without failing, while dynamic angle of repose refers to the angle that a slope relaxes to after a slide.

In dry flow models, the dark color of RSL is explained by the removal of higher-albedo dust during a flow, which reveals lower-albedo material underneath (Dundas, 2020; Dundas et al., 2017). Similarly, RSL fading is explained by the gradual redeposition of dust over many sols (i.e., Martian solar days). Dust certainly seems to play some role in RSL formation because more RSL than are usual were observed following global dust events in Mars years 28 and 34 (McEwen et al., 2021; Stillman et al., 2014). However, even dry flow hypotheses require some role for a volatile to explain how RSL can occur seasonally.

3.1.3 Dehydrating Slopes as a Trigger for RSL

The connection between RSL appearance and seasonal temperatures has been extensively studied, but any role for RH has received less attention. RH is the vapor pressure as a fraction of the saturation vapor pressure at a given temperature. When RH is high, soils hydrate as water vapor adsorbs to regolith grains, forming thin films of tightly bound H_2O (e.g., Fanale & Cannon, 1971; Savijärvi & Harri, 2021; Shumway et al., 2023). Conversely, during low RH, soils dehydrate as water desorbs and is released back to the atmosphere. RH anticorrelates with temperature, so colder seasons (i.e., autumn, winter) are more humid than warmer seasons (i.e., summer). RH also varies greatly over diurnal cycles, generally reaching a maximum just before sunrise, then dropping to single digits or even zero during the day (e.g., Fischer et al., 2019; Harri et al., 2014; Polkko et al., 2023). Here, we will focus on seasonal cycles of average RH, as this is the timescale over which RSL are observed (i.e., through repeat HiRISE images, several sols apart).

In this work, we test a formation mechanism that reconciles various wet and dry hypotheses to explain RSL appearance, morphology, and seasonality consistent with known environmental conditions on Mars. This model posits that RSL are granular flows triggered by seasonal dehydration of slopes during periods of low RH (e.g., Gough et al., 2020; McEwen et al., 2011). Specifically, seasonal mass wasting could occur during low relative humidity (RH) conditions as water desorbs from granular slopes, lowering cohesive forces between grains and destabilizing slopes. When RH rises again during a later season, slopes would rehydrate as water vapor readsorbs. Adsorbed water forms thin films that can bridge grains of regolith, increasing cohesivity and allowing the slope to be built up to steeper angles. As with other granular flow hypotheses, the recurrence of RSL between years requires replenishment of granular material, which could be supplied by aeolian transport of sands upslope (e.g., Dundas 2017; 2020), and/or by deposition of dust suspended in the atmosphere (McEwen et al., 2021). Dust deposition also explains the slow fading and disappearance of RSL in this and other grain flow models (McEwen et al., 2021). The desorption model is favored in this work because it explains seemingly contradictory wet and dry characteristics that RSL exhibit, while requiring only water vapor supplied to the soil via adsorption.

Desorption as the trigger mechanism for RSL was first hypothesized upon their discovery (McEwen et al., 2011), but this hypothesis has never been tested directly through laboratory investigations of water adsorption and slope stability. Previous work has investigated whether dehydrating salts could play a role in RSL formation, and found that RSL at one site appear during conditions that would cause perchlorate salts to fully dehydrate (Gough et al., 2020). However, the link between salt (de)hydration, soil cohesivity, and slope stability was assumed.

In this work, we focus on adsorption and desorption processes in salt-free regolith to investigate slope failure as a function of RH and adsorbed water content. This desorption mechanism involves only soil and adsorbed water, and does not rely on a high abundance of salts—which have never been conclusively linked to RSL. (Previous identifications of hydrated perchlorates at RSL sites can be plausibly interpreted as artifacts in the spectroscopy data; Leask et al., 2018; Ojha et al., 2015.) The results of these experiments provide broad physical insights that are relevant across many RSL sites and to granular slopes on Mars generally.

3.2 Methods

To determine the effect of RH and regolith hydration on slope stability, we measured the water content and angle of repose in a Martian regolith simulant at several RH values between 0 and 96%. The sediment used was Mojave Mars Simulant (MMS), a natural regolith analog composed of mechanically crushed, oxidized basaltic rocks (Peters et al., 2008). The MMS used in this experiment was sieved to grain size of <500 microns and baked at 100°C overnight in a vacuum chamber to remove all water prior to the experiments.

Adsorbed water content and RH were measured using the isopiestic method (Rard & Platford, 1991). In the isopiestic method, a reference solution with a well-defined vapor pressure as a function of concentration controls the RH of the system by exchanging water vapor with the headspace, which can then be adsorbed onto the regolith simulant. The system was initially evacuated to increase the rate at which water vapor diffused through the system. The entire apparatus was held at a constant temperature of 25°C for 3 days to allow adequate time for water to exchange and for the regolith to reach equilibrium with the headspace. Gravimetric analysis (i.e., weighing before and after) was used to measure the adsorbed water content of the regolith, and the concentration of the reference solution. RH was calculated from the concentration of the reference solution, which has a well-defined vapor pressure as a function of concentration. The reference solution was prepared from a 99.999% pure solution of H_2SO_4 manufactured by Sigma Aldrich. This method and the apparatus used are described in more detail in Shumway, et al. (2023) and Toner & Catling (2018).

First, the adsorption properties of the simulant were characterized by measuring adsorbed water content as a function of RH for a small mass of regolith (~0.5 g). Next, the same method was used to set RH and measure wt. % H_2O for a larger mass of regolith (~100 g), which was later used to investigate slope failure (see below). The results for the two sample sizes were compared to ensure the larger mass of regolith had reached equilibrium with the measured RH.

Once RH and adsorbed water content were known, we measured slope angles using a transparent, cylindrical, acrylic tumbler (~9 cm in diameter). The tumbler was laid horizontally on top of a pair of wheels, and driven by a motor to rotate slowly (~4 rotations per hour; see Fig. 3-1). A level video camera filmed the transparent face of the tumbler while it rotated, monitoring the gradually steepening profile of the regolith simulant within.

Eventually, the inclination of the soil simulant would exceed the maximum stable angle of the regolith inside (i.e., static angle of repose), and the slope would fail, avalanching downslope until coming to rest at a lower stable angle (i.e., the dynamic angle of repose). Over 100 slope failures were filmed in each experiment to collect sufficient data to allow statistical analysis of many events at the same conditions. Frames from one video showing a slope immediately before and after failure are displayed in Fig. 3-1.

In each video, we tracked the slope to detect failure events and measure the static and dynamic angles of repose (from the frames immediately before and after each slope failure event, respectively). Each video was compressed to two frames per second to reduce file size without loss of information. Each frame of the video was cropped to a circle containing only the tumbler face, then brightened and smoothed using a Gaussian blur to emphasize the slope and reduce noise. Finally, a Canny edge detection algorithm was applied to identify the slope, and a smoothed spline was fit through the pixels to represent the slope mathematically.

In each frame of the video, we checked for a reduction in slope relative to the prior frame to identify slope failure events. In the frames immediately before and after a failure event, slope angles were calculated by taking the derivative of the spline that was fit to the slope. Because each slope was a complex profile that could not always be represented by a single dominant angle, we calculated the slope angle at one hundred points across the length of the slope, excluding the first and last 10% points on the slope, which were closest to the edge of the cylinder and prone to edge effects.

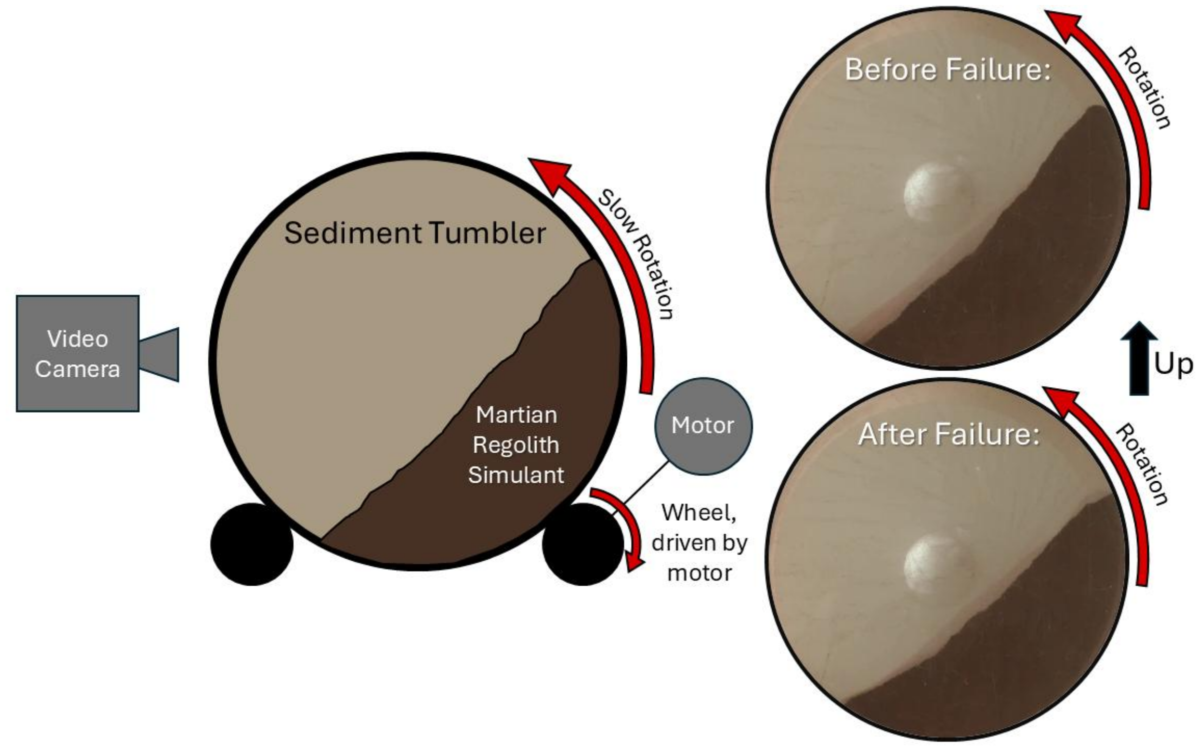

Figure 3-1. Schematic (left) and still images (right) showing the tumbler apparatus that was used to measure angle of repose as a function of relative humidity (RH). Within, Mars regolith simulant (dark brown) was equilibrated at a known RH and the water content was measured. Driven by a motor, the tumbler slowly rotates counterclockwise, gradually increasing the profile of the sediment within, until the slope fails. Still images from the experimental video show examples of the maximum slope reached before a failure event (top right) and the slope relaxed to after failure (bottom right). In the images shown, RH = 36% and H_2O content = 1.85 wt. %. Red arrows indicate direction of rotation.

3.3 Results

3.3.1 Soil Hydration and Relative Humidity

Results from the isopiestic experiments demonstrate how the adsorbed water content of the regolith simulant varies with RH (i.e., an adsorption isotherm; Fig. 3-2). When adsorbing or desorbing water, soils experience a hysteresis effect in which the water content depends on whether the soil is gaining or losing water (Hillel, 1971). Such hysteresis has been previously observed in several other Martian regolith simulants (e.g., Pommerol et al., 2009; Shumway et al., 2023). For the regolith simulant used in this study, we document hysteresis by measuring water content as a function of RH for both wetting and drying curves (black and white circles in Fig. 3-2, respectively). As with other granular materials, the soil studied here retains more water while drying compared to a wetting sample at the same RH.

Results show correlation between RH and adsorbed water content, for both wetting and drying curves, with a maximum of ~7 wt. % H_2O adsorbed at ~96% RH. The water content as a function of RH for the tumbler apparatus (magenta squares) generally agrees with the measured adsorption isotherm (black circles), confirming that the entirety of the regolith had equilibrated with the set headspace RH (within ~1 wt. % H_2O) prior to the measuring of the slope angle.

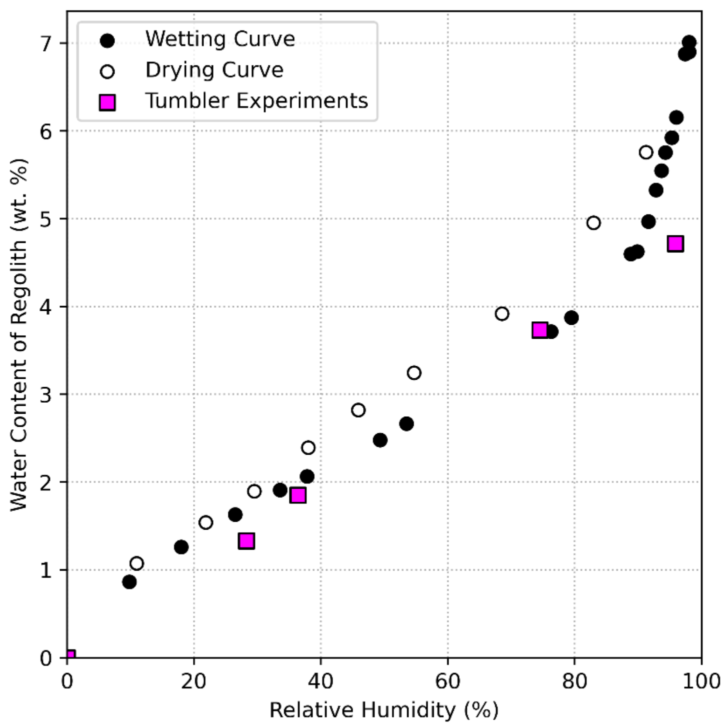

Figure 3-2. Adsorption isotherm for fine-grained (<500 μm) regolith analog Mojave Mars Simulant (MMS), showing the adsorbed water content at various relative humidity (RH). Hysteresis in wetting vs. drying regolith results in different water content at any given RH, dependent on whether the sample is gaining or losing water (i.e., wetting and drying curves, black and white circles, respectively). Measured RH and water content of tumbler chamber

(magenta squares) generally agree with the wetting curve data (i.e., the larger mass of sediment in the tumbler reached equilibrium with the water vapor in the headspace).

3.3.2 Angle of Repose and Relative Humidity

We analyzed thousands of slope angles measured across hundreds of slope failure events to compile statistical distributions of angles of repose in sediment equilibrated at 0-96% RH. Slope angles calculated from frames immediately before and after failure are interpreted as the static and dynamic angles of repose, respectively. Fig. 3-3 shows histograms of the measured static (blue) and dynamic (orange) angles of repose, as well as the mean of each dataset (circles). The standard error of the mean is also plotted, but is smaller than the points displayed. A probability density function is also fit to each distribution (solid lines). Various statistical parameters for each distribution are listed in Table 3-1.

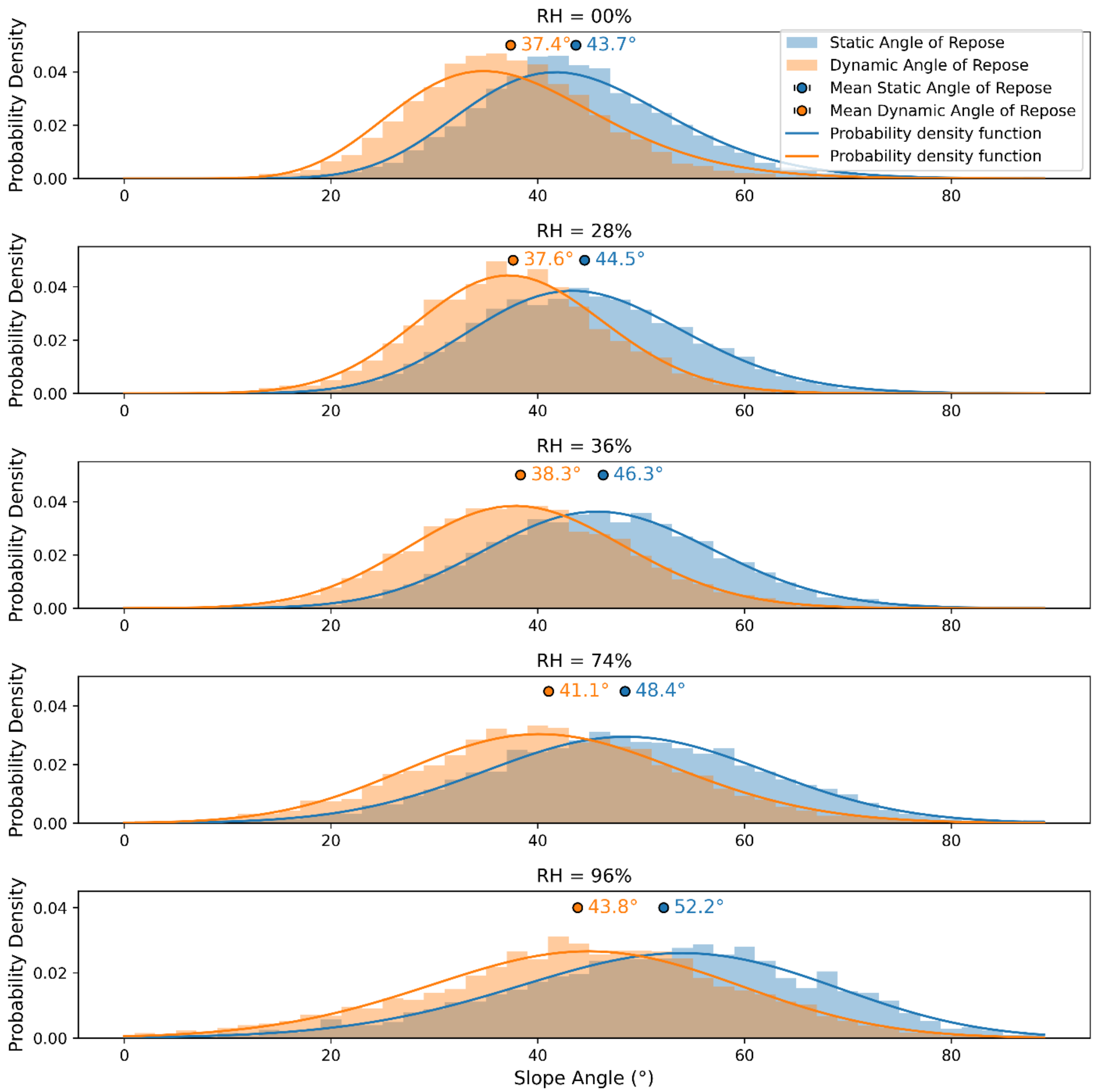

Figure 3-3. Histograms show the distribution of slope angles measured immediately before (static) and after (dynamic) slope failure events. The mean angle of repose is represented by a solid circle, with a standard error of the mean smaller than the point plotted. See Table 3-1 for more statistical information about these distributions.

	RH (%)	N	Median	Mean	Standard Deviation	Standard Error	Skewness	Kurtosis
Static Angles of Repose	0%	10692	42.89	43.55	9.78	0.117	0.413	1.031
	28%	10197	44.12	44.54	10.42	0.127	0.232	0.098
	36%	9999	46.10	46.32	10.98	0.136	0.094	-0.028
	74%	8118	48.21	48.41	13.48	0.185	-0.038	-0.014
	96%	6138	53.08	51.97	15.11	0.240	-0.332	-0.052
Dynamic Angles of Repose	0%	10692	36.58	37.01	9.17	0.110	0.465	1.651
	28%	10197	37.36	37.61	9.02	0.110	0.116	0.482
	36%	9999	38.09	38.32	10.40	0.128	0.090	0.173
	74%	8118	40.72	41.01	13.08	0.180	0.133	0.351
	96%	6138	44.33	43.79	14.93	0.238	-0.186	-0.001

Table 3-1. Relevant data and statistical parameters from each slope angle experiment. RH is relative humidity, and N is the number of slopes measured.

Results show that the mean static and dynamic angles of repose both increased with RH (Fig. 3-4). Static angle of repose increased by 8.4° from 43.7° at 0% RH to 52.2° at 96% RH. Dynamic angle of repose increased by 6.8° from 37.0° at 0% RH to 43.8° at 96% RH. Linear regressions were performed to describe the first order trend of angle of repose with RH. Static angles of repose followed a trend of $\theta_s = (0.079 \pm 0.0022)\, RH + (43.1 \pm 0.97)$ with $R^2 = 0.93$; dynamic angles of repose followed a trend of $\theta_d = (0.063 \pm 0.0023)\, RH + (36.4 \pm 0.90)$ with $R^2 = 0.91$, as shown in Fig. 3-4.

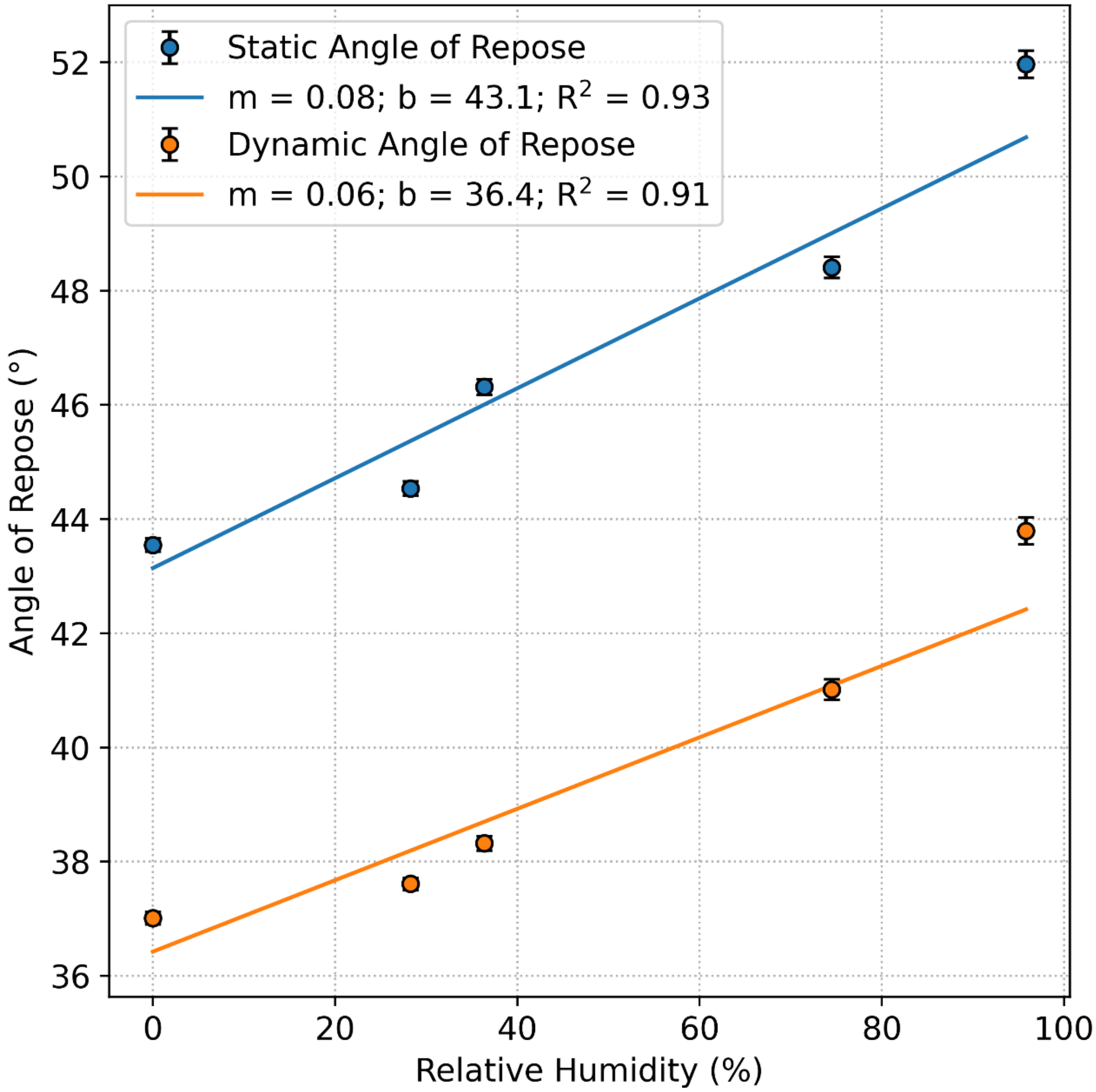

Figure 3-4. Mean static (blue) and dynamic (orange) angles of repose measured in simulated Martian regolith equilibrated at RH = 0%, 28%, 36%, 74%, and 96%. Angle of repose increases at higher RH. Error bars show the standard error of the mean. Linear regressions are also shown.

3.4 Discussion

3.4.1 Support for the Water Desorption Model

Results show a strong correlation between RH, soil hydration, and slope stability, which suggests that seasonal RH cycles could alter the angle of repose to alternatively stabilize and destabilize granular slopes on Mars. This finding supports the hypothesis that RSL are granular flows triggered by seasonal water desorption. If present, perchlorate salts might further augment these cohesivity cycles (e.g., Gough et al., 2020), but our experimental results emphasize that salts are not required to explain seasonal granular flows.

These findings suggest that in high-RH conditions (such as autumn and winter), slopes will hydrate by adsorbing thin films of water, which can bridge the pore space between grains and increase cohesivity. High adsorbed water content therefore stabilizes slopes, allowing them to reach steeper stable angles without failing. During this phase of the cycle, RSL are not active, but are "recharging" as slopes are built up to steep angles by windblown sediment and/or air fall dust (e.g., see Dundas, 2020; Dundas et al., 2017; McEwen et al., 2021). The maximum angle that a slope could be built to depends on the RH, which our results suggest could be up to several degrees higher than an equivalent dry slope.

Subsequently, when RH drops (e.g., in the spring and summer), water will desorb from slopes, lowering cohesivity and decreasing the angle of repose. Experiments show that the resulting decrease in static angle of repose could be as large as 8.4° (i.e., if RH decreased from 96% to 0%). If the static angle of repose ever falls below the actual inclination of a slope, the slope will become unstable and fail. The resulting granular flow would remove the uppermost layer of high-albedo dust, revealing low-albedo material underneath, which would explain the dark appearance of RSL (Dundas, 2020; McEwen et al., 2021). Gradual deposition of airfall dust explains why RSL fade over time (e.g., Dundas, 2020; McEwen et al., 2021).

These results also provide a novel explanation for how RSL grow incrementally over a season. If slope stability is controlled by RH, gradually decreasing RH could repeatedly destabilize slopes, triggering multiple grain flows. Specifically, when RH decreases, the top layer of sediment will dehydrate first, likely before sediment at depth has a chance to equilibrate with the newly dry atmosphere. When the dehydrated top layer fails, it could expose sediment that is still hydrated and therefore stable. Now in direct contact with the dry atmosphere, the newly exposed layer will rapidly dehydrate and fail as well, increasing the length of the RSL.

Over the course of the drying season, new material would be repeatedly exposed, dehydrated, and moved downslope, which from orbit would appear as an incremental lengthening of individual linea.

Some recharge mechanism is required to explain how RSL recur between years. As in other grain flow models, we suggest windblown deposition of sediment onto the lee faces of outcrops could serve as the source of sediment resupply. One case study Garni crater found a connection between local patterns of eolian deposition and erosion and the size and location of RSL (King et al., 2019). In Garni, the majority of RSL occur on the leeward side—where sediment is deposited—while no RSL occur on the wind-scoured side—where erosive processes dominate (King et al., 2019). This connection to wind explains why RSL are associated with rocky outcrops, since steep, rocky slopes create a lee effect that traps sediment near points where RSL initiate. The results presented here build on these prior studies and further support a dry flow hypothesis by demonstrating how slopes can be resupplied by new material during the RSL-dormant seasons (i.e., because hydrated slopes are more cohesive therefore are able to retain more sediment).

Results are also consistent with the measured upper limit of ~0.5-3 wt. % H_2O in RSL (Edwards & Piqueux, 2016). This amount of water is equivalent to the adsorbed water content of the tested regolith simulant at < 60% RH (Fig. 3-2). At RH values between 0% and 60%, the change in angle of repose is large enough to potentially trigger grain flows ($\Delta\theta_s$ = ~5°; Fig. 3-4).

While these experimental results provide compelling evidence in support of the desorption model, future spacecraft measurements are needed to validate the hypothesis. For example, this model predicts a change in RSL slopes between seasons, which may be measured through the construction of digital terrain models (DTMs) of RSL-bearing slopes during both RSL-active and RSL-inactive seasons. However, the resulting change in slope may be below the vertical resolution of current DTMs. Another remote sensing observation that could help test this hypothesis is frequent monitoring of water vapor abundances at RSL sites throughout different seasons, which could be used to interpret the amount of water being seasonally adsorbed and desorbed from RSL-bearing slopes. Furthermore, studies of potential sources of granular material which could resupply RSL have shown some promise (e.g., in Garni Crater; King et al., 2019; Stillman et al., 2020). Similar studies could be conducted on other RSL sites to identify plausible sources of granular material that resupply RSL, and any correlation with local wind patterns that would suggest eolian transported sediment.

3.4.2 Comparison to Spacecraft Data

A key piece of evidence in support grain flow hypotheses is that RSL frequently occur on slopes near the angle of repose measured for Martian dunes. Analysis of DTMs constructed from HiRISE images for three dune fields revealed angles of repose in the range of 30-35° (Atwood-Stone & McEwen, 2013), while the *Curiosity* rover measured static and dynamic angles of repose as 33° and 29°, respectively, in the Bagnold dunes (Ewing et al., 2017). Meanwhile, many RSL exist on slopes near 28-35° (Dundas et al., 2017). At one site, RSL were observed to initiate at on a mean slope of 32.6° and terminate on a mean slope of 30.7°, which are interpreted as the static and dynamic angles of repose, respectively (Stillman et al., 2020). However, many RSL have also been observed to exist on slopes that deviate from the angle of repose (Stillman et al., 2020; Tebolt et al., 2020).

By comparison, the angles measured in these experiments (43°-52° static; 37°- 43° dynamic) are notably higher than both the angle of repose and the RSL slope angles measured on Mars. There are several plausible explanations for the discrepancy between laboratory and field measurements. First, the experiments were conducted at a much higher gravitational acceleration compared to Mars' surface (i.e., 9.81 m/s^2 vs. 3.72 m/s^2). While angle of repose is likely independent of gravity (Atwood-Stone & McEwen, 2013), one experimental study of angles of repose under Mars-like gravitational acceleration (achieved through parabolic flights) measured higher static angles of repose and lower dynamic angles of repose compared to terrestrial gravity (Kleinhans et al., 2011). The wider gap between static and dynamic angles of repose at lower gravitational acceleration observed by Kleinhans, et al. (2011) would further strengthen the effect of desorption on RSL formation, as it suggests slopes could reach yet higher angles in the high-RH seasons, then relax to shallower angles post-collapse.

Another potential explanation for the discrepancy in measured angles is that the experiments only tested stability under the force of gravity, whereas actual Martian slopes will have many complex factors that affect slope stability. Additional random forces, such as winds or dust devils, which may act to destabilize slopes at lower angles. This may be supported by observations of many more RSL than were expected following a planet-wide dust storms in Mars year 34 (McEwen et al., 2021). Such real-world forces may prevent slopes from reaching the highest stable angles predicted by experiments conducted in ideal laboratory conditions.

Angle of repose is also a function of a material's roughness, cohesivity, grain size, and angularity (Sullivan et al., 2011). The regolith simulant used in these experiments is a natural analog that is a good compositional match for Martian regolith, but it may not perfectly emulate all properties of Martian regolith that affect angle of repose. Thermal inertia measurements of RSL-bearing slopes are consistent with sand-to-gravel-sized grains (Tebolt et al., 2020). The grain size of the regolith used in these experiments was < 500 microns (i.e., medium sand and finer), which could also explain the higher measured angles of repose (i.e., because finer grained materials have a higher angle of repose). Finally, the tumbling of sediments in the acrylic chamber likely resulted in triboelectric charging, which may have introduced electrostatic cohesion that artificially increased the angles measured in the experiment.

While experimental limitations led to laboratory slope angles that were systematically higher than values measured on Mars, the finding of a *relative* change in angle of repose as a function of RH, which supports the desorption model for RSL, would remain valid even at lower, Mars-like slope angles.

3.4.3 Significance for Astrobiology and Planetary Protection

Understanding the quantity and role (if any) of water in RSL is critically important to astrobiology and planetary protection measures. If RSL are caused by flowing or seeping water (freshwater or brines), they may constitute habitable environments in which to search for life. However, if RSL are purely dry flows, they may not be an interesting astrobiological target, and may not merit protected status.

The evidence presented here supports a semi-dry model, where RSL may contain up to several weight percent of water in the form of thin, adsorbed films. The adsorbed water involved is ephemeral—forming and persisting through high-RH seasons, then seasonally drying out when RH is low. Adsorbed water is distinct from liquid water, though it hypothetically could be habitable (Möhlmann, 2005). Seasonal dry periods would pose an additional barrier to any organisms, particularly during periods when water activity drops below the known lower limit for cell division (a_w = 0.585; Stevenson et al., 2017). Nonetheless, terrestrial organisms are known to survive seasonal wet-dry cycles, and in fact desiccating conditions may even preserve organisms (Hallsworth, 2021).

Because of their putative connection to water, RSL are assigned a protected status such that any spacecraft seeking to encounter them would have to meet strict sterilization requirements (Rummel et al., 2014). However, if RSL do not contain sufficient liquid water to support life, this classification may need to be reconsidered. Further studies will be needed to investigate the habitability of transient, seasonal thin films of adsorbed water to assess whether RSL in the desorption model are likely to be habitable.

3.5 Conclusion

We tested a semi-dry, desorption-triggered mechanism for RSL formation through laboratory analog experiments measuring slope stability of Martian regolith simulant. We demonstrated that slope hydration and angle of repose are linked to RH, which indicates that annual RH cycles could seasonally stabilize/destabilize Martian slopes. During periods of low RH, dehydrating slopes could destabilize, leading to grain flows with morphology and seasonality matching those of RSL. As average RH conditions increase, slopes rehydrate and become more cohesive, retaining windblown sediments and/or dust, which resupplies material to cause RSL to recur year-after-year.

Despite initial excitement over their connection to liquid water, a growing body of evidence suggests RSL are more appropriately described as granular flows. The likely limited role of water in RSL formation further constrains their potential habitability and informs planetary protection protocols. While the amount of water involved in the desorption model is less favorable to life compared to wetter models (i.e., brine flows), the desorption model does not preclude habitability. However, neither would RSL merit additional protected status, since regolith hydration through adsorption occurs across Mars.

4. Mineralogically Diverse and Salt-rich Regolith in Jezero Crater Characterized using X-ray Spectroscopy

At the time of writing, this chapter is under review for publication:

Shumway, A. O., Kizovski, T. V., Catling, D. C., VanBommel, S. J., Jones, M. W. M., Orenstein, B. J., Schmidt, M. E., Tice, M. M., Hurowitz, J. A., Knight, A. L., Clark, B. C., Wade, L., Cardarelli, E. L., Li, A. Y., Zawaski, M. J., Klevang, D. A., Elam, W. T., Hausrath, E. M., Treiman, A. H., Henneke, J., Tosca, N. J., Liu, Y., Cable, M. L., Allwood, A. C., & the PIXL team (*in review*). Mineralogically Diverse and Salt-rich Regolith in Jezero Crater Characterized using X-ray Spectroscopy. *Journal for Geophysical Review: Planets*

Abstract

The Planetary Instrument for X-ray Lithochemistry (PIXL) onboard the Perseverance rover has characterized the composition of Martian regolith at a scale of hundreds of microns using micro-focus X-ray fluorescence spectroscopy. PIXL data reveal a diverse population of regolith grains with distinct spectral, chemical, and crystallographic properties, through which we identified the mineralogy of individual regolith components. Olivine, phyllosilicate, carbonate-bearing phases, Cr-Ti-spinel, plagioclase, and Fe-sulfate are all inferred from the data, and potential local and regional bedrock sources are proposed for each. PIXL also inspected dust and soil components, which are found to be geochemically similar to analogous components characterized elsewhere by preceding missions. Unlike other sites, regolith on the western fan front of Jezero crater contains fewer sulfates, but is highly enriched in Cl (up to 2.0 ± 0.5 wt. %), which likely includes chlorides, chlorates, and/or perchlorates. PIXL also finds evidence of hydration in the regolith, potentially carried by salts, as interstitial water, and/or in adsorbed phases. PIXL's observations of diverse amorphous and crystalline components, multiple styles of aqueous alteration, and

enrichments of brine-forming salts provide exciting new justification for the return of a Martian regolith sample to Earth for further study.

Plain Language Summary

We investigated Martian regolith (i.e., soil) in Jezero crater using the Planetary Instrument for X-ray Lithochemistry (PIXL) on NASA's *Perseverance* rover. PIXL provides an unprecedented level of detail about the chemical make-up of soils, which we used to identify minerals at the scale of individual grains. By comparing PIXL's results to other measurements throughout Jezero crater and across Mars, we infer the likely origins for various components, which tells us about past environments over a wide geographic area. The coarser grains appear to originate from nearby sources, while the finer grained material closely resembles soils at other sites and is likely global in its origin. Jezero soils are saltier (enriched in chlorine) compared to previous sites, which may be the result of previous, wet environments. Presently, chlorine salts (such as perchlorates) strongly interact with water, and likely play a major role in moving water between the atmosphere and the surface. Our analyses provide crucial chemical and geologic context for two regolith samples cached by *Perseverance*, one of which may be returned to Earth for future analysis using techniques that are not available on Mars.

4.1 Introduction

Much of Mars' surface is blanketed with regolith—loose, unconsolidated rocky material that is also frequently called soil in the literature. Regolith likely formed from primary basaltic materials that were subsequently mechanically and chemically altered, but the precise formation and alteration mechanisms remain unclear (e.g., Clark et al., 1982; Taylor & McLennan, 2009). Regolith mineralogy can record episodes of aqueous alteration; for example, the discovery of hematite spherules (i.e., "blueberries") in regolith and bedrock in Meridiani Planum revealed that acidic groundwater once flowed in the region (Squyres et al., 2006). Across Mars, regolith is rich in salts like sulfates and perchlorates, which also hold clues about past environmental conditions (e.g., Cull et al., 2010; Yen et al., 2005). Some of these salts can deliquesce into liquid brine under modern Martian conditions, which presents a form of (highly saline) liquid water that might exist on the surface today (Gough et al., 2011; Nuding et al., 2014; Rivera-Valentín et al., 2020). Continued study of regolith composition and mineralogy at new locations using novel techniques improves our understanding of Mars' geologic history and climates through the present. Future human exploration also benefits from a thorough characterization of potential resources or hazards contained within Martian regolith (Beaty et al., 2019).

4.1.1 Previous Analyses of Martian Regolith

The Viking Landers conducted the first X-ray fluorescence (XRF) measurements of Martian regolith and found it to be composed of basaltic fines, dust, salts, and lithic fragments (Clark et al., 1982). The compositional similarities between regolith at the two distant Viking landing sites first suggested a global, geochemically uniform soil unit—a hypothesis that was subsequently confirmed by later missions (e.g., Bell III et al., 2000; O'Connell-Cooper et al., 2017; Taylor & McLennan, 2009; Yen et al., 2005). The geochemical similarity of regolith across Mars suggests either a uniform basaltic source, or global mixing to homogeneity at the resolution of current instruments (e.g., Blake et al., 2013; Hausrath et al., 2025)

Deviations from the global soil composition can be introduced by components originating from local sources (e.g., Bell III et al., 2000; Squyres et al., 2006; Yen et al., 2005). For example, the Alpha Particle X-ray Spectrometers (APXS) onboard the Mars Exploration Rovers (MER) measured soils that were chemically similar to each other and to previously measured soils, but also contained locally derived components: basalt enrichments in Gusev and hematite in Meridiani Planum (Yen et al., 2005). APXS is also carried by the Mars Science Laboratory (MSL) *Curiosity* rover, where it has been used to characterize soils and sands in Gale crater (O'Connell-Cooper et al., 2017, 2018). In this work, we distinguish between regolith (i.e., soil) and aeolian sediments (i.e., sand), the latter which is sorted via transport, resulting in physical and chemical differences (following the convention used in, e.g., Berger et al., 2020; O'Connell-Cooper et al., 2017, 2018).

4.1.1.1 Dust in Regolith

The finest-grain component of regolith is airfall dust. Because of its size (~100 nm to ~10 μm diameter), dust can be lifted and suspended in the atmosphere (Knight et al., 2024; Schmidt et al., 2018). As such, dust plays a major role in weather patterns locally (e.g., dust devils and dust lifting events) and globally (e.g., seasonal global dust storms; e.g., Newman et al., 2002). Dust also affects spectroscopic measurements where it coats samples (Henneke et al., 2022; Rice et al., 2023) and can degrade the effectiveness of spacecraft hardware (e.g., by covering solar panels). Characterization of the physical properties and chemistry of dust is a high priority for preparing for future exploration, since dust poses a potential biohazard to humans (Beaty et al., 2019).

The origin of Martian dust is an open question. Dust has an apparently uniform composition that is similar to that of soils, which suggests planet-scale mixing (Berger et al., 2016; Knight et al., 2024; McSween & Keil, 2000). One hypothesis is that dust represents an average crustal composition, dominated by basalts and evaporitic salts (Berger et al., 2024; McSween & Keil, 2000). Another hypothesis is that dust is largely sourced from a specific region on Mars, such as the Medusae Fossae Formation (Ojha et al., 2018). Geochemical investigations of dust at sites across Mars can help further constrain its origin(s).

4.1.1.2 Salts in Regolith

In every location where Martian regolith has been studied, sulfur and chlorine have been present (Bell III et al., 2000; Clark et al., 1982; Hausrath et al., 2025; Hecht et al., 2009; O'Connell-Cooper et al., 2017; Yen et al., 2005). While the abundances of S and Cl in regolith vary between sites, APXS investigations on three rovers (MER-A, MER-B, and MSL) have observed a consistent molar trend of S / Cl = 3.7 +/- 0.7 (Berger et al., 2016). In regolith, S and Cl frequently exist as sulfate and oxychlorine species, respectively (Archer et al., 2014; Blake et al., 2013; Hecht et al., 2009; Kounaves et al., 2010; Sutter et al., 2017), which are strongly linked to past aqueous episodes (e.g., Benison et al., 2024; Scheller et al., 2022; Siljeström et al., 2024; Tice et al., 2022). Presently, such salts may also play a role in carrying soil hydration (David et al., 2022), exchanging water between the surface and atmosphere (Jakosky et al., 1997), forming soil crusts (Hausrath et al., 2023).

Perchlorate (ClO_4) salts are particularly interesting because of their presumed ubiquity in Martian regolith (Clark & Kounaves, 2016) and their ability to absorb water vapor and dissolve into brine (i.e., deliquesce) at Mars-relevant conditions (e.g., Gough et al., 2011; Nuding et al., 2014; Rivera-Valentín et al., 2020). Once formed, perchlorate brines can remain liquid at extremely low temperatures because of their depressed freezing points and low eutectic temperatures (e.g., -74.6°C in the case of Ca-perchlorate; Pestova et al., 2005). Additionally, perchlorates are prone to supercooling, a metastable liquid state that can persist at temperatures well below the equilibrium freezing point (Toner et al., 2014b). Regolith further stabilizes perchlorate brines against freezing and salt precipitation, allowing them to persist at colder and drier conditions (Shumway et al., 2023b). Understanding perchlorate-rich regolith is critical because it presents a plausible pathway for quasi-liquid water to exist on modern Mars—water which could enable geochemical reactions, increase soil cohesion, mobilize soluble species, and potentially create habitable environments.

4.1.2 Mars 2020 Mission

The *Perseverance* rover is investigating the geologic history of Mars, searching for signs of life, and collecting a variety of unique samples to eventually be returned to Earth for further study (Farley et al., 2020). To achieve these goals, *Perseverance* utilizes a diverse suite of instruments. The Mars Environmental Dynamics Analyzer (MEDA) collects meteorological data including temperature, pressure, and relative humidity (Rodriguez-Manfredi et al., 2021). Mast Camera Zoom (Mastcam-Z) is a stereoscopic, multispectral imager (Bell et al., 2021). The SuperCam instrument suite includes a remote micro imager (RMI), laser induced breakdown spectroscopy (LIBS), and visible and infrared (VISIR) spectroscopy (Maurice et al., 2021; Wiens et al., 2020). *Perseverance* also has a suite of engineering cameras, including the Hazard Avoidance Cameras (Hazcams), which provide context images for operations and analysis (Maki et al., 2020). Mounted on the robotic arm, proximity science instrument SHERLOC (Scanning Habitable Environments with Raman and Luminescence for Organics and Chemicals) uses Raman spectroscopy and fluorescence to characterize mineralogy and detect organics, while its WATSON (Wide Angle Topographic Sensor for Operations and eNgineering) subsystem provides high-resolution stereo color images (~13 μm/pixel; Bhartia et al., 2021). The Planetary Instrument for X-ray Lithochemistry (PIXL) is a micro-scale X-ray spectrometer described in detail in section 2.1 (Allwood et al., 2020).

In February 2021, *Perseverance* landed in Jezero crater (Fig. 4-1), a ~45 km, 3.82 - 3.96 billion year old impact crater that once contained a lake, located on the western rim of the Isidis impact basin (Farley et al., 2020; Mangold et al., 2020; Werner, 2008). Jezero was selected as the landing site for *Perseverance* in part due to its large, well-preserved, clay and carbonate-bearing sedimentary fan deposit located on the western edge of the crater (Bosak et al., 2024; Ehlmann, Mustard, Fassett, et al., 2008; Fassett & Head III, 2005; Goudge et al., 2015; Mangold et al., 2020; Stack et al., 2024). This fan is estimated to have formed approximately 3.2-3.8 billion years ago (Ga) when ancient streams flowed into the Jezero crater lake, depositing sediments into the fan complex over time (Fassett & Head, 2008; Mangold et al., 2020). Thus, the fan may preserve clues about ancient aqueous environments and the astrobiological potential of the crater through time (Farley et al., 2020).

Mineralogical studies of Jezero crater with the Compact Reconnaissance Imaging Spectrometer for Mars (CRISM) instrument have revealed spectral signatures of olivine, phyllosilicate (smectite), pyroxene, and carbonate (Ehlmann et al., 2008a, 2008b; Horgan et al., 2020). CRISM data also show a spatial correlation between olivine and carbonate in the region around Jezero, interpreted as a regional olivine-carbonate lithology (Brown et al., 2020). These orbital spectroscopy measurements are influenced by regolith mineralogy on the surface, so *in situ* measurements of regolith at a submillimeter scale can provide crucial ground truthing for orbital data.

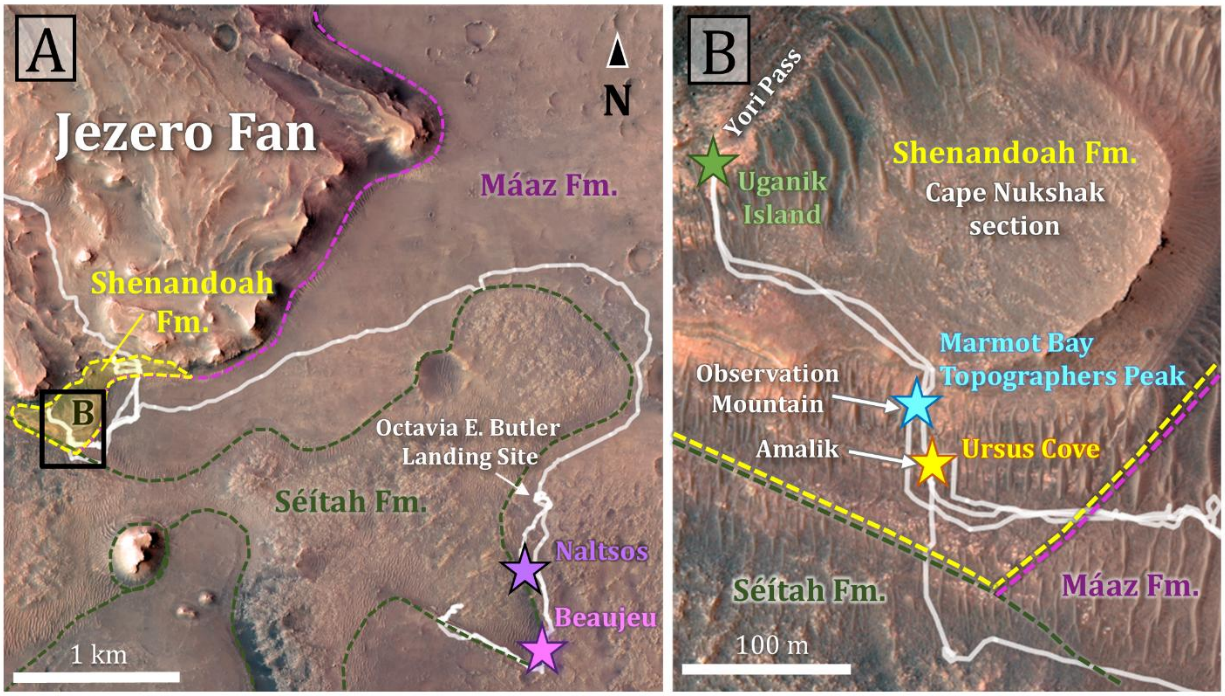

Figure 4-1. Orbital context images of Jezero crater taken by the High Resolution Imaging Science Experiment (HiRISE; McEwen et al., 2007). The white line represents the path travelled by the *Perseverance* rover. Approximate boundaries for the Séítah (green), Máaz (purple), and Shenandoah (yellow) formations are shown, adapted from Royer et al. (2025) and Stack et al. (2024). Informal names for features and outcrops are also shown in white text. Stars and corresponding labels indicate PIXL scans that are relevant to this work: unabraded rock targets *Naltsos* and *Beaujeu*, abraded bedrock *Uganik Island*; and regolith targets *Ursus Cove*, *Topographers Peak*, and *Marmot Bay*. (B) shows a zoomed-in view of the Cape Nukshak section of the Shenandoah formation on the fan front, where PIXL's regolith scans took place. Image credits: NASA/JPL/University of Arizona.

4.2 Methods

4.2.1 Overview of PIXL

PIXL is a micro-scale XRF spectrometer mounted on the arm of the *Perseverance* rover that produces high-spatial-resolution, quantitative elemental maps by scanning targets with its narrow X-ray beam (Allwood et al., 2020). PIXL's Rh-anode X-ray tube produces characteristic Rh fluorescence peaks and a bremsstrahlung radiation continuum that are focused onto the sample surface using polycapillary optics (Allwood et al., 2020). The X-ray beam size varies with energy, and is modeled to range from 173 μm full width at half maximum (FWHM) at 3.5 keV to 45 μm FWHM at 20 keV (Das et al., 2025). The number and pattern of XRF measurement spots in a single scan are chosen to balance science objectives with operational constraints (e.g., power and duration). Line and map scans interrogate a target with a high density of closely spaced measurements, which provides contiguous information on texture and chemistry in one or two dimensions, respectively. In contrast, grid scans typically sample a larger area, but with sparse, non-contiguous measurements. During each scan, the PIXL flight software uses the Optical Fiduciary System (OFS) to track relief and maintain focus of the X-ray beam (Allwood et al., 2020; Klevang et al., 2024). It also measures and can compensate for positional drift of the instrument induced by thermal expansion and contraction of rover body and arm, rover slippage, and settling into the Martian surface. PIXL also provides context images for each target using its micro context camera (MCC), which illuminates the target with light emitting diodes (LEDs) in each of four wavelengths: ultraviolet (UV, 385 nm), blue (B, 450 nm), green (G, 530 nm) and near-infrared (NIR, 735 nm; Allwood et al., 2020). MCC data are used to create false-color and color-ratio images of the target, and typically image a wider area around the footprint of the XRF scan (Henneke et al., 2023). Complete specifications and pre-flight calibration for PIXL are provided by Allwood et al. (2020) and Klevang et al. (2023).

During XRF mapping, the X-ray beam remains at any given point for 10 seconds, acquiring an energy-dispersive X-ray spectrum in each of PIXL's two detectors (Allwood et al., 2020). PIXL is sensitive to elements with atomic number (Z) between 10 and 40 (i.e., Na to Zr), which are quantified as oxides. Oxide abundances are determined via a spectral model—derived from first principles—implemented through the PIQUANT software (Barber & Davidoff, 2022; Heirwegh et al., 2022). PIQUANT assumes the target material is homogeneous within the X-ray-energy-dependent sample volume (e.g., Das et al., 2025; VanBommel, 2024; VanBommel et al., 2024) and addresses matrix effects including depth effects such as self-absorption, pile-up and escape peaks, and spectral overlap (e.g., Cr K_β at 5.95 keV and Mn K_α at 5.90 keV) during analyses of acquired spectra (e.g., Heirwegh et al., 2022; VanBommel et al., 2025). The spectral and compositional data can then be analyzed via the PIXLISE software, which provides analytical tools that allow rapid interpretation of data, including spatial variations, as each beam is precisely localized on several context images (Allwood et al., 2020; Nemere et al., 2024).

While PIXL is primarily an XRF instrument, it also detects diffracted X-rays, which can reveal information about a target's crystallinity—or lack thereof (Jones et al., 2025; Liu et al., 2022; Orenstein et al., 2024; Schmidt et al., 2025; Tice et al., 2022). Monocrystalline regions diffract X-rays anisotropically, so diffraction can be identified by comparing X-ray counts as a function of energy between PIXL's two detectors (Wright et al., 2023). PIXL detects diffraction peaks from monocrystalline domains with a spatial extent larger than ~ 30 - 50 μm, with the absence of diffraction peaks suggesting either a finely crystalline (< ~ 30 - 50 μm) or amorphous material (Tice et al., 2022). Multiple adjacent PIXL beam locations with diffraction peaks at the same energies indicates the presence of a monomineralic crystalline domain larger than PIXL's beam width (Liu et al., 2022; Orenstein et al., 2024; Tice et al., 2022). Diffracted X-rays can also interfere with the quantification of elemental abundance when they overlap spectrally with fluorescence peaks. PIQUANT does not account for diffraction peaks when quantifying elements, so instead all elemental and oxide abundances reported here have been corrected for effects caused by diffraction, as well as topographic slope and surface roughness, following the methods described in Schmidt et al. (2025) and Tice et al. (2023).

4.2.2 Geologic Context

Perseverance began its surface mission at the Octavia E. Butler landing site (Fig. 4-1A), then explored two aqueously altered igneous units that make up the crater floor: the Séítah and Máaz formations. Séítah is an olivine-cumulate with secondary carbonate (Beyssac et al., 2023; Liu et al., 2022; Tice et al., 2022), while Máaz consists of Fe-rich serpentinized basaltic to trachyandesitic lavas rich in pyroxene and feldspar (Schmidt et al., 2025; Tosca et al., in review; Udry et al., 2023). Next, the rover traversed to the fan front region to investigate the contact between Jezero's Western fan and the crater floor (Fig. 4-1B). At the fan front, the rover encountered its first sedimentary rocks at a stratigraphic sequence informally named the Shenandoah formation (Stack et al., 2024). PIXL conducted its regolith investigations in the Cape Nukshak region of the Shenandoah formation (Fig. 4-1B). Within Cape Nukshak, PIXL also probed abraded bedrock in the Amalik (target *Novarupta*) and Yori Pass members (target *Uganik Island;* Fig. 4-1; Hurowitz et al., 2023).

Amalik and Yori Pass consist of laminated sandstones and mudstones (Fig. 4-1B; Stack et al., 2024). Geochemically, Amalik is rich in olivine and silicate alteration products, as well as carbonates (possibly a ferrodolomite cement), and includes planar lags of heavy minerals including Cr-spinels, zircon or baddeleyite, and Ca-phosphates (Hurowitz et al., 2023; Kizovski et al., 2023). At *Uganik Island* (Yori Pass), PIXL found evidence of phyllosilicates and Fe, Mg-sulfates cut with veins and vugs of anhydrite (Hurowitz et al., 2023; Jones et al., 2025). Observations of diagenetic sulfate features and concretions suggest that saline groundwater once flowed in this region, which is astrobiologically interesting because of the presence of liquid water and the high biosignature preservation potential of sulfates, phyllosilicates, and concretions (Benison et al., 2024; Kalucha et al., 2024).

The regolith of Jezero crater has been investigated by other instruments onboard *Perseverance*. Mastcam-Z observed that soils have been spectrally consistent across the rover's traverse, with signs of olivine among the coarser grains and pyroxene among the finer grains (Bell et al., 2022; Rice et al., 2023). A multi-instrument investigation of regolith across the crater floor found fines consistent with pyroxene and a ferric-oxide phase, while coarser grains (~1-2 mm) showed signatures of olivine (Vaughan et al., 2023). Among the fines of the crater floor and fan front, SuperCam observed H_2O absorption features indicative of hydration (Cousin et al., 2025; Hausrath et al., 2023). SHERLOC measurements of regolith resulted in Raman spectra consistent with olivine, plagioclase, carbonate, and sulfate (Cardarelli et al., 2023). Across the crater, PIXL and Mastcam-Z have observed a widespread type of coating that is spectrally and chemically similar to dust and fine-grained regolith, though interpretations vary as to the origin of these coatings (Garczynski et al., 2022; Schmidt et al., 2024).

PIXL has also previously measured regolith on two occasions where grains overlaid uncleared, unabraded bedrock (Fig. 4-1A, purple and pink stars). The *Naltsos* target (sol 125) was partially covered with dust and regolith, and PIXL's single-line scan passed over a ~1-2 mm particle of Fe, Mg silicate, interpreted as an olivine sand grain (Fig. 5 in Hausrath et al., 2023). Similarly, at the dust- and regolith-covered target *Beaujeu*, PIXL again observed a ~1 mm diameter olivine sand grain inside of a pit on the rock surface (Schmidt et al., 2025).

4.2.3 PIXL Regolith Scans

Between sols 577 and 601, PIXL conducted five scans on regolith targets, summarized in Table 4-1. Each scan occurred in the Cape Nukshak region of the Shenandoah formation on the fan front of the western Jezero fan (Fig. 4-1B). PIXL's first regolith target was *Ursus Cove*, an armored megaripple adjacent to the *Amalik* outcrop (type locality of the Amalik member; Figs. 4-1B and 4-2). PIXL next scanned regolith at *Observation Mountain,* a larger armored megaripple approximately 40 m NNE of *Ursus Cove* (Figs. 4-1B and 4-3). Two samples of regolith were also collected from *Observation Mountain* (samples *Atmo Mountain* and *Crosswind Lake*), which are cached and could eventually be returned to Earth by a future mission (Hausrath et al., 2025). *Observation Mountain* was selected for study and sampling due to the variety of grains present, and for its presumed inactivity, which is suggested by its morphology and the presence of soil crusts (Hausrath et al., 2025).

Location	Target	Target type	Sol	Scan Type	Scan Size (mm)	Step Size (mm)	No. of Points
Amalik	*Ursus Cove*	Undisturbed surface regolith	577	3-Line	15 x 2	0.125	363
			589	Grid	14 x 14	1	225
Observation Mountain (regolith sampling site)	*Topographers Peak*	Subsurface regolith (excavated by wheel scuff)	598	Map	5 x 5	0.125	1681
	Marmot Bay	Undisturbed surface regolith	600	Grid	21 x 21	1.5	225
			601	Map	3.5 x 7	0.125	1653

Table 4-1. Details of PIXL's regolith scans on the fan front. "Sol" refers to a Martian solar day, with sol 1 indicating the start of the landed mission. Scan size describes the approximate footprint of the XRF map. Step size refers to the average distance between consecutive measurements in a scan. Duplicate regolith samples were collected from Observation Mountain and cached for potential return by a future mission.

PIXL probed both undisturbed surface regolith (*Ursus Cove* and *Marmot Bay*) and subsurface regolith excavated via a wheel scuff (*Topographers Peak*). The surfaces of the armored bedforms consisted of both coarse (> 1 mm) and fine (< 0.5 mm) grains (Figs. 4-2 and 4-3). The subsurface regolith was primarily composed of finer-grained regolith, with a mean grain size of ~ 125 μm (Hausrath et al., 2025), though some coarse grains and clumps can be seen outside of the PIXL scan area (Fig. 4-3D).

Typically, PIXL targets are cleared of dust using the Gas Dust Removal Tool (gDRT); however, the gDRT was not used on any regolith target because it presumably would have displaced coarser grains as well, preventing study of undisturbed surface regolith. As a result, PIXL's elemental and oxide abundances likely reflect compositional mixing with dust.

The relatively high topographic variability of the regolith targets (Fig. A-1) posed a challenge to interpreting the data because PIXL's analytical routine assumes a fixed standoff distance, so derived oxide quantifications are sensitive to the distance between the target and the instrument. PIXL periodically checks its location relative to the target and adjusts its position to maintain a constant standoff distance (Allwood et al., 2020). However, a sudden change in vertical relief over a short lateral distance (e.g., a coarse grain rising above the background topography) can result in PIQUANT miscalculating the composition, leading to, for example, artificially high or low total element abundances (Tice et al., 2022). The impact of topography is mitigated in the data analyzed and presented herein (i.e., Table A-1) using the methods described in Schmidt et al. (2025) and Tice et al. (2023).

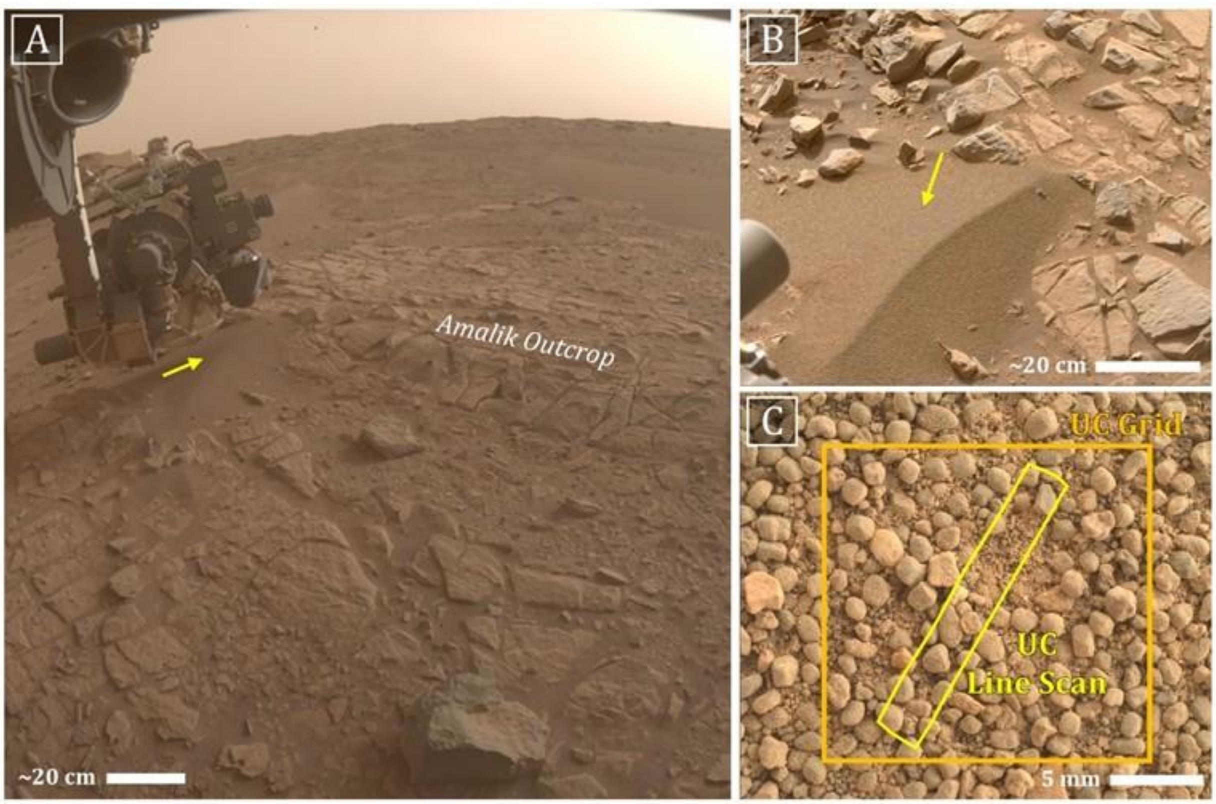

Figure 4-2: Context images for the PIXL scans at the *Amalik* workspace. Yellow arrows point to the approximate locations of the *Ursus* Cove PIXL target on the bedform. A) Front Hazcam image showing PIXL deployed over the *Ursus Cove* target. B) MastCam-Z Left image of the

Ursus Cove target. C) Close-up WATSON image of *Ursus Cove*, with approximate footprints of the two PIXL scans. All image files are listed in Table A-2.

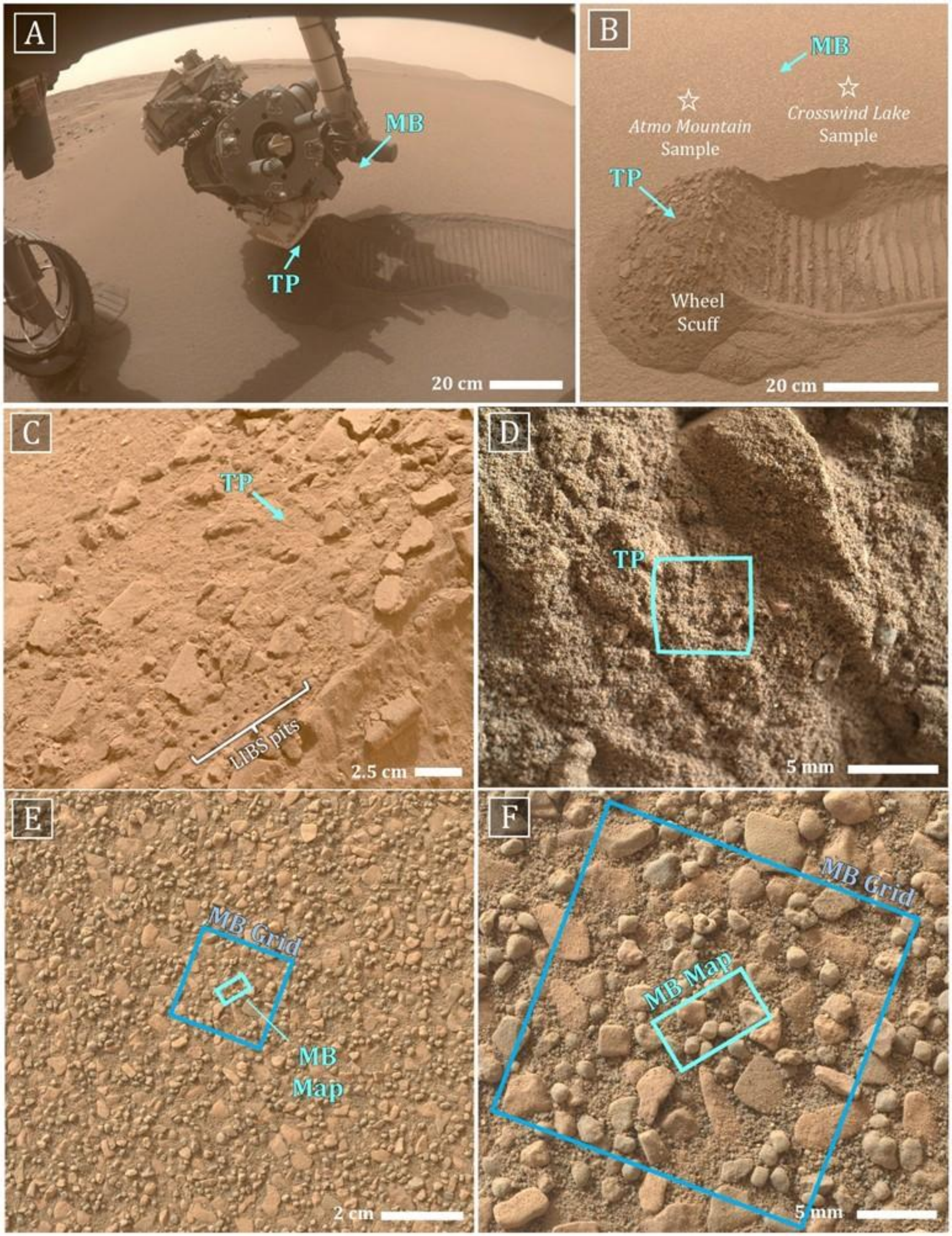
A
MB
TP
20 cm
B
MB
Atmo Mountain
Sample
Crosswind Lake
Sample
TP
Wheel
Scuff
20 cm
C
TP
LIBS pits
2.5 cm
D
TP
5 mm
E
MB Grid
MB
Map
2 cm
F
MB Grid
MB Map
5 mm

Figure 4-3: Context images for the PIXL targets at *Observation Mountain*. Blue arrows point to the approximate locations of the PIXL scans. *Topographers Peak* (TP) is comprised of regolith that was excavated by a wheel scuff maneuver, while *Marmot Bay* (MB) is undisturbed surface regolith. A) Front Hazcam image of PIXL deployed over *Topographers Peak*. B) Front Hazcam image of the scuff. The locations from which the two regolith samples were later collected are indicated with stars. C) Mastcam-Z Right image of the *Topographers Peak* target. The line of small depressions near the bottom of this image are LIBS pits created by SuperCam analyses of this target (see Cousin et al., 2025). D) WATSON image of *Topographers Peak,* with the approximate footprint of the PIXL scan shown as a blue box. E) WATSON image of *Marmot Bay* with the approximate footprints of the PIXL grid (large square) and map (rectangle) scan footprints. F) Close-up WATSON image of *Marmot Bay*, with the approximate footprints of the PIXL scans. All image files are listed in Table A-2.

4.3 Results

4.3.1 Micro Context Image (MCC) Images

Across the three regolith targets, PIXL observed a heterogenous mixture of regolith with considerable variety in size, angularity, color, chemistry, and diffraction properties (Figs. 4-4 and 4-5). Among the coarser grains, there are three distinct categories of grains with similar spectral reflectance values: dark-toned grains, light-toned grains, and intermediate-toned grains (indicated by the black, white, and orange arrows in Fig. 4-4, respectively). Meanwhile, the fines are a mixture of many spectrally heterogeneous grains with a mean grain size of ~125 μm (Hausrath et al., 2025). Each target is covered with dust, which strongly reflects in the NIR channel (Henneke et al., 2022), and therefore precludes mineral identification via multispectral analysis. Still, the MCC data provide valuable evidence to support mineral identifications made via analysis of elemental composition and diffraction results.

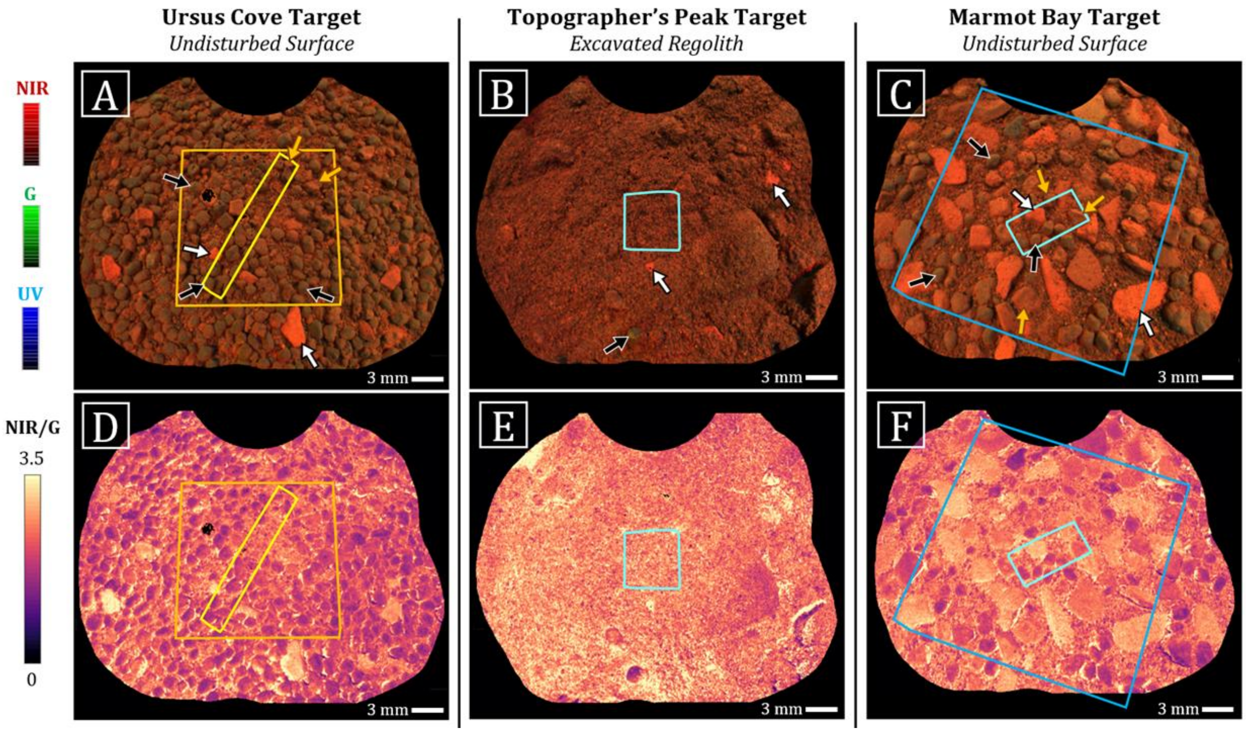

Figure 4-4. PIXL Micro Context Camera (MCC) images of the three regolith targets. (A-C) False color images of each target in the near-infrared (NIR; 735 nm), green (G; 530 nm), and blue (B; 450 nm) channels, flat-fielded and enhanced. (D-E) MCC ratio image of NIR/G reflectance values. Note that distinct populations of grains with similar spectral signatures are distinguishable within and between scans. The black, white, and orange arrows point to examples of the dark-, light-, and intermediate-toned grains, respectively. Rectangles show the extents of PIXL's XRF measurements.

4.3.2 Elemental and Diffraction Results

Regolith composition at each site was predominantly mafic, with some feldspathic and non-silicate components. Major oxide abundances for each regolith component are reported in Table 4-2, with additional XRF results in Table A-3. Each of the spectrally distinct grain types observed in MCC images also had specific corresponding chemical composition and diffraction properties (cf. Figs. 4-4 and 4-5). Below, we analyze the reflectance, fluorescence, and diffraction results to infer mineralogy for several regolith components. Other PIXL studies have sometimes identified minerals using the Mineral Identification by

SToichiometry (MIST) algorithm (Moreland et al., submitted; Siebach et al., submitted); however, MIST was not used here because the targets are covered with dust, which causes the measured stoichiometry to deviate from any pure mineral endmember. Instead, we infer mineralogy by analyzing mixing trends between dust and plausible mineral endmembers on ternary diagrams and by using the dust layer model described in section B1.

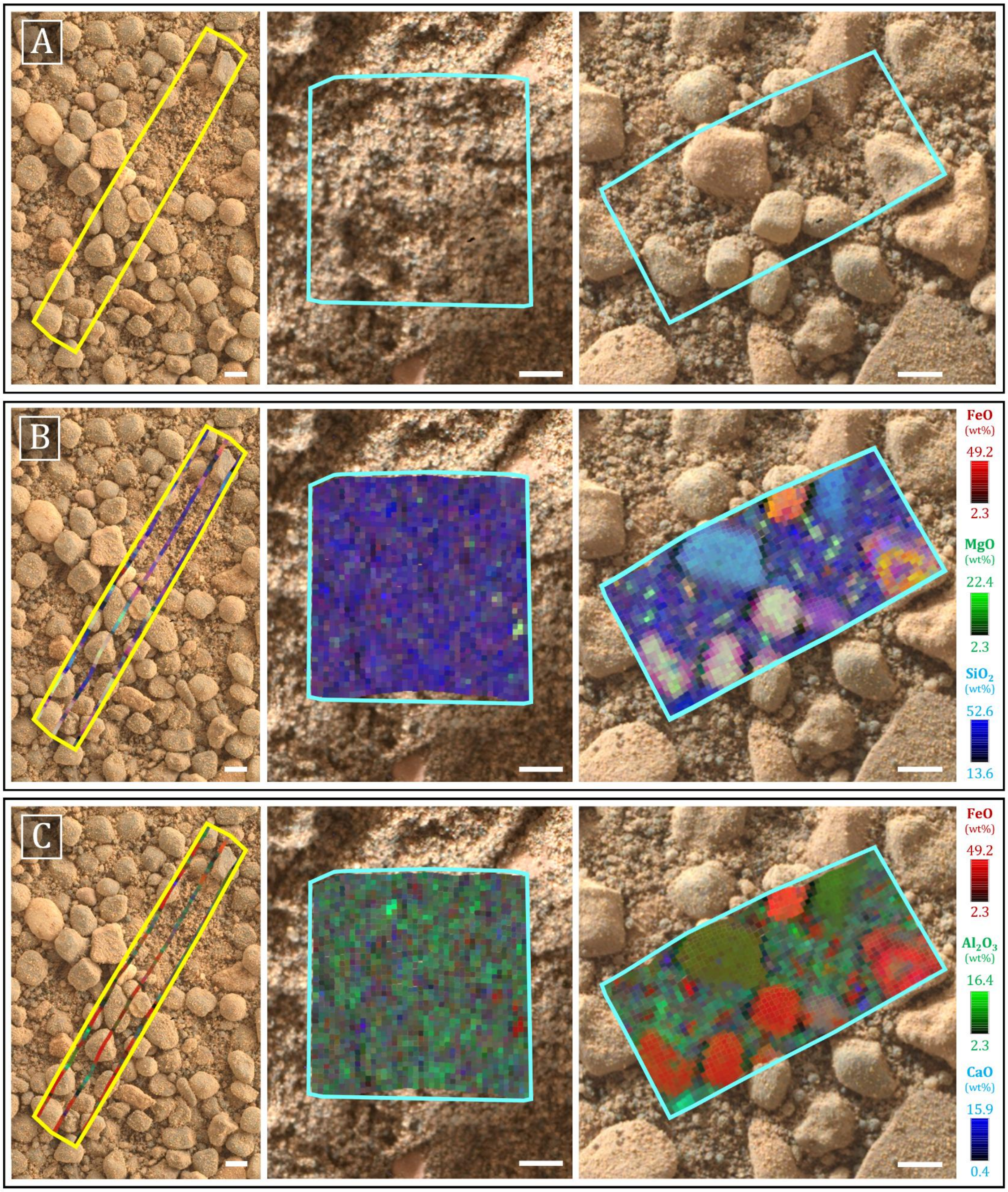
A
B
FeO
(wt%)
49.2
2.3
MgO
(wt%)
22.4
2.3
SiO2
(wt%)
52.6
13.6
C
FeO
(wt%)
49.2
2.3
Al2O3
(wt%)
16.4
2.3
CaO
(wt%)
15.9
0.4

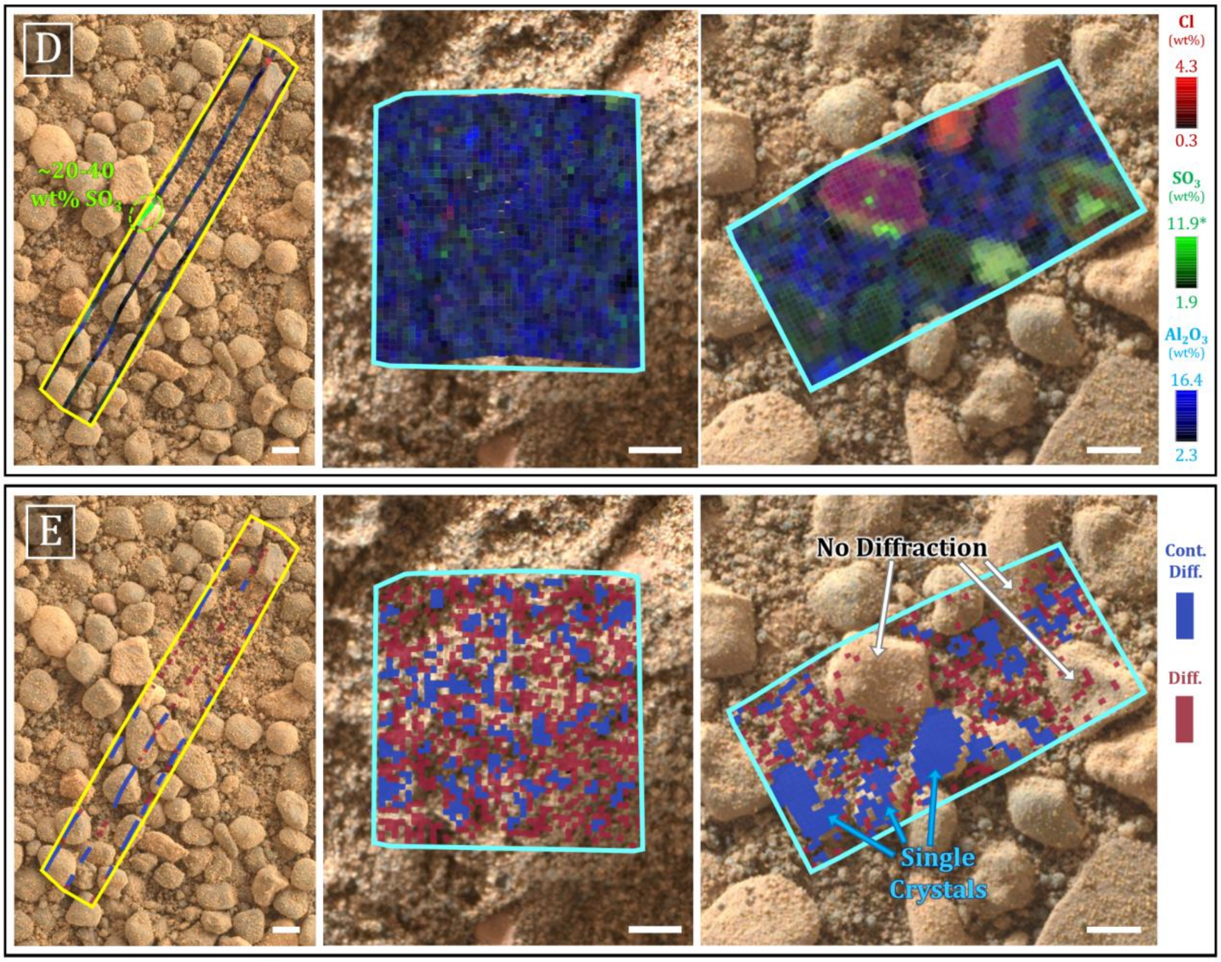

Figure 4-5. Visualizations of abundances of key oxides, as well as diffraction results, for *Ursus Cove* (left), *Topographers Peak* (center), and *Marmot Bay* (right). A) WATSON images with the approximate PIXL footprints (aligned manually). B) Red, green, blue (RGB) map illustrating abundances of FeO_T, MgO, and SiO_2, respectively. C) RGB map showing FeO_T, Al_2O_3, and CaO abundances, D) RGB map showing Cl, SO_3, and Al_2O_3 abundances. SO_3 (green) is scaled to the maximum value from *Marmot Bay* (11.9 wt. %) for visual clarity, but note several points in *Ursus Cove* contain up to ~40 wt.% SO_3 (see section 4.3.2.5). E) Map showing diffraction results. Blue illustrates regions where multiple contiguous points exhibit identical diffraction peaks (i.e., larger monocrystalline domains), while red indicates points that diffract, but are not related to a larger crystal. Transparent regions exhibited no detectable diffraction peaks (white arrows indicate examples of non-diffracting grains). 1 mm white scale bars are shown throughout.

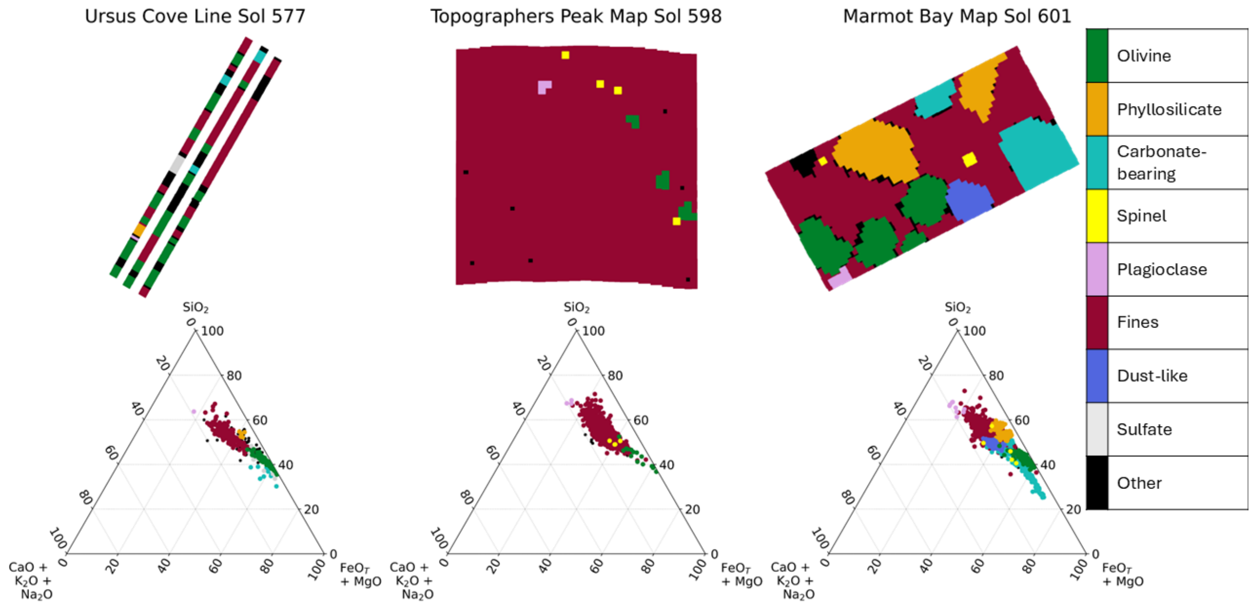

Figure 4-6: (Top row) Maps illustrating locations of identified components within three PIXL scans. (Bottom row) SiO_2 vs. FeO_T + MgO vs. CaO + K_2O + Na_2O ternary diagrams visualizing the compositions of the corresponding regolith components displayed above.

4.3.2.1 Olivine

Surface targets *Ursus Cove* and *Marmot Bay* contained a class of grains that were ~ 1 - 2 mm in size, rounder, and darker-toned, which stood out for their low NIR/G reflectance ratio (i.e., they are greener than their surroundings; Fig. 4-4 D & F). This grain type accounts for ~29 % of the XRF measurements in the *Ursus Cove* line scan on sol 577, and ~ 13 % of the *Marmot Bay* map scan on sol 601 (Table A-1). XRF results revealed these grains were primarily composed of FeO_T (35.9 ± 1.8 wt. %), MgO (15.3 ± 0.8 wt. %), and SiO_2 (37.5 ± 1.9 wt. %), with lower levels of Na_2O (not detected), K_2O (0.1 ± 0.1 wt. %), CaO (1.9 ± 0.5 wt. %), Cl (1.0 ± 0.3 wt. %), and SO_3 (4.5 ± 0.4 wt. %), compared to the bulk regolith composition (Fig. 4-5 and Table 4-2). Across each of these grains, spectra measured from adjacent points exhibited identical diffraction peaks, which indicates each grain is a single crystal with a dominant orientation (Fig. 4-5E; Orenstein et al., 2024). These reflectance, stoichiometric, and diffraction properties are consistent with dust-covered olivine.

This interpretation agrees with Mastcam-Z and SuperCam observations, which have previously reported olivine grains of similar size, color, and roundness throughout the regolith on the crater floor and fan front (Cousin et al., 2025; Rice et al., 2023; Vaughan et al., 2023). PIXL has also previously encountered similar olivine sand, albeit inadvertently, on the *Naltsos* and *Beaujeu* natural surface (i.e., unabraded and uncleared) rock targets in the Máaz unit on the crater floor (Hausrath et al., 2023; Schmidt et al., 2025). At the *Observation Mountain* megaripple, SuperCam and SHERLOC both also observed olivine on the undisturbed surface targets (Cardarelli et al., 2023; Cousin et al., 2025; Hausrath et al., 2025).

4.3.2.2 Phyllosilicate

Another class of coarse surface regolith consisted of larger (~2 - 4 mm), more-angular, lighter-toned grains, which were spectrally distinct due to their bright NIR reflectance (Fig. 4-4). These grains accounted for ~ 13% of the XRF measurements *Marmot Bay* map scan (sol 601), but were less prevalent at *Ursus Cove* (~1% of the measurements in the sol 577 line scan; Table A-1). Compositionally, the most abundant elements were FeO_T (17.1 ± 0.9 wt. %), MgO (12.2 ± 0.6 wt. %), and SiO_2 (41.9 ± 2.1 wt. %), with SiO_2 enriched and FeO_T depleted relative to the olivine component (Fig. 4-5; Table 4-2). They are also highly enriched in Cl (2.0 ± 0.5 wt. %) and Br (1606 ± 642 ppm) relative to the average value for each scan (Fig. 4-5D; Table 4-2). Very few diffraction peaks were observed from these grains (only 6 % of points), suggesting they are either finely crystalline (i.e., < ~ 30 - 50 μm) or X-ray amorphous (Fig. 4-5E). The bright NIR reflectance, composition, and lack of diffraction peaks are all consistent with phyllosilicates (discussed further in section 4.1.2). Phyllosilicates were also identified at this site by SuperCam (Cousin et al., 2025).

4.3.2.3 Carbonate-bearing

At both surface targets, a third class of coarse grain was intermediate between the olivine and phyllosilicate components in terms of spectral reflectance, size, angularity, and degree of rounding (Fig. 4-4). Their composition was rich in FeO_T (36.1 ± 1.8 wt. %) and poor in SiO_2 (32.8 ± 1.6 wt. %), with high Cl abundance (1.8 ± 0.5 wt. %), relative to the average composition (Fig. 4-5). Diffraction peaks were not observed in 91% of points on these grains (Fig. 4-5E). We interpret this non-diffracting component that trends towards a zero-SiO_2 composition as a carbonate-bearing phase. This interpretation is consistent with SuperCam and SHERLOC's detections of Fe, Mg-carbonate in the regolith at *Observation Mountain* (Cardarelli et al., 2023; Cousin et al., 2025; Hausrath et al., 2025).

Although PIXL cannot directly measure CO_3 (C and O are below PIXL's detection limit of $Z \geq 11$), the presence of carbonates can be inferred based on compositional mixing trends, X-ray backscattering, and light element abundance. First, these grains spanned a compositional mixing trend between dust and a zero-silicate endmember (Fig. 4-6), which is consistent with the compositions of Fe, Mg-carbonates observed previously on the crater floor (Tice et al., 2022). The spectra for these grains also exhibited high X-ray backscattering, which has been shown to correlate with light element abundance in previous analyses (Tice et al., 2023). The abundance of light elements can also be inferred by summing all quantified elements and oxides (i.e., the analytical totals, Table 4-2), then inferring that any shortfall below 100% is likely caused by undetectable low-Z elements. This method has been used previously to identify carbonates on the Jezero crater floor (Tice et al., 2022) and is possible due to PIXL's fixed geometry (i.e., consistent and known position relative to the sample surface). If present, oxalates (Applin et al., 2015) or carboxylic acids (Benner et al., 2000) would also contribute to low totals in a minor or trace way, but presently there is no evidence for such compounds from any instrument on *Perseverance*. In these regolith scans, the feasibility of this approach was limited due to complications introduced by compositional mixing and topographic effects. The carbonate-bearing regolith grains had analytical totals of ~100%, which could result from carbonate (low totals) mixing with a high-total endmember (e.g., olivine). Additionally, the topography of the scans (Fig. A-1) may have artificially inflated the totals for these grains, as targets that rise above the mean topography of the scan result in increased X-ray counts due to the reduced sample to detector distance, which can lead to inflated elemental abundances and totals. Matrix effects could also skew totals here, particularly given the presence of multiple endmembers of distinct composition within the analytical footprint (e.g., Sherman, 1955).

4.3.2.4 Cr-, Ti- Spinel

Several points across the three regolith targets were highly enriched in Cr_2O_3 and/or TiO_2 (>5 wt. %), which were correlated with FeO_T (22.2 ± 1.1 wt. %) and anticorrelated with SiO_2 (31.0 ± 1.6 wt. %; Fig. A-2). We interpret these grains as Fe-Ti-Cr spinel. Compositional analysis was limited by small sample size (12 points across five scans), as well as a grain size smaller than PIXL's beam width, which resulted in compositional mixing with surrounding material. Still, we can infer the composition of these spinels by projecting a mixing trend to zero SiO_2 (Fig. A-2). Most Cr-rich points fall along a mixing trend between silicate minerals and chromite. At *Topographers Peak*, one point is highly enriched in TiO_2 (8.9 ± 0.3 wt. %) with no Cr_2O_3 detected, but we were not able to conclusively determine the mineralogy from a single measurement. Only one point with Cr_2O_3 > 5 wt. % was observed at *Ursus Cove* (in the sol 589 grid scan; Fig. A-2), but more grains may have been present outside of the XRF scan areas, which were more limited than the maps at *Topographers Peak* and *Marmot* Bay (i.e., 588 points versus 1681 and 1878 points, respectively).

4.3.2.5 Fe-Sulfate

One coarser grain at *Ursus Cove* contained ~ 20 - 40 wt. % SO_3, correlated with FeO_T (27.0 ± 1.4 wt. %; Fig. 4-5D). The grain is overexposed in MCC images (Fig. 4-4F), which precludes multispectral analysis. The dust coverage and few measurements on this grain (N=8) complicate attempts to determine its specific mineralogy, but it appears to follow a mixing trend between dust and Fe-sulfate. No diffraction peaks were detected from this grain, which is consistent with an amorphous phase (Fig. 4-5E). Note that Fe-sulfate was only detected at *Ursus Cove* and not at the *Observation Mountain* regolith sampling site.

4.3.2.6 Plagioclase

PIXL observed at least one grain at *Marmot Bay* that was enriched in Na_2O (3.4 ± 0.6 wt. %), Al_2O_3 (13.5 ± 0.7 wt. %), SiO_2 (39.3 ± 2.0 wt. %), and CaO (8.0 ± 0.4 wt. %), and depleted in MgO (4.6 ± 0.4 wt. %) and FeO_T (4.1 ± 0.5 wt. %) compared with the surrounding regolith (cf. Fig. 4-5C, pink region in Fig. 4-6). The grain was ~0.5 mm in diameter, but PIXL's footprint only partially covered the grain, resulting in few measurements (N = 9). Other grains with similar feldspathic compositions were detected in the sparser grid scan on *Marmot Bay* (sol 600), and in the fine-grained subsurface regolith at *Topographers Peak* (Fig. 4-6).

Based on analysis of mixing trends using ternary diagrams, we interpret this feldspathic grain as plagioclase partially covered by fines and dust (Fig. 4-6). This interpretation is consistent with measurements by other instruments on *Perseverance*, as SHERLOC detected Raman peaks indicative of weathered plagioclase at this location (Cardarelli et al., 2023) and some SuperCam LIBS spots measured compositions that trended towards plagioclase (Cousin et al., 2025).

		Olivine	Phyllosilicate	Carbonate-bearing	Cr, Ti Spinel	Fe-Sulfate	Plagioclase	Fines	Dust-like
	Total	**103.5**	**93.5**	**100.4**	**91.7**	**96.8**	**79.9**	**81.2**	**104.9**
Na_2O	**wt. %**	0	2.4	0	2.6	4.2	3.42	2.78	3.66
	1σ	0	0.55	0	0.65	0.57	0.59	0.57	0.54
MgO	**wt. %**	15.25	12.22	11.36	6.77	5.96	4.58	6.76	7.5
	1σ	0.77	0.62	0.57	0.36	0.32	0.37	0.34	0.38
Al_2O_3	**wt. %**	5.41	8.18	6.31	8.06	5.46	13.45	7.94	8.31
	1σ	0.27	0.41	0.32	0.41	0.28	0.68	0.4	0.42
SiO_2	**wt. %**	37.52	41.92	32.77	31.02	22.75	39.26	35.01	39.04
	1σ	1.88	2.1	1.64	1.56	1.14	1.97	1.75	1.96
P_2O_5	**wt. %**	0.79	1.14	0.95	0.67	0.63	0.7	0.9	1.4
	1σ	0.27	0.36	0.31	0.24	0.22	0.24	0.3	0.42
SO_3	**wt. %**	4.35	4.47	5.65	3.73	26.7	4.18	3.8	8.71
	1σ	0.42	0.39	0.3	0.52	1.42	0.45	0.51	0.46
Cl	**wt. %**	0.98	1.99	1.8	0.82	0.86	0.79	0.89	2.22
	1σ	0.32	0.51	0.49	0.28	0.29	0.27	0.3	0.54
K_2O	**wt. %**	0.13	0.26	0.18	0.17	0.24	0.36	0.39	0.5
	1σ	0.14	0.22	0.18	0.17	0.21	0.23	0.23	0.18
CaO	**wt. %**	1.9	2.29	3.99	4.3	1.89	7.97	5.36	6.32
	1σ	0.5	0.54	0.48	0.42	0.5	0.4	0.27	0.32
TiO_2	**wt. %**	0.19	0.7	0.29	2.02	0.25	0.65	0.87	0.85
	1σ	0.18	0.24	0.23	0.52	0.21	0.23	0.29	0.28
Cr_2O_3	**wt. %**	0.14	0.3	0.08	8.87	0.12	0.16	0.29	0.17
	1σ	0.15	0.23	0.09	0.44	0.13	0.16	0.23	0.17
MnO	**wt. %**	0.7	0.17	0.78	0.33	0.56	0.05	0.35	0.47
	1σ	0.24	0.18	0.27	0.23	0.2	0.06	0.23	0.2
FeO_T	**wt. %**	35.87	17.16	36.05	22.15	26.95	4.14	15.72	25.55
	1σ	1.79	0.86	1.8	1.11	1.35	0.45	0.79	1.28
Ni	**ppm**	257	348	188	147	270	111	218	351
	1σ	333	244	328	297	327	250	338	238
Zn	**ppm**	251	245	562	447	231	132	212	521
	1σ	345	346	235	190	348	283	344	218
Br	**ppm**	659	1606	245	20	249	184	91	120
	1σ	269	642	421	90	425	375	229	284

Table 4-2. Abundances of major oxides measured in each regolith component. 1σ uncertainties are derived from PIQUANT (Heirwegh et al., 2022). Additional trace element abundances are reported in Table A-3.

4.3.3 Fines and Dust

The finer-grained fraction of regolith at each target was geochemically uniform (Fig. A-3), which suggests mixing between the sites (within ~40 m of each other; see Fig. 4-1B) as well as between the surface and subsurface (i.e., *Marmot Bay* vs. *Topographers Peak*). Relative to the coarser grains, the finer-grained regolith component (mean grain size 125 μm; Hausrath et al., 2025) was enriched in Na_2O (2.8 ± 0.6 wt. %), K_2O (0.4 ± 0.2 wt. %), and CaO (5.4 ± 0.3 wt. %), and had a higher abundance of SiO_2 (35.0 ± 1.8 wt. %) than MgO (6.8 ± 0.3 wt. %) and FeO_T (15.7 ± 0.8 wt. %). Diffraction peaks were observed in 50% of the measurements on fines, which suggests a mix of crystalline and amorphous components (Fig. 4-5E). For comparison, the X-ray amorphous component of Gale crater regolith of comparable size (sieved to < 150 μm) was 35 – 40 wt. % (±15 wt. %, 1σ uncertainty) (Achilles et al., 2017; Rampe et al., 2018, 2020).

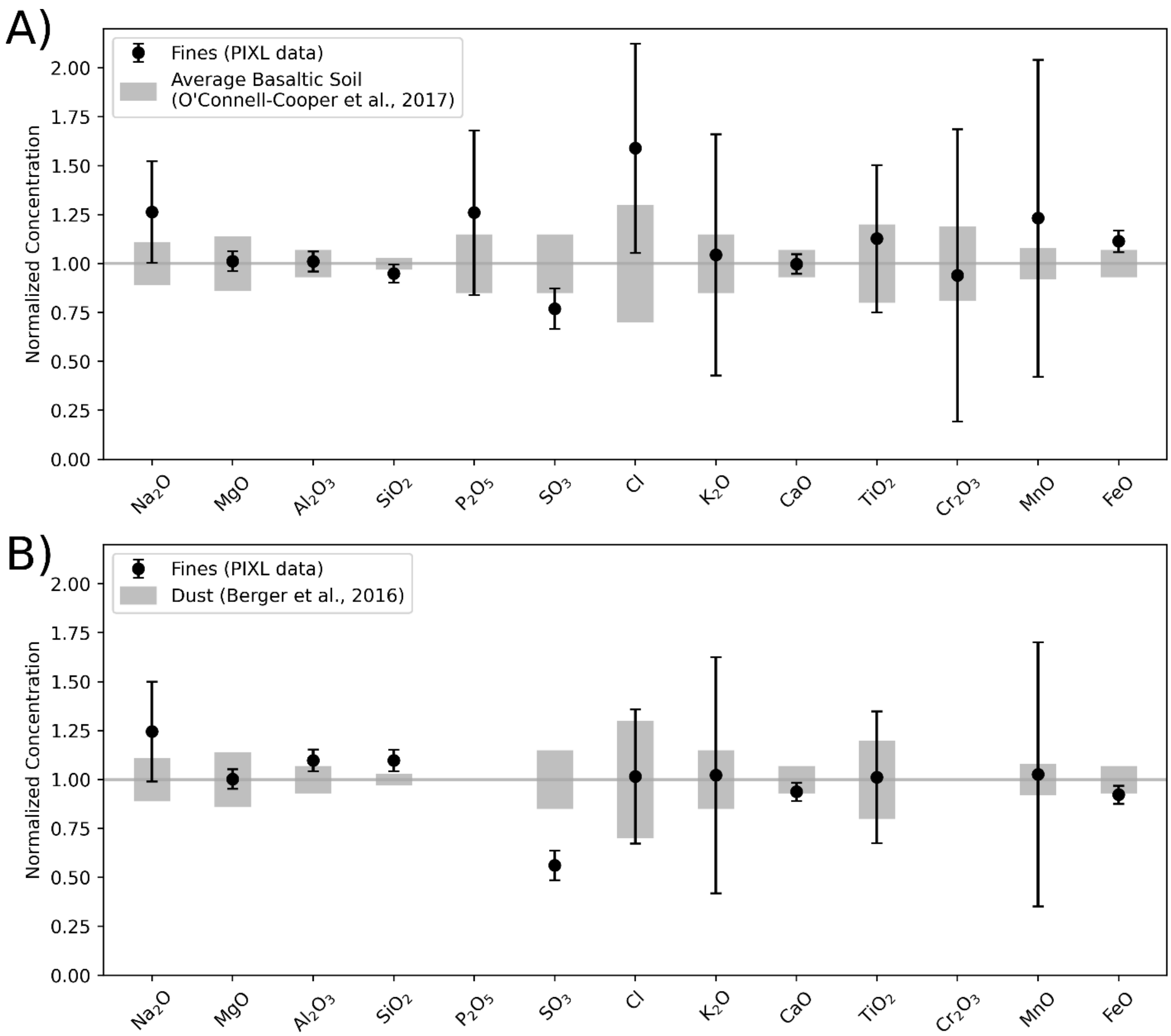

Figure 4-7. A) Composition of finer-grained regolith measured by PIXL (black) normalized to Average Basaltic Soil (gray; O'Connell-Cooper et al., 2017). B) PIXL fines (black) normalized to Martian dust (gray; Berger et al., 2016). P_2O_5 and Cr_2O_3 not shown in B) because they were not detected and not reported by APXS, respectively (Berger et al., 2016). 1σ uncertainties are shown for PIXL data (Heirwegh et al., 2022; Schmidt et al., 2025); accuracy errors are shown for APXS data (Gellert et al., 2015).

4.3.3.1 Global Soils

The finer-grained fraction of regolith at each PIXL target ("Fines" in Fig. 4-6 and Table 4-2) was a close geochemical match for the global soil component that has been identified at sites across Mars (Bell III et al., 2000; Clark et al., 1982; O'Connell-Cooper et al., 2017; Yen et al., 2005). Fig. 4-7 compares the bulk composition of the fines across the three PIXL targets to the chemistry of global soils and dust. For a global soil standard we use "Average Basaltic Soil" (ABS), which is derived from APXS soil measurements across three sites (O'Connell-Cooper et al., 2017). For dust, we use APXS observation tray measurements reported by Berger et al. (2016). To enable comparisons between PIXL (which reports oxides in absolute abundances) and APXS (which reports relative abundances), PIXL results were first normalized to 100 wt. %, then plotted as a ratio of the APXS-measured values. For each oxide, the PIXL fines match ABS, within error. Variable mixing with dust between sites may explain why PIXL's results are enriched in FeO and depleted in SiO_2 relative to ABS (Fig. 4-7).

Assessing the precise mineralogy of the fines was more difficult because each measurement had multiple fine grains within the beam area, so the results reflect a mix of several different compositions (e.g., VanBommel et al., 2023). However, compositional mixing trends can give hints to plausible mineral endmembers. The fines contained mixing trends towards a mafic endmember (potentially, a finer-grained counterpart to the coarse olivine grains), as well as towards feldspathic and pyroxene endmembers (Fig. 4-6). These findings agree with conclusions drawn from SuperCam data that fines are likely a mix of olivine, feldspar, and pyroxene (Cousin et al., 2025).

4.3.3.2 Dust

Strong NIR reflectance in the MCC images suggests that dust is prevalent in each regolith target (Fig. 4-4; Henneke et al., 2022). Dust is also visible across the regolith targets in the high resolution WASTON images (Fig. 4-5A). The signs of ubiquitous dust in the regolith supports the hypothesis that soils are a mix of basaltic sands and dust (e.g., Berger et al., 2024).

One coarse grain at *Marmot Bay* appeared visually identical to the darker-toned, rounded olivine grains, but its composition was more like that of airfall dust ("Dust-like" region in Fig. 4-6; Berger et al., 2016). A few spots on the grain instead followed a mixing trend between dust and a composition resembling that of the neighboring olivine grains. The dust-like grain did not exhibit any diffraction peaks, except in spots with an olivine-like composition, where there were multiple contiguous points with diffraction peaks at the same energy (Fig. 4-5E). One interpretation of these results is that this was an olivine grain with a thicker dust cover than its neighboring olivine grains.

A second interpretation is that this grain could have been related to a common type of coating observed throughout the crater, which is spectrally and chemically similar to dust (Garczynski et al., 2022; Schmidt et al., 2024). PIXL detected these coatings in the nearby Amalik outcrop at the *Novarupta* and *Chiniak Offset* targets (Schmidt et al., 2024), and this regolith grain might have been a weathered fragment from one of these coated rocks. Despite being a close compositional match for the coatings, the dust-like regolith grain lacks the coatings' characteristic purple- or maroon-ish color. The coatings are hypothesized to be either indurated dust (Garczynski et al., 2022), or vapor deposits from a volcanic plume (Schmidt et al., 2024).

4.3.4 Chlorine and Sulfur

Across all targets, PIXL detected higher levels of Cl and lower levels of SO_3 compared to previous APXS measurements of Martian soils (Fig. 4-7). Within the fines, PIXL measured 0.89 ± 0.30 wt. % Cl, with the highest Cl abundances observed in the coarser dust-like (2.22 ± 0.54 wt. %), phyllosilicate (1.99 ± 0.51 wt. %), and carbonate-bearing (1.80 ± 0.49 wt. %) grains (Fig. 4-5D, Table 4-2). The SO_3 concentration in the fines was 3.81 ± 0.51 wt. %, while SO_3 was most abundant in the Fe-sulfate grain (26.70 ± 1.42 wt.%) and the dust-like grain (8.71 ± 0.46 wt. %). Ca and K are plausible cations associated with Cl; while Ca, Mg, and K are correlated with SO_3 (Fig. A-4). Note that while PIQUANT reports sulfur as SO_3, reduced forms of sulfur are also possible.

Prior APXS measurements of soils and dust have observed that S and Cl follow a molar trend of S/Cl = 3.7 ± 0.7 (Berger et al., 2016; O'Connell-Cooper et al., 2017). We fit an orthogonal distance regression (which considers error in both variables) to PIXL's measurements of fines and found a slope of S/Cl = 2.43 ± 0.06 (Fig. 4-8). Recent modeling suggests that matrix corrections can lead to a misestimation of sulfur abundance in the case of sulfate on a basaltic matrix (e.g., dust on regolith), which may contribute to differences between PIXL and APXS measurements of SO_3 (figure 3 in VanBommel, 2024). PIXL's findings are consistent with SuperCam observations of higher Cl and fewer sulfates compared to analogous measurements of Gale crater regolith (Cousin et al., 2025).

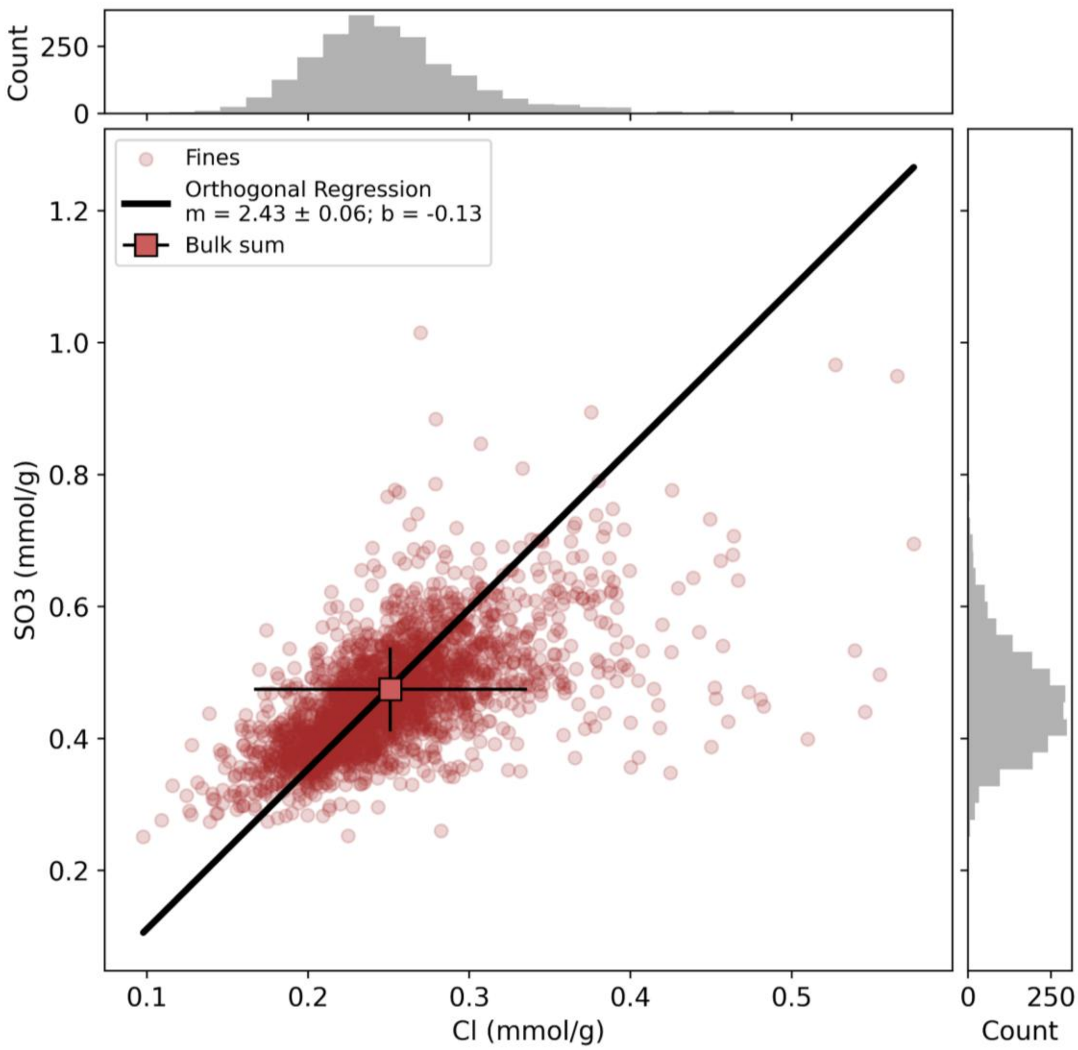

Figure 4-8. Cl vs. SO_3 (molar) for fine-grained regolith across three targets (*Marmot Bay*, *Topographers Peak*, and *Ursus Cove*). Individual measurements (circles) and the bulk sum value (square) are shown. Gray histogram plots on either axis show the distribution of the overlapping PIXL measurements. An orthogonal regression (black line) fit through the data has a slope of S/Cl = 2.43 ± 0.06 and an intercept of -0.13.

4.4 Discussion:

4.4.1 Potential source regions of regolith components

PIXL results reveal several mineralogically distinct regolith components (Fig. 4-6) that are likely derived from many distinct sources, and which record multiple styles of alteration. Detailed chemical and mineralogical analyses can provide insights into the lithological diversity and past environmental conditions within Jezero and beyond. The finer-grained components (i.e., dust and fines) could have been transported over longer distances because dust can be suspended (McSween & Keil, 2000) and fines are prone to saltation (e.g., Hausrath et al., 2025; Preston et al., 2024). The geochemical similarity of these components to analogous material at other sites further supports the hypothesis of a globally uniform dust and soil component. Conversely, the coarser-grained material (e.g., olivine, phyllosilicate, carbonate-bearing, sulfate) apparently originated from more proximate regional or local sources.

4.4.1.1 Olivine

To constrain potential source(s) for the olivine grains, we compared their chemistry to olivine-bearing outcrops PIXL has encountered elsewhere up to sol 1100 by calculating the forsterite number (Fo#; Fig. 4-9). Forsterite is the pure-Mg endmember of olivine, and Fo# is the molar ratio of Mg to Fe, i.e, Fo# = Mg / (Mg + Fe) * 100. PIXL has observed olivine in bedrock targets throughout Jezero crater, including the Máaz and Séítah formations, the fan top region (Tenby, Otis Peak), and the Margin unit (Fig. 4-9; Hernández-Montenegro et al., 2025; Liu et al., 2022; Moreland et al., submitted; Orenstein et al., 2024; Schmidt et al., 2025; Tice et al., 2022). However, we note that different criteria for classifying olivine applied across different investigations may result in differing values and ranges for Fo#s.

Olivine grains at *Ursus Cove* and *Marmot Bay* have average Fo# = 40.74 ± 4.34 (Fig. 4-9). This composition is similar to the olivine sand grains previously encountered as loose grains on bedrock at the *Naltsos* ($Fo_{33.5 \pm 2.0}$; Hausrath et al., 2023) and *Beaujeu* ($Fo_{40.5 \pm 3.2}$; Schmidt et al., 2025) targets. Similar Fo#s suggest a common source for this geographically widespread grain type, or preferential loss of a more Fe-rich olivine component by chemical weathering. These calculations are also likely influenced by compositional mixing with dust, which has an Mg:Fe molar ratio of ~0.41 (Berger et al., 2016). To account for the effects of dust, we modelled dust layers on olivine substrates from Fo_0 to Fo_{100} in increments of 10 and found that Fo_{40} was the best match for the observed spectra (section S1).

The closest compositional match to a bedrock source is the *Quartier* target in the Séítah formation ($Fo_{46 \pm 1}$; Hernández-Montenegro et al., 2025). We conclude that these grains are likely sourced from a Séítah-like unit (i.e., an olivine cumulate), or the Séítah unit itself. This conclusion agrees with independent findings from Mastcam-Z, which observed that olivine regolith grains were similar in size and spectral properties to olivine in the Séítah formation bedrock, interpreted as the likely source (Vaughan et al., 2023). Similarly, SuperCam measured the chemistry of this class of olivine sand via LIBS and calculated $Fo_{52\text{-}69}$ (Cousin et al., 2025), which is consistent with LIBS analyses of olivine in Séítah bedrock ($Fo_{54\text{-}73}$; Beyssac et al., 2023). Despite the different values derived from the different techniques, PIXL and SuperCam results both point to Séítah-like olivine-rich bedrock as a probable source for the olivine sand grains.

An alternative hypothesis is that these olivine grains could be sourced from the olivine-carbonate lithologies in the Nili Planum region surrounding Jezero crater. CRISM estimates the composition of olivine in this region at $Fo_{40\text{–}66}$ (Brown et al., 2020), which is consistent with the PIXL-derived chemistry of the olivine sand ($Fo_{40.7 \pm 4.3}$; Fig. 4-9). This hypothesis could be directly tested with future PIXL scans on outcrops of the regional olivine-carbonate unit as *Perseverance* continues to explore the region beyond Jezero crater. These probable sources indicate that the olivine grains likely represent either a local or regional contribution to the regolith in Jezero crater.

4.4.1.2 Phyllosilicates

Phyllosilicate-group minerals are present throughout Jezero crater, and have been identified by PIXL on the crater floor, the fan front, the upper fan, and the margin unit (Moreland et al., submitted). In the Shenandoah formation (where PIXL's regolith scans occurred), phyllosilicates were observed in the laminated mudstones of the Yori Pass member (Bosak et al., 2024; Hurowitz et al., 2023). We compared the composition of the phyllosilicate regolith component with several previous PIXL measurements of phyllosilicate-bearing bedrock, and found a close geochemical match to the *Uganik Island* abrasion patch in the Yori Pass member. At *Uganik Island,* PIXL observed a phyllosilicate- and sulfate-rich matrix cut with veins of anhydrite (Hurowitz et al., 2023; Jones et al., 2025). Stoichiometric analysis identified the phyllosilicate component of *Uganik Island* as sepiolite (Moreland et al., submitted).The composition of the phyllosilicate regolith grains is consistent with *Uganik Island* bulk rock (i.e., excluding the $CaSO_4$ veins) mixed with dust, which suggests they are lithic fragments of the Yori Pass member partially covered by dust. The absence of diffraction peaks is also consistent with a Yori Pass source, since PIXL similarly did not observe diffraction in the phyllosilicate matrix at *Uganik Island* (Jones et al., 2025). The proximity to the likely source (~180 m between *Uganik Island* and *Observation Mountain*, Fig. 4-1B) suggests that these grains are a local contribution to the regolith, which is also consistent with their grain size and angularity.

However, one notable compositional difference is that the regolith phyllosilicate grains contained much less SO_3 than the *Uganik* Island bulk rock (4.5 wt. % vs. ~17 wt. %, respectively). One explanation for this depletion in SO_3 is that soluble sulfates could have been dissolved and mobilized by past aqueous episodes, or by more recent thin brine films, similar to the mobilization of ClO_4 by brine films at the *Phoenix* landing site (Cull et al., 2010). A high abundance of Cl (1.99 ± 0.51 wt. %)in these grains supports the hypothesis of thin brine films, which is discussed further in section 4.3 (Fig. 4-5D; Table 4-2).

The presence of phyllosilicates in Jezero regolith is interesting because phyllosilicates were not detected in the Gale crater Rocknest samples by the CheMin instrument (Blake et al., 2013; Morris et al., 2015). A local origin for this grain type (supported by their size, angularity, and chemical similarity to nearby outcrop) would account for the difference between sites. Another possible explanation for the difference is that these grains may belong to the amorphous fraction of regolith, since PIXL did not detect diffracted X-rays.

4.4.1.3 Carbonate-bearing

There are several local or regional carbonate-rich lithologies which could be plausible sources for the carbonate-bearing regolith component. PIXL previously observed carbonates associated with olivine in the Séítah formation on the crater floor (Liu et al., 2022; Tice et al., 2022), and carbonates were also present in the fan top region and the margin unit (Horgan et al., 2020, 2024; Wiens et al., 2024). However, the carbonate-bearing regolith component is compositionally distinct from other carbonates PIXL has investigated in bedrock, possibly due to compositional mixing with dust and another phase (potentially olivine). Alternatively, these grains may originate from a bedrock source not yet inspected with PIXL, for example the regional olivine-carbonate unit beyond Jezero crater (Brown et al., 2020). Future PIXL measurements on Nili Planum olivine-carbonate outcrops could test this hypothesis. A final hypothesis is that these grains could have formed from the direct aqueous alteration of precursor regolith. While the provenance of the carbonate-bearing grains remains unconstrained, all of these plausible sources indicate that this component is a local or regional contribution to the regolith, which is consistent with the observed grain size.

4.4.1.4 Cr-, Ti- Spinel

Mixing with surrounding material and few measurements (N=12) limited our ability to identify a likely source for the spinel grains. However, we infer that the spinels are a local contribution to the regolith, and could originate from lithologies where PIXL has previously identified Cr- and Ti-rich spinels. Chromite was present in various igneous units on the crater floor (Liu et al., 2022; Schmidt et al., 2025), and Cr-spinels were also seen in planar lags in the Amalik member (Hurowitz et al., 2023), which was geographically closest to the regolith study sites (Fig. 4-1B). Alternatively, such spinels may be a global contribution to regolith, as Cr- and Ti-enriched phases were also observed in the basaltic sands of the Bagnold Dunes in Gale crater (O'Connell-Cooper et al., 2018).

4.4.1.5 Fe-Sulfate

Sulfates have been observed throughout the bedrock of the fan front region, though mostly as $CaSO_4$ (e.g., Benison et al., 2024; Jones et al., 2025; Phua et al., 2024). Ferric sulfate was present as a clast in the *Uganik Island* PIXL target in Yori Pass (Hurowitz et al., 2023), and its composition was a close match for the Fe-sulfate regolith grain. Therefore, we infer that this grain was likely a local contribution to the regolith from Yori Pass-style bedrock. However, one compositional difference was that the *Uganik Island* ferric sulfate follows a mixing trend towards an endmember with equal molar abundances of Fe and Mg, while the regolith grain trends towards a pure Fe-sulfate endmember. Lower MgO abundances in the regolith grain could be a result of preferential weathering or alteration.

4.4.1.6 Plagioclase

The plagioclase grain does not have a clear compositional match with any previous PIXL measurement on bedrock. PIXL observed plagioclase in outcrops throughout the Máaz formation on the crater floor (Schmidt et al., 2025). The Máaz formation is a plausible candidate for the origin of these grains, or the source could be a lithology not yet encountered by PIXL as of sol 1100. However, with few measurements (N = 9), possible alteration, and compositional mixing with dust and fine-grained regolith, we cannot conclusively link the plagioclase regolith component to a particular source lithology.

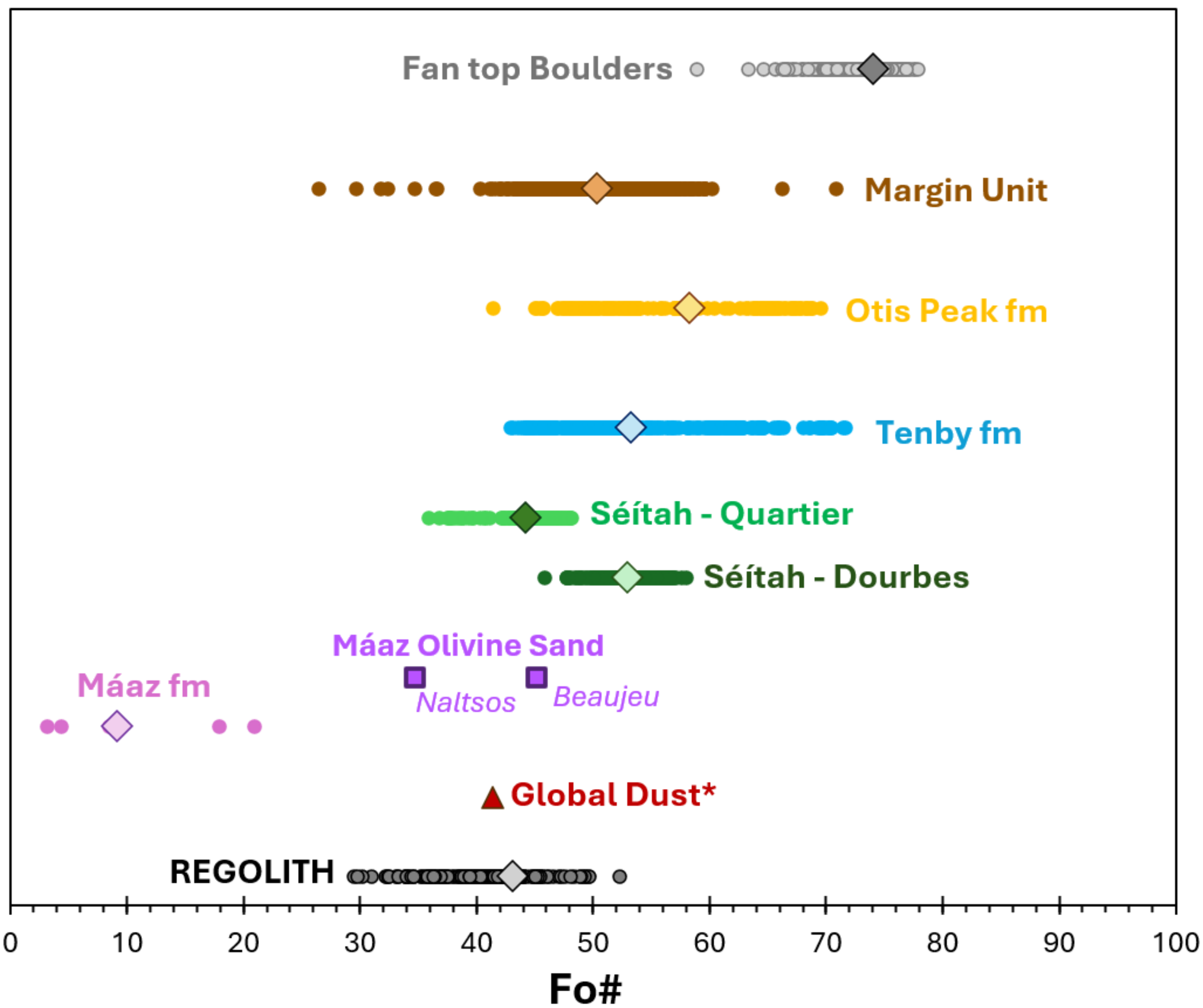

Figure 4-9. Forsterite number (Fo#) of olivine regolith grains (dark gray; this work) compared to olivine identified by PIXL in the fan top and Séítah regions (Moreland et al., submitted) and the Máaz formation (Schmidt et al., 2025). Squares show the Fo#s for two instances where PIXL scanned similar olivine sand on top of bedrock at *Naltsos* (Hausrath et al., 2023) and *Beaujeu* (Schmidt et al., 2025). The Mg:Fe molar ratio of dust is indicated with a triangle (Berger et al., 2016). Circles represent individual PIXL points identified as olivine. Diamonds show the bulk sum value across a target or formation.

Regolith Component	Notable Spectral Properties	Notable Chemistry	Diffraction	UC	TP	MB	Potential source(s)
Olivine	Low NIR / G	FeO_T (36 wt. %), MgO (15 wt. %), SiO_2 (38 wt. %); Na not detected	Yes, single crystal	x	x	x	Local: Séítah-like unit Regional: olivine-carbonate unit
Phyllosilicate	High NIR	FeO_T (17 wt. %), MgO (12 wt. %), SiO_2 (42 wt. %); high Cl (2 wt. %) and Br (1600 ppm)	No	x		x	Local: Shenandoah Formation, Yori Pass member
Carbonate-bearing	N/A	High FeO_T (36 wt. %); MgO (11 wt. %); low SiO_2 (33 wt. %); high Cl (2 wt. %); Na not detected	No	x		x	Local: Séítah-like unit Regional: olivine-carbonate unit
Cr-,Ti-Spinel	N/A	Very high Cr_2O_3 (9 wt.%) & TiO_2 (2 wt.%), correlated with FeO_T	Mixed		x	x	Local: Shenandoah formation, Amalik member; Séítah formation; Global: basaltic sands
Fe-sulfate	Over-exposed	Very high SO_3 (>20 wt. %)	No	x			Local: Shenandoah formation, Yori Pass member
Plagioclase	N/A	High SiO_2 (39 wt.%), Al_2O_3 (13 wt.%); Very low FeO_T (4 wt.%), MgO (5 wt.%)	Mixed		x	x	*Inconclusive*
Fines	Heterogenous mixture	Higher Na_2O + CaO + K_2O (9 wt. %)	Mixed	x	x	x	Global: Global soil unit[a]
Dust-like	Low NIR / G (identical to olivine component)	High SO_3 (9 wt. %), correlated with CaO (6 wt. %); High P (>1 wt. %)	None (dust comp.); Single crystal (olivine comp.)			x	Local: Dust-like coating[b] Global: Airfall dust[c]

Table 4-3. Summary of identified regolith components, notable reflectance, chemistry, and diffraction properties, where they were detected, and potential sources. MB = *Marmot Bay*, TP = *Topographers Peak*, UC = *Ursus Cove*. [a]O'Connell-Cooper et al. (2017), [b]Schmidt et al. (2024), [c]Knight et al. (2024).

4.4.2 Evidence of Aqueous Activity and Alteration

Multiple styles of aqueous alteration were observed in the regolith, which provide clues about past environmental conditions. For example, phyllosilicate grains may have originated from lithologies that formed *in-situ* as direct precipitates (Benison et al., 2024), or from the alteration of primary mafic minerals. Such alteration could have occurred either within the original source region(s) in the Jezero crater catchment area (Ehlmann et al., 2008a), or after they were incorporated into the Yori Pass sandstones. If formed locally, clays are excellent at preserving biosignatures, as organic material can be trapped within the layered clay structure (Bosak et al., 2024).

The carbonate-bearing grains imply alteration of primary silicate phases took place under the influence of dissolved CO_2, potentially at a low water:rock ratio. This style of alteration has been previously observed in the Séítah formation (Tice et al., 2022). If these carbonate-bearing grains originated from the Nili Planum olivine-carbonate unit, they would present a unique opportunity to study alteration products from outside Jezero crater and interpret environmental conditions on a regional scale.

The abundances of S and Cl in the regolith also suggest a history of aqueous activity, consistent with other evidence of saline fluids in Jezero's past (e.g., Benison et al., 2024; Farley et al., 2022; Hurowitz et al., 2023; Scheller et al., 2022; Tice et al., 2022). Such salts may have been precipitated from saline aqueous solutions (potentially groundwater; e.g., Benison et al., 2024). Subsequently, thin brine films could have mobilized and redistributed S and Cl in the regolith, in a similar manner to the concentration of salts at the *Phoenix* landing site (Cull et al., 2010).

4.4.3 Regolith Hydration and Brine-Forming Salts

Regolith plays a key role in Mars' hydrosphere because it exchanges water with the atmosphere, storing H_2O in adsorbed phases, hydrated salts and/or minerals, and potentially thin films of brine (Anderson & Tice, 1979; Cull et al., 2010). Understanding the amount of water stored in each of these potential reservoirs is critical for assessing the global water inventory and the astrobiological potential of modern Mars. The Viking landers measured 1 to 3 wt. % water in soils (Anderson & Tice, 1979), and the Sample Analysis at Mars instrument onboard the *Curiosity* rover similarly measured 1.5 to 3 wt. % water in the Rocknest sand shadow (Leshin et al., 2013). Meslin et al. (2013) observed ubiquitous hydration in the fine-grained regolith in Gale crater, which was associated with and apparently carried by amorphous phases. Similarly, in Jezero crater SuperCam measured hydration bands in the fines at *Observation Mountain* (Cousin et al., 2025).

PIXL's results build on these previous observations by inferring that hydration is most associated with the fines and the phyllosilicate regolith components. Although PIXL cannot directly measure H_2O, any water in the scan area would result in low analytical totals, since H and O are low-Z elements that would be absent from the instrument's quantifications. PIXL measured lower analytical totals in the fines (81%) and the coarse phyllosilicate grains (93%; Table 4-2). Note that a high abundance of low-Z elements can also be caused by carbonates, but in this case the fines and phyllosilicates lack any indication of a carbonate composition (i.e., no mixing towards a zero-silicate endmember; Fig. 4-6). In the fines, hydration can be explained by adsorbed water, which would be more abundant due to the higher specific surface area of the fines. In the coarse phyllosilicate grains, water may exist between mineral layers, and/or adsorbed to mineral surfaces. In both the fines and phyllosilicates, water could also plausibly exist in hydrated salts (e.g., sulfates, perchlorates), since both components were enriched in SO_3 and Cl (Fig. 4-5D, Table 4-2). The latter interpretation is consistent with ChemCam results, which showed amorphous sulfates as the main carrier of hydration in Gale crater soils (David et al., 2022). Additionally, analog laboratory experiments have shown that perchlorate-rich regolith can hold several wt. % water, dependent on salt abundance, relative humidity (RH), and temperature—a result of simultaneous adsorption and deliquescence (e.g., figure 2 in Shumway et al., 2023).

Although PIXL cannot directly distinguish between different oxidation states of Cl, we infer that both chlorides and oxychlorine species (i.e., chlorate and/or perchlorate) are likely present in the studied regolith, since they are thought to be essentially ubiquitous in Martian soils (Clark & Kounaves, 2016; Sutter et al., 2017). On the crater floor, perchlorate salts were interpreted as late stage precipitates formed during episodes of aqueous alteration by saline water (Scheller et al., 2022; Tice et al., 2022). Similarly, the enrichment of Cl (likely including ClO_4) in Jezero soils relative to global averages may also be a product of past aqueous activity. Among the coarser grains, the correlation of high Cl with the most altered phases (i.e., phyllosilicate and carbonate-bearing grains) could be evidence of aqueous alteration by past brines (Fig. 4-5D).

The inferred presence of perchlorates is fascinating because of their ability to absorb water vapor and dissolve into liquid brine (i.e., deliquesce) under certain Mars-relevant conditions (e.g., Gough et al., 2011; Nuding et al., 2014; Toner et al., 2014). In regolith, deliquescent perchlorate salts would form thin films of brine that could chemically weather the surface, mobilize soluble species, and possibly create habitable niches. Perchlorate brines form when RH exceeds the deliquescent relative humidity (DRH), and remain stable as a liquid so long as temperature and RH exceed the brine's eutectic point. For example, liquid Ca-perchlorate brine is stable at temperatures and RH values above its eutectic point of 199K and 52% RH (Nuding et al., 2014; Pestova et al., 2005; Toner et al., 2014b).

At the *Observation Mountain* regolith sampling site, MEDA measured temperatures and RHs that were below the eutectic point of Ca-perchlorate, which indicates that liquid perchlorate brines were not stable while the rover was there (figure 26 in Hausrath et al., 2025). Other plausible perchlorates (i.e., Mg- and Na-perchlorate) have higher eutectic temperatures, so similarly would not have been able to form stable liquid brine. Instead, any putative perchlorates in the regolith would have likely existed as hydrated salts, though their hydration state may have changed following diurnal cycles in temperature and RH.

However, *Perseverance* only visited *Observation Mountain* during the Northern winter ($L_s \approx$ 325 - 350°), and it is feasible that liquid perchlorate brines might be able to form during a warmer and/or more humid season. Once formed, perchlorate brines are remarkably persistent due to hysteresis in freeze-thaw and deliquescence-efflorescence cycles. For example, perchlorate brines are prone to supercooling, and can remain in a metastable liquid phase at temperatures well below their eutectic (Toner et al., 2014b). Similarly, perchlorate brines effloresce (dehydrate into salt) at humidities below their DRH—in other words, they persist as liquids under drier conditions than are required for their formation (Nuding et al., 2014). Finally, perchlorate brines are further stabilized by regolith, which allows thin films of unfrozen water to persist at yet more extreme conditions, even indefinitely under certain conditions (Shumway et al., 2023b).

PIXL measured relatively lower levels of SO_3 compared to other sites, despite the local bedrock of Jezero crater containing many sulfate features, particularly within the Shenandoah formation (Benison et al., 2024; Jones et al., 2025; Phua et al., 2024; Siljeström et al., 2024). Sulfates in the soil may have been contributed from those nearby SO_3-rich lithologies, or from dust, which recent PIXL measurements suggest could contain $CaSO_4$ (Knight et al., 2024). PIXL regolith measurements agree with recent SuperCam analyses, which independently concluded that Jezero regolith contains fewer Mg-sulfates than analogous measurements in Gale crater (Cousin et al., 2025). Martian soil contains some fraction of soluble sulfate (Kounaves et al., 2010), and amorphous sulfates may be the main carrier of hydration in regolith (David et al., 2022). At *Observation Mountain*, the measured temperature and RH changes may have caused the sulfate salts in the regolith to transition between hydration states (see figure 26 in Hausrath et al., 2025).

4.4.4 Relevance for Mars Sample Return

PIXL observation in sampled regolith	**Questions raised which could be answered with a returned regolith sample**
Global soil and dust component	What is the origin of global soils and dust? How homogenous are these components within each sample?
	What hazards do regolith pose for future crewed missions–for example

Cl enrichment	fine particulates (dust) and toxic oxychlorine species? (Beaty et al., 2019)
	What is the speciation of the salts in regolith? Could those salts deliquesce to form (potentially habitable) brines under modern surface conditions?
	What is the relative abundance of chlorides vs. oxychlorine species? How oxidizing is the modern Martian regolith, and what does that imply for the destruction of organics on the surface?
	Are there valuable resources (e.g., perchlorates, water) contained within regolith? (Beaty et al., 2019)
Hydrated fines & phyllosilicates	How is water stored in regolith (e.g., adsorbed and interfacial water, hydrated minerals and salts, brine films)? How much water is in each of these reservoirs?
Multiple amorphous and crystalline components	How is water stored in the amorphous fraction (e.g., as hydrated salts, interstitial water, etc.)? Is the amorphous material compositionally homogeneous?
Mineralogically diverse components	Are there regolith components from lithologies for which no bedrock sample was collected? Could characterization of these materials expand the geographic extent of *Perseverence*'s sampling campaign?
Multiple styles of (aqueous) alteration	What environmental conditions are recorded in the various regolith grains? How long-lived and widespread were these environments? Were they ever habitable?

Table 4-4. Summary of several key PIXL observations about the sampled regolith, which raise questions that could be answered through analysis of a Martian regolith sample in terrestrial labs using instrumentation not available on spacecraft hardware.

PIXL results demonstrate that the regolith samples collected and cached by *Perseverance* contain salt-rich and mineralogically diverse material representing local, regional, and global components. A complete, multi-instrument description of the duplicate regolith samples (*Atmo Mountain* and *Crosswind Lake*) is provided by Hausrath et al. (2025). Here, we will focus on how PIXL's observations specifically contribute to the Mars Sample Return (MSR) campaign and further motivate the return of a regolith sample (summarized in Table 4-4).

Chemical maps produced by PIXL reveal that the sampled regolith represents geographically and lithologically diverse sources, including lithic fragments from nearby bedrock, contributions from regional sources (i.e., grains possibly sourced from the Nili Planum olivine-carbonate unit), as well as global components like soil and dust. Some components (e.g., carbonate-bearing and olivine grains) have compositions unique from any other sample, offering an opportunity to infer lithologies from beyond the rover's traverse. PIXL further documented how these components were arranged prior to mixing during sampling (i.e., differences between surface and subsurface regolith). These results will provide crucial *in situ* geological context for future investigations that will be conducted on these samples upon delivery to Earth.

PIXL geochemically confirms the presence of global soils and dust at the regolith sampling site, which demonstrates that the samples are representative of regolith observed elsewhere by previous missions (see also Hausrath et al., 2025). Analysis of these globally uniform components in terrestrial labs would pave the way for future exploration of Mars by characterizing potential hazards and resources that may be encountered (i.e., objectives 6 and 7 in Beaty et al., 2019). Additionally, analyses of the composition and homogeneity of the finest-grain component at a high spatial resolution not presently available on spacecraft hardware could test hypotheses for the origins of soil and dust. For example, fines that are geochemically homogenous on the scale of individual grains would point to a single source region (e.g., Ojha et al., 2018), whereas heterogeneity would instead suggest material derived from many sources that was subsequently mixed to homogeneity at the resolution of current spacecraft instrumentation.

The high abundances of Cl in this regolith emphasizes unanswered questions about the oxidation state and speciation of Cl on Mars' surface, which could be conclusively answered with a returned sample. Though several missions have detected Cl in regolith, very few have been able to distinguish between and measure the abundance of different (oxy)chlorine species (e.g., Cl^- vs. ClO_3^- vs. ClO_4^-). The relative abundances of chloride, chlorate, and perchlorate and their associated cations would tell us which hydrated salts exist on the surface, and whether they are likely to form brine under modern conditions. Oxychlorine species are also strong oxidizers capable of destroying organics, so measuring the oxidation state would greatly influence our understanding of the habitability and biosignature preservation potential of Mars' surface. Perchlorate in particular is toxic to humans, so their quantification is crucial for assessing biohazards and developing mitigating strategies and technologies to enable future human exploration (Beaty et al., 2019; Niziński et al., 2021). Conversely, perchlorates could also be assessed as a resource, since Mars-relevant perchlorate salts may be viable as propellants (Hoganson et al., 2024).

Water is another important resource for future missions. PIXL data suggest hydration in the fines and phyllosilicate grains, but rover instrumentation cannot distinguish whether this water exists as adsorbed or interfacial water, in hydrated minerals and salts, or as thin brine films. Terrestrial labs could determine the amount of water stored in each of these potential reservoirs, which would greatly advance our understanding of the modern hydrological cycle, global water inventory, and accessibility of H_2O for future missions.

4.5 Conclusion

PIXL mapped the elemental composition of Martian regolith at a higher resolution than any previous investigation (< 1 mm), which generated new insights into how regolith is formed, transported, and aqueously altered. Regolith on the Jezero crater's Western fan front consists of global soil and airfall dust, plus coarser-grained components that are likely contributed from nearby lithologies. PIXL data were interpreted to infer mineralogy and potential bedrock sources of several regolith components: olivine and carbonate-bearing components likely originated from lithologies similar to the Séítah formation or the Nili Planum olivine-carbonate unit, phyllosilicates and Fe-sulfate grains were likely sourced from bedrock similar in composition to the Yori Pass member, while spinels may have been contributed from an outcrop similar to the Amalik member. The finer-grained regolith fraction is a close geochemical match for the global soils previously analyzed across Mars, and global airfall dust blankets the regolith targets. A high abundance of low-Z elements suggests hydration in the fines and the coarse phyllosilicate grains, potentially as adsorbed water or as hydrated minerals or salts. Regolith in Jezero apparently contains fewer sulfates than in Gale, but is highly enriched in Cl, potentially in the form of hydrated oxychlorine salts. Jezero's salty regolith may be further evidence of past saline aqueous environments, and likely plays a role in modern water exchange between the atmosphere and the surface. PIXL provides a crucial first look at the chemistry of the two mineralogically diverse regolith samples collected and cached by *Perseverance*. The local, regional, and global components, as well as the interesting salt enrichments, emphasize the unique value of a regolith sample to the MSR campaign.

4.6 Acknowledgements

This work is supported by Mars 2020 Phase E funding for the PIXL instrument under a contract with the National Aeronautics and Space Administration (80NM0018D0004).

4.7 Data Availability Statement

All data, including separate file uploads for tables S1 and S3, are archived on the NASA Planetary Data System: Geosciences node (Allwood & Hurowitz, 2021; https://pds-geosciences.wustl.edu/m2020/). Source code for PIXLISE and PIQUANT software are available via (Barber & Davidoff, 2022; Nemere et al., 2024).

5. Conclusion

5.1 Chapter Summaries

Much of the Martian surface is blanketed with salt-rich regolith, which holds a large reservoir of H_2O in the form of hydrated salts and minerals, adsorbed water, and possibly liquid brine. Soil, salt, and water each play a key role in shaping the chemistry, cohesivity, and habitability of Mars' surface, yet studies of systems containing all three components remain uncommon. **Chapter 2** began to fill this gap in the literature through analog laboratory experiments studying the behaviors of realistic briny regolith analogs over a range of Mars-relevant temperatures, relative humidities, and salt concentrations. Results show that when regolith is accounted for, perchlorate brines contain more water and better resist salt precipitation and freezing, which likely improves their potential to sustain life. These findings greatly expand the conditions where potentially habitable brines could exist on Mars today, which informs future astrobiological and geochemical investigations of the planet.

Soil, salt, and water have also been invoked to explain the puzzling, seasonal slope features known as RSL. Literature speculates that RSL could be wet brine flows, and they are protected as "Special Regions" for their putative connection to liquid water and possible habitability. **Chapter 3** describes several factors that may contribute to RSL, experimentally validating the hypothesis that RSL could be granular flows triggered by seasonally desorbing water. Results demonstrate that soil hydration and slope stability depend linearly on relative humidity (RH), suggesting that seasonal swings between high and low RH could stabilize then destabilize slopes, respectively, causing sand avalanches. Evidence supports a semi-dry formation mechanism for RSL, which only requires adsorbed water supplied from the atmosphere, and does not rely on hidden reservoirs of water or high abundances of deliquescent salts. The minimal amount of (adsorbed) water involved calls into question whether RSL are relevant as astrobiological targets, and whether they merit their current planetary protection designation.

Fifty years after the first XRF instruments were launched to Mars on the Viking Landers, **Chapter 4** carries the torch by reporting brand new XRF investigations of regolith from PIXL onboard the *Perseverance* rover. This work results in the highest resolution (< 1 mm) geochemical maps ever produced for Martian regolith and reveals a mineralogically diverse and salt-rich regolith. Regolith in Jezero crater is enriched in chlorine (possibly as perchlorates), yet contains fewer sulfates than previous sites, suggesting a unique local aqueous history. The regolith investigated consists of local, regional, and global components, each which record clues about past environments and Mars' geologic history. These data also describe the composition and geologic context of a duplicate pair of regolith samples collected and cached by *Perseverance*, one of which may be returned to Earth for future study using techniques not available on any spacecraft. This information will be critical for future researchers as they plan how to curate and eventually analyze these regolith samples in terrestrial labs.

5.2 Future work

This dissertation lays a solid foundation for understanding Mars' salty soils and raises several novel science questions to be explored in future work. This work has focused on the top-most layer of Martain regolith, which is in direct contact with the atmosphere. In fact, all exploration of Mars to this point has just scratched the surface—literally accessing only the top few 10s of centimeters. This will change soon, as both the ESA's upcoming *Rosalind Franklin* rover and the Mars Life Explorer mission concept (prioritized for NASA funding in the mid-2030s) would drill up to 2m beneath the surface into regolith and/or subsurface ice (*Origins, Worlds, and Life*, 2023; Williams, 2021). Beneath the harsh surface, conditions may be more favorable for life, as temperatures are more stable over diurnal cycles, and harmful radiation is rapidly attenuated by regolith. Future experiments and thermodynamic models that consider the stability and habitability of water in salty, ice-cemented regolith *at depth* will be crucial for enabling the success of these upcoming missions, as well as future human exploration.

PIXL's detections of chlorine-enriched regolith are exciting, but also frustrating due to our inability to confidently distinguish between chloride (Cl^-), chlorate (ClO_3^-), and perchlorate (ClO_4^-). Each of these anions form salts that interact differently with water, hydrating or possibly by deliquescing into brine at different temperature and RH conditions. Existing XRF instruments are insensitive to low atomic number elements like oxygen, which hampers attempts to determine the oxidation state of Cl or S. Recently, combined analyses of X-ray fluorescence and scattering data have been used to examine light-element abundances, which contributed to the *Curiosity* rover's recent discovery of elemental sulfur (i.e., by discerning S^0 from SO_3). Similar scattering analyses could be applied to XRF datasets across Mars to detect and possibly quantify oxychlorine species. Combined with environmental measurements (e.g., temperature and relative humidity from landed instruments), new identifications of perchlorates could improve our understanding of how much water is stored in hydrated salts and/or brines across multiple landing sites.

Mars planetary science is rapidly evolving from a data-poor field, where a few missions return limited quantities of data that are interpreted and reinterpreted over decades, to a data-rich field, where more data is returned each day than can be manually analyzed. This phase change in Mars data science comes at a time when advances in machine learning and artificial intelligence allow efficient processing of large volumes of data; however, the implementation of these methods into planetary datasets has so far been growing slowly. This dissertation briefly explored machine learning techniques in Chapter 4 (and Appendix A.2), using K-means clustering to identify trends in geochemical datasets and automatically group points by similar composition and diffraction peaks. Presently, most analysis of planetary geochemical datasets is conducted manually—a time intensive process that can be a hurdle for the rapid decision making required for operating a mission in real time. Further development and integration of machine learning tools could automate and speed up geochemical analyses, both improving rover operations and possibly teasing new insights from an archive of almost 50 years of surface exploration.

Finally, the most revolutionary future research stemming from this work will be analyses of returned samples of Martian regolith, studied using all manner of instruments and techniques available in Earth's laboratories. Just as the Apollo lunar samples transformed our understanding of Earth's place in the Solar System, so too will the return of Martian samples revolutionize planetary science and astrobiology, leading to breakthroughs and paradigm shifts that cannot be predicted today. Preparations for the handling, preliminary analyses, and release of these samples is already underway (Carrier et al., 2024), and further preparatory work will be needed to determine how to properly curate these samples to minimize any loss of science (e.g., Tosca et al., 2022). Future astrobiological studies of returned Martian samples could be modelled on the successes of the OSIRIS-REX mission, which recently discovered salts, amino acids, and nucleobases in returned asteroid samples (Glavin et al., 2025; McCoy et al., 2025). The discovery of remnants of a salty ocean and the building blocks for life in returned asteroid samples begs the question: what evidence of life will be found the rocks and regolith retrieved from Mars?

References

Abotalib, A. Z., & Heggy, E. (2019). A deep groundwater origin for recurring slope lineae on Mars. *Nature Geoscience*, *12*(4), 235–241. https://doi.org/10.1038/s41561-019-0327-5

Achilles, C. N., Downs, R. T., Ming, D. W., Rampe, E. B., Morris, R. V., Treiman, A. H., Morrison, S. M., Blake, D. F., Vaniman, D. T., Ewing, R. C., Chipera, S. J., Yen, A. S., Bristow, T. F., Ehlmann, B. L., Gellert, R., Hazen, R. M., Fendrich, K. V., Craig, P. I., Grotzinger, J. P., … Morookian, J. M. (2017). Mineralogy of an active eolian sediment from the Namib dune, Gale crater, Mars. *Journal of Geophysical Research: Planets*, *122*(11), 2344–2361. https://doi.org/10.1002/2017JE005262

Allwood, A. C., & Hurowitz, J. A. (2021). *Mars 2020 PIXL Raw and Processed Data Bundle* (Archive No. urn:nasa:pds:mars2020_pixl::2.0). NASA Planetary Data System. https://doi.org/10.17189/1522645

Allwood, A. C., Wade, L. A., Foote, M. C., Elam, W. T., Hurowitz, J. A., Battel, S., Dawson, D. E., Denise, R. W., Ek, E. M., Gilbert, M. S., King, M. E., Liebe, C. C., Parker, T., Pedersen, D. A. K., Randall, D. P., Sharrow, R. F., Sondheim, M. E., Allen, G., Arnett, K., … Zimmerman, R. (2020). PIXL: Planetary Instrument for X-Ray Lithochemistry. *Space Science Reviews*, *216*(8), 134. https://doi.org/10.1007/s11214-020-00767-7

Anderson, D. M. (1967). Ice Nucleation and the Substrate-ice Interface. *Nature*, *216*(5115), 563–566. https://doi.org/10.1038/216563a0

Anderson, D. M., & Tice, A. R. (1979). The analysis of water in the Martian regolith. *Journal of Molecular Evolution*, *14*(1), 33–38. https://doi.org/10.1007/BF01732365

Appelo, C. A. J., & Postma, D. (2004). *Geochemistry, Groundwater and Pollution* (2nd ed.). CRC Press. https://doi.org/10.1201/9781439833544

Applin, D. M., Izawa, M. R. M., Cloutis, E. A., Goltz, D., & Johnson, J. R. (2015). Oxalate minerals on Mars? *Earth and Planetary Science Letters*, *420*, 127–139. https://doi.org/10.1016/j.epsl.2015.03.034

Archer, P. D., Franz, H. B., Sutter, B., Arevalo Jr., R. D., Coll, P., Eigenbrode, J. L., Glavin, D. P., Jones, J. J., Leshin, L. A., Mahaffy, P. R., McAdam, A. C., McKay, C. P., Ming, D. W., Morris, R. V., Navarro-González, R., Niles, P. B., Pavlov, A., Squyres, S. W., Stern, J. C., … Wray, J. J. (2014). Abundances and implications of volatile-bearing species from evolved gas analysis of the Rocknest aeolian deposit, Gale Crater, Mars. *Journal of Geophysical Research: Planets*, *119*(1), 237–254. https://doi.org/10.1002/2013JE004493

Arvidson, R. E., Anderson, R. C., Bartlett, P., Bell, J. F., Blaney, D., Christensen, P. R., Chu, P., Crumpler, L., Davis, K., Ehlmann, B. L., Fergason, R., Golombek, M. P., Gorevan, S., Grant, J. A., Greeley, R., Guinness, E. A., Haldemann, A. F. C., Herkenhoff, K., Johnson, J., … Wilson, J. (2004). Localization and Physical Properties Experiments Conducted by Spirit at Gusev Crater. *Science*, *305*(5685), 821–824. https://doi.org/10.1126/science.1099922

Arvidson, R. E., Anderson, R. C., Bartlett, P., Bell, J. F., Christensen, P. R., Chu, P., Davis, K., Ehlmann, B. L., Golombek, M. P., Gorevan, S., Guinness, E. A., Haldemann, A. F. C., Herkenhoff, K. E., Landis, G., Li, R., Lindemann, R., Ming, D. W., Myrick, T., Parker, T., … Wilson, J. (2004). Localization and Physical Property Experiments Conducted by

Opportunity at Meridiani Planum. *Science*, *306*(5702), 1730–1733. https://doi.org/10.1126/science.1104211

Arvidson, R. E., Bonitz, R. G., Robinson, M. L., Carsten, J. L., Volpe, R. A., Trebi-Ollennu, A., Mellon, M. T., Chu, P. C., Davis, K. R., Wilson, J. J., Shaw, A. S., Greenberger, R. N., Siebach, K. L., Stein, T. C., Cull, S. C., Goetz, W., Morris, R. V., Ming, D. W., Keller, H. U., … Mehta, M. (2009). Results from the Mars Phoenix Lander Robotic Arm experiment. *Journal of Geophysical Research: Planets*, *114*(E1). https://doi.org/10.1029/2009JE003408

Atwood-Stone, C., & McEwen, A. S. (2013). Avalanche slope angles in low-gravity environments from active Martian sand dunes. *Geophysical Research Letters*, *40*(12), 2929–2934. https://doi.org/10.1002/grl.50586

Banin, A., & Anderson, D. M. (1974). Effects of Salt Concentration Changes During Freezing on the Unfrozen Water Content of Porous Materials. *Water Resources Research*, *10*(1), 124–128. https://doi.org/10.1029/WR010i001p00124

Barber, T., & Davidoff, S. (2022). *pixlise/piquant: 3.2.11 Open Source* (Version v3.2.11) [Computer software]. Zenodo. https://doi.org/10.5281/zenodo.6959225

Beaty, D. W., Grady, M. M., McSween, H. Y., Sefton-Nash, E., Carrier, B. L., Altieri, F., Amelin, Y., Ammannito, E., Anand, M., Benning, L. G., Bishop, J. L., Borg, L. E., Boucher, D., Brucato, J. R., Busemann, H., Campbell, K. A., Czaja, A. D., Debaille, V., Des Marais, D. J., … Zorzano, M. P. (2019). The potential science and engineering value of samples delivered to Earth by Mars sample return. *Meteoritics & Planetary Science*, *54*(S1), S3–S152. https://doi.org/10.1111/maps.13242

Beck, P., Pommerol, A., Schmitt, B., & Brissaud, O. (2010). Kinetics of water adsorption on minerals and the breathing of the Martian regolith. *Journal of Geophysical Research: Planets*, *115*(E10). https://doi.org/10.1029/2009JE003539

Bell III, J. F., McSween Jr., H. Y., Crisp, J. A., Morris, R. V., Murchie, S. L., Bridges, N. T., Johnson, J. R., Britt, D. T., Golombek, M. P., Moore, H. J., Ghosh, A., Bishop, J. L., Anderson, R. C., Brückner, J., Economou, T., Greenwood, J. P., Gunnlaugsson, H. P., Hargraves, R. M., Hviid, S., … Soderblom, L. (2000). Mineralogic and compositional properties of Martian soil and dust: Results from Mars Pathfinder. *Journal of Geophysical Research: Planets*, *105*(E1), 1721–1755. https://doi.org/10.1029/1999JE001060

Bell, J. F., Maki, J. N., Alwmark, S., Ehlmann, B. L., Fagents, S. A., Grotzinger, J. P., Gupta, S., Hayes, A., Herkenhoff, K. E., Horgan, B. H. N., Johnson, J. R., Kinch, K. B., Lemmon, M. T., Madsen, M. B., Núñez, J. I., Paar, G., Rice, M., Rice, J. W., Schmitz, N., … Yingling, R. (2022). Geological, multispectral, and meteorological imaging results from the Mars 2020 Perseverance rover in Jezero crater. *Science Advances*, *8*(47), eabo4856. https://doi.org/10.1126/sciadv.abo4856

Bell, J. F., Maki, J. N., Mehall, G. L., Ravine, M. A., Caplinger, M. A., Bailey, Z. J., Brylow, S., Schaffner, J. A., Kinch, K. M., Madsen, M. B., Winhold, A., Hayes, A. G., Corlies, P., Tate, C., Barrington, M., Cisneros, E., Jensen, E., Paris, K., Crawford, K., … Wolff, M. J. (2021). The Mars 2020 Perseverance Rover Mast Camera Zoom (Mastcam-Z) Multispectral, Stereoscopic Imaging Investigation. *Space Science Reviews*, *217*(1), 24. https://doi.org/10.1007/s11214-020-00755-x

Benison, K. C., Gill, K. K., Sharma, S., Siljeström, S., Zawaski, M., Bosak, T., Broz, A., Clark, B. C., Cloutis, E., Czaja, A. D., Flannery, D., Fornaro, T., Gómez, F., Hand, K., Herd, C. D. K., Johnson, J. R., Madariaga, J. M., Madsen, M. B., Martinez-Frías, J., … Yanchilina, A. (2024). Depositional and Diagenetic Sulfates of Hogwallow Flats and Yori Pass, Jezero Crater: Evaluating Preservation Potential of Environmental Indicators and Possible Biosignatures From Past Martian Surface Waters and Groundwaters. *Journal of Geophysical Research: Planets*, *129*(2), e2023JE008155. https://doi.org/10.1029/2023JE008155

Benner, S. A., Devine, K. G., Matveeva, L. N., & Powell, D. H. (2000). The missing organic molecules on Mars. *Proceedings of the National Academy of Sciences*, *97*(6), 2425–2430. https://doi.org/10.1073/pnas.040539497

Berger, J. A., Gellert, R., Boyd, N. I., King, P. L., McCraig, M. A., O’Connell-Cooper, C. D., Schmidt, M. E., Spray, J. G., Thompson, L. M., VanBommel, S. J. V., & Yen, A. S. (2020). Elemental Composition and Chemical Evolution of Geologic Materials in Gale Crater, Mars: APXS Results From Bradbury Landing to the Vera Rubin Ridge. *Journal of Geophysical Research: Planets*, *125*(12), e2020JE006536. https://doi.org/10.1029/2020JE006536

Berger, J. A., Schmidt, M. E., Gellert, R., Campbell, J. L., King, P. L., Flemming, R. L., Ming, D. W., Clark, B. C., Pradler, I., VanBommel, S. J. V., Minitti, M. E., Fairén, A. G., Boyd, N. I., Thompson, L. M., Perrett, G. M., Elliott, B. E., & Desouza, E. (2016). A global Mars dust composition refined by the Alpha-Particle X-ray Spectrometer in Gale Crater. *Geophysical Research Letters*, *43*(1), 67–75. https://doi.org/10.1002/2015GL066675

Berger, J. A., VanBommel, S. J., Rampe, E. B., Knight, A. L., Ustunisik, G. K., & Righter, K. (2024). *Ancient Lithified Sands of the Stimson Formation in Gale Crater Preserve Moderately Volatile Element Enrichment Linked to Magmatic Degassing*. 10th International Conference on Mars, Pasadena, CA.

Besley, L. M., & Bottomley, G. A. (1969). The water vapour equilibria over magnesium perchlorate hydrates. *The Journal of Chemical Thermodynamics*, *1*(1), 13–19. https://doi.org/10.1016/0021-9614(69)90032-9

Beyssac, O., Forni, O., Cousin, A., Udry, A., Kah, L. C., Mandon, L., Clavé, O. E., Liu, Y., Poulet, F., Quantin Nataf, C., Gasnault, O., Johnson, J. R., Benzerara, K., Beck, P., Dehouck, E., Mangold, N., Alvarez Llamas, C., Anderson, R. B., Arana, G., … Team, T. S. (2023). Petrological Traverse of the Olivine Cumulate Séítah Formation at Jezero Crater, Mars: A Perspective From SuperCam Onboard Perseverance. *Journal of Geophysical Research: Planets*, *128*(7), e2022JE007638. https://doi.org/10.1029/2022JE007638

Bhartia, R., Beegle, L. W., DeFlores, L., Abbey, W., Razzell Hollis, J., Uckert, K., Monacelli, B., Edgett, K. S., Kennedy, M. R., Sylvia, M., Aldrich, D., Anderson, M., Asher, S. A., Bailey, Z., Boyd, K., Burton, A. S., Caffrey, M., Calaway, M. J., Calvet, R., … Zan, J. (2021). Perseverance's Scanning Habitable Environments with Raman and Luminescence for Organics and Chemicals (SHERLOC) Investigation. *Space Science Reviews*, *217*(4), 58. https://doi.org/10.1007/s11214-021-00812-z

Bing, H., & Ma, W. (2011). Laboratory investigation of the freezing point of saline soil. *Cold Regions Science and Technology*, *67*(1–2), 79–88. https://doi.org/10.1016/j.coldregions.2011.02.008

Blake, D. F., Morris, R. V., Kocurek, G., Morrison, S. M., Downs, R. T., Bish, D., Ming, D. W., Edgett, K. S., Rubin, D., Goetz, W., Madsen, M. B., Sullivan, R., Gellert, R., Campbell, I., Treiman, A. H., McLennan, S. M., Yen, A. S., Grotzinger, J., Vaniman, D. T., … Zorzano Mier, M.-P. (2013). Curiosity at Gale Crater, Mars: Characterization and Analysis of the Rocknest Sand Shadow. *Science*, *341*(6153), 1239505. https://doi.org/10.1126/science.1239505

Bosak, T., Shuster, D. L., Scheller, E. L., Siljeström, S., Zawaski, M. J., Mandon, L., Simon, J. I., Weiss, B. P., Stack, K. M., Mansbach, E. N., Treiman, A. H., Benison, K. C., Brown, A. J., Czaja, A. D., Farley, K. A., Hausrath, E. M., Hickman-Lewis, K., Herd, C. D. K., Johnson, J. R., … Williams, A. (2024). Astrobiological Potential of Rocks Acquired by the Perseverance Rover at a Sedimentary Fan Front in Jezero Crater, Mars. *AGU Advances*, *5*(4), e2024AV001241. https://doi.org/10.1029/2024AV001241

Boxe, C. S., Hand, K. P., Nealson, K. H., Yung, Y. L., Yen, A. S., & Saiz-Lopez, A. (2012). Adsorbed water and thin liquid films on Mars. *International Journal of Astrobiology*, *11*(3), 169–175. https://doi.org/10.1017/S1473550412000080

Brown, A. J., Viviano, C. E., & Goudge, T. A. (2020). Olivine-Carbonate Mineralogy of the Jezero Crater Region. *Journal of Geophysical Research: Planets*, *125*(3), e2019JE006011. https://doi.org/10.1029/2019JE006011

Byrne, S. (2009). The Polar Deposits of Mars. *Annual Review of Earth and Planetary Sciences*, *37*(Volume 37, 2009), 535–560. https://doi.org/10.1146/annurev.earth.031208.100101

Cannon, K. M., Britt, D. T., Smith, T. M., Fritsche, R. F., & Batcheldor, D. (2019). Mars global simulant MGS-1: A Rocknest-based open standard for basaltic martian regolith simulants. *Icarus*, *317*, 470–478. https://doi.org/10.1016/j.icarus.2018.08.019

Cardarelli, E. L., Vaughan, A., Siljeström, S., Minitti, M. E., Paar, G., Sullivan, R., Buckner, D. K., Hausrath, E. M., Johnson, J. R., Wu, M., Uckert, K., Bhartia, R., Hand, K., Bell, J. F., Conrad, P., Panossian, L., & Burgos, R. (2023). *The First In-Situ Regolith Observations on the Delta Front of Jezero Crater, Mars Characterized by the Mars 2020 SHERLOC and Mastcam-Z Investigations*. *2806*, 2671. 54th Lunar and Planetary Science Conference.

Carrier, B. L., Graham, H. V., Herd, C. D. K., Sefton-Nash, E., Haltigin, T., Paardekooper, D., & Viotti, M. (2024). *Planning Measurements on Samples from Mars: Status Report from the Mars Sample Return (MSR) Sample Receiving Project (SRP) Measurement Definition Team (MDT-1)*. *3040*, 1615. 55th Lunar and Planetary Science Conference.

Catling, D. C., Claire, M. W., Zahnle, K. J., Quinn, R. C., Clark, B. C., Hecht, M. H., & Kounaves, S. (2010). Atmospheric origins of perchlorate on Mars and in the Atacama. *Journal of Geophysical Research: Planets*, *115*(E1). https://doi.org/10.1029/2009JE003425

Catling, D. C., & Kasting, J. F. (2017). *Atmospheric Evolution on Inhabited and Lifeless Worlds*. Cambridge University Press.

Chevrier, V. F., Hanley, J., & Altheide, T. S. (2009). Stability of perchlorate hydrates and their liquid solutions at the Phoenix landing site, Mars. *Geophysical Research Letters*, *36*(10). https://doi.org/10.1029/2009GL037497

Chojnacki, M., McEwen, A., Dundas, C., Ojha, L., Urso, A., & Sutton, S. (2016). Geologic context of recurring slope lineae in Melas and Coprates Chasmata, Mars. *Journal of Geophysical Research: Planets*, *121*(7), 1204–1231. https://doi.org/10.1002/2015JE004991

Clark, B. C., Baird, A. K., Weldon, R. J., Tsusaki, D. M., Schnabel, L., & Candelaria, M. P. (1982). Chemical composition of Martian fines. *Journal of Geophysical Research: Solid Earth*, *87*(B12), 10059–10067. https://doi.org/10.1029/JB087iB12p10059

Clark, B. C., & Kounaves, S. P. (2016). Evidence for the distribution of perchlorates on Mars. *International Journal of Astrobiology*, *15*(4), 311–318. https://doi.org/10.1017/S1473550415000385

Cousin, A., Meslin, P.-Y., Forni, O., Beyssac, O., Clavé, E., Hausrath, E., Beck, P., Dehouck, E., Schröder, S., Fouchet, T., Bedford, C., Johnson, J., Pilleri, P., Lasue, J., Gasnault, O., Martin, N., Chide, B., Udry, A., Sullivan, R., … Wiens, R. C. (2025). Soil diversity at Jezero crater and Comparison to Gale crater, Mars. *Icarus*, 116299. https://doi.org/10.1016/j.icarus.2024.116299

Cull, S. C., Arvidson, R. E., Catalano, J. G., Ming, D. W., Morris, R. V., Mellon, M. T., & Lemmon, M. (2010). Concentrated perchlorate at the Mars Phoenix landing site: Evidence for thin film liquid water on Mars. *Geophysical Research Letters*, *37*(22). https://doi.org/10.1029/2010GL045269

Das, A., Heirwegh, C. M., Gao, N., Elam, W. T., Wade, L. A., Clark III, B. C., Hurowitz, J. A., VanBommel, S. J., Jones, M. W. M., & Allwood, A. C. (2025). Energy dependence of x-ray beam size produced by polycapillary x-ray optics. *X-Ray Spectrometry*, *54*(2), 203–213. https://doi.org/10.1002/xrs.3450

David, G., Dehouck, E., Meslin, P.-Y., Rapin, W., Cousin, A., Forni, O., Gasnault, O., Lasue, J., Mangold, N., Beck, P., Maurice, S., Wiens, R. C., Berger, G., Fabre, S., Pinet, P., Clark, B. C., Smith, J. R., & Lanza, N. L. (2022). Evidence for Amorphous Sulfates as the Main Carrier of Soil Hydration in Gale Crater, Mars. *Geophysical Research Letters*, *49*(21), e2022GL098755. https://doi.org/10.1029/2022GL098755

Devoie, É. G., Gruber, S., & McKenzie, J. M. (2022). A repository of measured soil freezing characteristic curves: 1921 to 2021. *Earth System Science Data*, *14*(7), 3365–3377. https://doi.org/10.5194/essd-14-3365-2022

Dundas, C. M. (2020). An aeolian grainflow model for Martian Recurring Slope Lineae. *Icarus*, *343*, 113681. https://doi.org/10.1016/j.icarus.2020.113681

Dundas, C. M., McEwen, A. S., Chojnacki, M., Milazzo, M. P., Byrne, S., McElwaine, J. N., & Urso, A. (2017). Granular flows at recurring slope lineae on Mars indicate a limited role for liquid water. *Nature Geoscience*, *10*(12), 903–907. https://doi.org/10.1038/s41561-017-0012-5

Edwards, C. S., & Piqueux, S. (2016). The water content of recurring slope lineae on Mars. *Geophysical Research Letters*, *43*(17), 8912–8919. https://doi.org/10.1002/2016GL070179

Ehlmann, B. L., & Edwards, C. S. (2014). Mineralogy of the Martian Surface. *Annual Review of Earth and Planetary Sciences*, *42*(Volume 42, 2014), 291–315. https://doi.org/10.1146/annurev-earth-060313-055024

Ehlmann, B. L., Mustard, J. F., Fassett, C. I., Schon, S. C., Head III, J. W., Des Marais, D. J., Grant, J. A., & Murchie, S. L. (2008). Clay minerals in delta deposits and organic preservation potential on Mars. *Nature Geoscience*, *1*(6), Article 6. https://doi.org/10.1038/ngeo207

Ehlmann, B. L., Mustard, J. F., Murchie, S. L., Poulet, F., Bishop, J. L., Brown, A. J., Calvin, W. M., Clark, R. N., Marais, D. J. D., Milliken, R. E., Roach, L. H., Roush, T. L., Swayze, G. A., & Wray, J. J. (2008). Orbital Identification of Carbonate-Bearing Rocks on Mars. *Science*, *322*(5909), 1828–1832. https://doi.org/10.1126/science.1164759

Ewing, R. C., Lapotre, M. G. A., Lewis, K. W., Day, M., Stein, N., Rubin, D. M., Sullivan, R., Banham, S., Lamb, M. P., Bridges, N. T., Gupta, S., & Fischer, W. W. (2017). Sedimentary processes of the Bagnold Dunes: Implications for the eolian rock record of Mars. *Journal of Geophysical Research: Planets*, *122*(12), 2544–2573. https://doi.org/10.1002/2017JE005324

Fanale, F. P., & Cannon, W. A. (1971). Adsorption on the Martian Regolith. *Nature*, *230*(5295), 502–504. https://doi.org/10.1038/230502a0

Farley, K. A., Stack, K. M., Shuster, D. L., Horgan, B. H. N., Hurowitz, J. A., Tarnas, J. D., Simon, J. I., Sun, V. Z., Scheller, E. L., Moore, K. R., McLennan, S. M., Vasconcelos, P. M., Wiens, R. C., Treiman, A. H., Mayhew, L. E., Beyssac, O., Kizovski, T. V., Tosca, N. J., Williford, K. H., … Zorzano, M.-P. (2022). Aqueously altered igneous rocks sampled on the floor of Jezero crater, Mars. *Science*, *377*(6614), eabo2196. https://doi.org/10.1126/science.abo2196

Farley, K. A., Williford, K. H., Stack, K. M., Bhartia, R., Chen, A., de la Torre, M., Hand, K., Goreva, Y., Herd, C. D. K., Hueso, R., Liu, Y., Maki, J. N., Martinez, G., Moeller, R. C., Nelessen, A., Newman, C. E., Nunes, D., Ponce, A., Spanovich, N., … Wiens, R. C. (2020). Mars 2020 Mission Overview. *Space Science Reviews*, *216*(8), 142. https://doi.org/10.1007/s11214-020-00762-y

Fassett, C. I., & Head III, J. W. (2005). Fluvial sedimentary deposits on Mars: Ancient deltas in a crater lake in the Nili Fossae region. *Geophysical Research Letters*, *32*(14). https://doi.org/10.1029/2005GL023456

Fassett, C. I., & Head, J. W. (2008). The timing of martian valley network activity: Constraints from buffered crater counting. *Icarus*, *195*(1), 61–89. https://doi.org/10.1016/j.icarus.2007.12.009

Fischer, E., Martínez, G. m., & Rennó, N. o. (2016). Formation and Persistence of Brine on Mars: Experimental Simulations throughout the Diurnal Cycle at the Phoenix Landing Site. *Astrobiology*, *16*(12), 937–948. https://doi.org/10.1089/ast.2016.1525

Fischer, E., Martínez, G. M., Rennó, N. O., Tamppari, L. K., & Zent, A. P. (2019). Relative Humidity on Mars: New Results From the Phoenix TECP Sensor. *Journal of Geophysical Research: Planets*, *124*(11), 2780–2792. https://doi.org/10.1029/2019JE006080

Garczynski, B. J., Bell, J. F., Horgan, B. H. N., Johnson, J. R., Rice, M. S., Vaughan, A., Nuñez, J. I., & Herd, C. D. K. (2022). *Perseverance and the Purple Coating: A Mastcam-Z*

Multispectral Story. Lunar and Planetary Science Conference, The Woodlands, TX, United States. https://www.hou.usra.edu/meetings/lpsc2022/pdf/2346.pdf

Gellert, R., Clark, B. C., III, & MSL and MER Science Teams. (2015). In Situ Compositional Measurements of Rocks and Soils with the Alpha Particle X-ray Spectrometer on NASA's Mars Rovers. *Elements*, *11*(1), 39–44. https://doi.org/10.2113/gselements.11.1.39

Gilichinsky, D. A. (2002). Permafrost Model of Extraterrestrial Habitat. In *Astrobiology* (pp. 125–142). Springer, Berlin, Heidelberg. https://doi.org/10.1007/978-3-642-59381-9_9

Gilichinsky, D. A., Soina, V. S., & Petrova, M. A. (1993). Cryoprotective properties of water in the Earth cryolithosphere and its role in exobiology. *Origins of Life and Evolution of the Biosphere*, *23*(1), 65–75. https://doi.org/10.1007/BF01581991

Glavin, D. P., Dworkin, J. P., Alexander, C. M. O., Aponte, J. C., Baczynski, A. A., Barnes, J. J., Bechtel, H. A., Berger, E. L., Burton, A. S., Caselli, P., Chung, A. H., Clemett, S. J., Cody, G. D., Dominguez, G., Elsila, J. E., Farnsworth, K. K., Foustoukos, D. I., Freeman, K. H., Furukawa, Y., … Lauretta, D. S. (2025). Abundant ammonia and nitrogen-rich soluble organic matter in samples from asteroid (101955) Bennu. *Nature Astronomy*, *9*(2), 199–210. https://doi.org/10.1038/s41550-024-02472-9

Goudge, T. A., Mustard, J. F., Head, J. W., Fassett, C. I., & Wiseman, S. M. (2015). Assessing the mineralogy of the watershed and fan deposits of the Jezero crater paleolake system, Mars. *Journal of Geophysical Research: Planets*, *120*(4), 775–808. https://doi.org/10.1002/2014JE004782

Gough, R. V., Chevrier, V. F., Baustian, K. J., Wise, M. E., & Tolbert, M. A. (2011). Laboratory studies of perchlorate phase transitions: Support for metastable aqueous perchlorate solutions on Mars. *Earth and Planetary Science Letters*, *312*(3), 371–377. https://doi.org/10.1016/j.epsl.2011.10.026

Gough, R. V., Chevrier, V. F., & Tolbert, M. A. (2016). Formation of liquid water at low temperatures via the deliquescence of calcium chloride: Implications for Antarctica and Mars. *Planetary and Space Science*, *131*, 79–87. https://doi.org/10.1016/j.pss.2016.07.006

Gough, R. V., Nuding, D. L., Archer Jr, P. D., Fernanders, M. S., Guzewich, S. D., Tolbert, M. A., & Toigo, A. D. (2020). Changes in Soil Cohesion Due to Water Vapor Exchange: A Proposed Dry-Flow Trigger Mechanism for Recurring Slope Lineae on Mars. *Geophysical Research Letters*, *47*(11), e2020GL087618. https://doi.org/10.1029/2020GL087618

Gough, R. V., Nuding, D. L., Martínez, G. M., Rivera-Valentín, E. G., Primm, K. M., & Tolbert, M. A. (2023). Laboratory Studies of Brine Growth Kinetics Relevant to Deliquescence on Mars. *The Planetary Science Journal*, *4*(3), 46. https://doi.org/10.3847/PSJ/acbd98

Grotzinger, J. P., & Milliken, R. E. (2012). The Sedimentary Rock Record of Mars: Distribution, Origins, and Global Stratigraphy. In J. P. Grotzinger & R. E. Milliken (Eds.), *Sedimentary Geology of Mars* (Vol. 102, p. 0). SEPM Society for Sedimentary Geology. https://doi.org/10.2110/pec.12.102.0001

Hallsworth, J. E. (2021). Mars' surface is not universally biocidal. *Environmental Microbiology*, *23*(7), 3345–3350. https://doi.org/10.1111/1462-2920.15494

Harri, A.-M., Genzer, M., Kemppinen, O., Gomez-Elvira, J., Haberle, R., Polkko, J., Savijärvi, H., Rennó, N., Rodriguez-Manfredi, J. A., Schmidt, W., Richardson, M., Siili, T., Paton, M., Torre-Juarez, M. D. L., Mäkinen, T., Newman, C., Rafkin, S., Mischna, M., Merikallio, S., … Urqui, R. (2014). Mars Science Laboratory relative humidity observations: Initial results. *Journal of Geophysical Research: Planets*, *119*(9), 2132–2147. https://doi.org/10.1002/2013JE004514

Hausrath, E. M., Adcock, C. T., Bechtold, A., Beck, P., Benison, K., Brown, A., Cardarelli, E. L., Carman, N. A., Chide, B., Christian, J., Clark, B. C., Cloutis, E., Cousin, A., Forni, O., Gabriel, T. S. J., Gasnault, O., Golombek, M., Gómez, F., Hecht, M. H., … the SuperCam team and the Regolith working group. (2023). An Examination of Soil Crusts on the Floor of Jezero Crater, Mars. *Journal of Geophysical Research: Planets*, *128*(10), e2022JE007433. https://doi.org/10.1029/2022JE007433

Hausrath, E. M., Sullivan, R., Goreva, Y., Zorzano, M. P., Vaughan, A., Cousin, A., Siljeström, S., Sharma, S., Shumway, A. O., Kizovski, T., VanBommel, S. J., Tice, M., Knight, A., Martinez, G., Vicente-Retortillo, A., Mandon, L., Adcock, C. T., Madariaga, J. M., Población, I., … Group, the R. W. (2025). Collection and In Situ Analyses of Regolith Samples by the Mars 2020 Rover: Implications for Their Formation and Alteration History. *Journal of Geophysical Research: Planets*, *130*(2), e2023JE008046. https://doi.org/10.1029/2023JE008046

Hecht, M. H., Kounaves, S. P., Quinn, R. C., West, S. J., Young, S. M. M., Ming, D. W., Catling, D. C., Clark, B. C., Boynton, W. V., Hoffman, J., DeFlores, L. P., Gospodinova, K., Kapit, J., & Smith, P. H. (2009). Detection of Perchlorate and the Soluble Chemistry of Martian Soil at the Phoenix Lander Site. *Science*, *325*(5936), 64–67. https://doi.org/10.1126/science.1172466

Heinz, J., Schulze-Makuch, D., & Kounaves, S. P. (2016). Deliquescence-induced wetting and RSL-like darkening of a Mars analogue soil containing various perchlorate and chloride salts. *Geophysical Research Letters*, *43*(10), 4880–4884. https://doi.org/10.1002/2016GL068919

Heirwegh, C. M., Elam, W. T., O'Neil, L. P., Sinclair, K. P., & Das, A. (2022). The focused beam X-ray fluorescence elemental quantification software package PIQUANT. *Spectrochimica Acta Part B: Atomic Spectroscopy*, *196*, 106520. https://doi.org/10.1016/j.sab.2022.106520

Henneke, J., Klevang, D., Liu, Y., Jørgensen, J., Denver, T., Rice, M., VanBommel, S., Toldbo, C., Hurowitz, J., Tice, M., Tosca, N., Johnson, J., Winhold, A., Allwood, A., & Bell, J. (2023). A Radiometric Correction Method and Performance Characteristics for PIXL's Multispectral Analysis Using LEDs. *Space Science Reviews*, *219*(8), 68. https://doi.org/10.1007/s11214-023-01014-5

Henneke, J., Pedersen, D. A. K., Leif Jørgensen, J., Liu, Y., Allwood, A. C., Hurowitz, J., Schmidt, M. E., & VanBommel, S. J. (2022). *Profiling Martian Dust Using PIXL Images*. EGU22-11769. https://doi.org/10.5194/egusphere-egu22-11769

Hernández-Montenegro, J. D., Kizovski, T. V., Treiman, A. H., Li, A. Y., Asimow, P. D., Schmidt, M. E., Liu, Y., Labrie, J., Knight, A. L., Tice, M. M., Klevang, D. A., VanBommel, S., Wade, L. A., Hurowitz, J. A., Brown, A. J., Cable, M. L., & Allwood, A. C. (2025). Petrogenesis of the olivine cumulate outcrop *Issole* – The missing link between the Séítah and Máaz formations in Jezero crater, Mars. *Icarus*, *437*, 116620. https://doi.org/10.1016/j.icarus.2025.116620

Hillel, D. (1971). *Soil and Water: Physical Principles and Processes*. Academic Press.

Hoekstra, P., & Miller, R. D. (1967). On the mobility of water molecules in the transition layer between ice and a solid surface. *Journal of Colloid and Interface Science*, *25*(2), 166–173. https://doi.org/10.1016/0021-9797(67)90020-3

Hoganson, A. C. C., Afriat, A., Wernex, C. M., Ferguson, R. E., Rathore, H., Patel, D. N., Tappan, B., & Son, S. F. (2024). Novel Solid Propellants Enabled Through In Situ Martian Perchlorates. *Journal of Propulsion and Power*, *40*(3), 388–396. https://doi.org/10.2514/1.B39269

Horgan, B. H. N., Anderson, R. B., Dromart, G., Amador, E. S., & Rice, M. S. (2020). The mineral diversity of Jezero crater: Evidence for possible lacustrine carbonates on Mars. *Icarus*, *339*, 113526. https://doi.org/10.1016/j.icarus.2019.113526

Horgan, B. H. N., Garczynski, B., Gupta, S., Jones, A., Barnes, R., Hurowitz, J., Tice, M., Cardarelli, E. L., Russell, P. S., Wiens, R., Siljeström, S., Stack, K., Sholes, S., Bell, J. F., Johnson, J. R., Núñez, J., Randazzo, N., Simon, J. I., & Mars 2020 Science Team. (2024). *Campaign Overview and Initial Results from Exploration of the Margin Unit in*

Jezero Crater by the Perseverance Rover. *3040*, 2624. https://ui.adsabs.harvard.edu/abs/2024LPICo3040.2624H

Huber, C., Ojha, L., Lark, L., & Head, J. W. (2020). Physical models and predictions for recurring slope lineae formed by wet and dry processes. *Icarus*, *335*, 113385. https://doi.org/10.1016/j.icarus.2019.07.019

Hunten, D. M., & McElroy, M. B. (1970). Production and escape of hydrogen on Mars. *Journal of Geophysical Research (1896-1977)*, *75*(31), 5989–6001. https://doi.org/10.1029/JA075i031p05989

Hurowitz, J. A., Tice, M. M., Allwood, A. C., Cable, M. L., Bosak, T., Broz, A., Caravaca, G., Clark, B. C., Dehouck, E., Fairén, A. G., Gomez, F., Grotzinger, J., Gupta, S., Johnson, J. R., Kah, L. C., Kalucha, H., Labrie, J., Li, A. Y., Mandon, L., … Yanchilina, A. (2023). The Petrogenetic History of the Jezero Crater Delta Front from Microscale Observations by the Mars 2020 PIXL Instrument. *54th Lunar and Planetary Science Conference 2023*, *54*. https://hal.science/hal-04045097

Ingersoll, A. P. (1970). Mars: Occurrence of Liquid Water. *Science*, *168*(3934), 972–973. https://doi.org/10.1126/science.168.3934.972

Jakosky, B. M. (2021). Atmospheric Loss to Space and the History of Water on Mars. *Annual Review of Earth and Planetary Sciences*, *49*(1), 71–93. https://doi.org/10.1146/annurev-earth-062420-052845

Jakosky, B. M., Zent, A. P., & Zurek, R. W. (1997). The Mars Water Cycle: Determining the Role of Exchange with the Regolith. *Icarus*, *130*(1), 87–95. https://doi.org/10.1006/icar.1997.5799

Jaramillo, E. A., Royle, S. H., Claire, M. W., Kounaves, S. P., & Sephton, M. A. (2019). Indigenous Organic-Oxidized Fluid Interactions in the Tissint Mars Meteorite. *Geophysical Research Letters*, *46*(6), 3090–3098. https://doi.org/10.1029/2018GL081335

Jones, M. W. M., Flannery, D. T., Hurowitz, J. A., Tice, M. T., Schrank, C. E., Allwood, A. C., Tosca, N. J., Catling, D. C., VanBommel, S. J., Knight, A. L., Ganly, B., Siebach, K. L., Benison, K. C., Broz, A. P., Zorzano, M.-P., Heirwegh, C. M., Orenstein, B. J., Clark, B. C., Sinclair, K. P., … O'Neil, L. P. (2025). In situ crystallographic mapping constrains sulfate precipitation and timing in Jezero crater, Mars. *Science Advances*, *11*(16), eadt3048. https://doi.org/10.1126/sciadv.adt3048

Kalucha, H., Broz, A., Randazzo, N., Aramendia, J., Madariaga, J. M., Garczynski, B., Lanza, N., Mandon, L., Fouchet, T., Catling, D. C., Fairén, A. G., Kivrak, L., Gasda, P. J., Núñez, J. I., Cloutis, E., Hand, K. P., Rice Jr., J. W., Fischer, W. W., Maurice, S., & Wiens, R. C. (2024). Probable Concretions Observed in the Shenandoah Formation of Jezero Crater, Mars and Comparison With Terrestrial Analogs. *Journal of Geophysical Research: Planets*, *129*(8), e2023JE008138. https://doi.org/10.1029/2023JE008138

King, S., Toner, J., & Lin, P.-C. (2019). New evidence that seasonal RSL flows on Mars are dry, windblown sand avalanches. *The Astrobiology Science Conference (AbSciCon) 2019*, 343–374. https://ui.adsabs.harvard.edu/abs/2019absc.conf43374K/abstract

Kite, E. S., & Conway, S. (2024). Geological evidence for multiple climate transitions on Early Mars. *Nature Geoscience*, *17*(1), Article 1. https://doi.org/10.1038/s41561-023-01349-2

Kizovski, T. V., O'Neil, L., Schmidt, M., Hurowitz, J., Treiman, A., Pedersen, D., Liu, Y., Tice, M., Herd, C., Labrie, J., Christian, J., Knight, A., VanBommel, S., Moreland, E., Simon, J., & Allwood, A. (2023). Minor Minerals in the Jezero Crater Delta Analyzed by PIXL — Provenance and Mars Sample Return Implications. *Lunar and Planetary Science Conference*, *2806*, 2855. https://ui.adsabs.harvard.edu/abs/2023LPICo2806.2855K

Kleinhans, M. G., Markies, H., de Vet, S. J., in 't Veld, A. C., & Postema, F. N. (2011). Static and dynamic angles of repose in loose granular materials under reduced gravity. *Journal of Geophysical Research: Planets*, *116*(E11). https://doi.org/10.1029/2011JE003865

Klevang, D. A., Henneke, J., Benn, M., Denver, T., Jørgensen, P. S., Jørgensen, J. L., Wade, L. A., Denise, R., Elam, W. T., Van Beek, J., Cable, M., Hurowitz, J., & Allwood, A. (2024). Pre- and In-flight Performance of Terrain Relative Navigation on PIXL's Micro Context Camera, M2020. *2024 IEEE Aerospace Conference*, 1–14. https://doi.org/10.1109/AERO58975.2024.10521246

Klevang, D. A., Liebe, C. C., Henneke, J., Jørgensen, J. L., Sharrow, R., Setterfield, T., Wade, L., Sondheim, M., Foote, M., Elam, W. T., Heirwegh, C. M., Hurowitz, J., & Allwood, A. (2023). Pre-flight Geometric and Optical Calibration of the Planetary Instrument for X-ray Lithochemistry (PIXL). *Space Science Reviews*, *219*(1), 11. https://doi.org/10.1007/s11214-023-00955-1

Knight, A. L., VanBommel, S. J., Ganly, B., Yingst, R. A., Schmidt, M. E., Martínez, G. M., Vicente-Retortillo, Á., Jones, M. W. M., Shumway, A. O., Clark, B. C., Liu, Y., Flannery, D. T., Allwood, A. C., & Hurowitz, J. A. (2024). *Dust Accumulation on the PIXL Calibration Target: Phosphorus Enrichment and Role of Electrostatic Effects*. *3007*, 3393. https://ui.adsabs.harvard.edu/abs/2024LPICo3007.3393K

Kounaves, S. P., Carrier, B. L., O'Neil, G. D., Stroble, S. T., & Claire, M. W. (2014). Evidence of martian perchlorate, chlorate, and nitrate in Mars meteorite EETA79001: Implications for oxidants and organics. *Icarus*, *229*, 206–213. https://doi.org/10.1016/j.icarus.2013.11.012

Kounaves, S. P., Chaniotakis, N. A., Chevrier, V. F., Carrier, B. L., Folds, K. E., Hansen, V. M., McElhoney, K. M., O'Neil, G. D., & Weber, A. W. (2014). Identification of the perchlorate parent salts at the Phoenix Mars landing site and possible implications. *Icarus*, *232*, 226–231. https://doi.org/10.1016/j.icarus.2014.01.016

Kounaves, S. P., Hecht, M. H., Kapit, J., Quinn, R. C., Catling, D. C., Clark, B. C., Ming, D. W., Gospodinova, K., Hredzak, P., McElhoney, K., & Shusterman, J. (2010). Soluble sulfate in the martian soil at the Phoenix landing site. *Geophysical Research Letters*, *37*(9). https://doi.org/10.1029/2010GL042613

Leask, E. K., Ehlmann, B. L., Dundar, M. M., Murchie, S. L., & Seelos, F. P. (2018). Challenges in the Search for Perchlorate and Other Hydrated Minerals With 2.1-μm Absorptions on Mars. *Geophysical Research Letters*, *45*(22), 12,180-12,189. https://doi.org/10.1029/2018GL080077

Leshin, L. A., Mahaffy, P. R., Webster, C. R., Cabane, M., Coll, P., Conrad, P. G., Archer, P. D., Atreya, S. K., Brunner, A. E., Buch, A., Eigenbrode, J. L., Flesch, G. J., Franz, H. B., Freissinet, C., Glavin, D. P., McAdam, A. C., Miller, K. E., Ming, D. W., Morris, R. V., … Moores, J. E. (2013). Volatile, Isotope, and Organic Analysis of Martian Fines with the Mars Curiosity Rover. *Science*, *341*(6153), 1238937. https://doi.org/10.1126/science.1238937

Liu, Y., Tice, M. M., Schmidt, M. E., Treiman, A. H., Kizovski, T. V., Hurowitz, J. A., Allwood, A. C., Henneke, J., Pedersen, D. A. K., VanBommel, S. J., Jones, M. W. M., Knight, A. L., Orenstein, B. J., Clark, B. C., Elam, W. T., Heirwegh, C. M., Barber, T., Beegle, L. W., Benzerara, K., … Zorzano, M.-P. (2022). An olivine cumulate outcrop on the floor of Jezero crater, Mars. *Science*, *377*(6614), 1513–1519. https://doi.org/10.1126/science.abo2756

Maki, J. N., Gruel, D., McKinney, C., Ravine, M. A., Morales, M., Lee, D., Willson, R., Copley-Woods, D., Valvo, M., Goodsall, T., McGuire, J., Sellar, R. G., Schaffner, J. A., Caplinger, M. A., Shamah, J. M., Johnson, A. E., Ansari, H., Singh, K., Litwin, T., … Algermissen, S. (2020). The Mars 2020 Engineering Cameras and Microphone on the Perseverance Rover: A Next-Generation Imaging System for Mars Exploration. *Space Science Reviews*, *216*(8), 137. https://doi.org/10.1007/s11214-020-00765-9

Mangold, N., Dromart, G., Ansan, V., Salese, F., Kleinhans, M. G., Massé, M., Quantin-Nataf, C., & Stack, K. M. (2020). Fluvial Regimes, Morphometry, and Age of Jezero Crater Paleolake Inlet Valleys and Their Exobiological Significance for the 2020 Rover

Mission Landing Site. *Astrobiology*, *20*(8), 994–1013. https://doi.org/10.1089/ast.2019.2132

Marion, G. M., & Kargel, J. S. (2007). *Cold Aqueous Planetary Geochemistry with FREZCHEM: From Modeling to the Search for Life at the Limits*. Springer Science & Business Media.

Maurice, S., Wiens, R. C., Bernardi, P., Caïs, P., Robinson, S., Nelson, T., Gasnault, O., Reess, J.-M., Deleuze, M., Rull, F., Manrique, J.-A., Abbaki, S., Anderson, R. B., André, Y., Angel, S. M., Arana, G., Battault, T., Beck, P., Benzerara, K., … Wong, K. W. (2021). The SuperCam Instrument Suite on the Mars 2020 Rover: Science Objectives and Mast-Unit Description. *Space Science Reviews*, *217*(3), 47. https://doi.org/10.1007/s11214-021-00807-w

McCoy, T. J., Russell, S. S., Zega, T. J., Thomas-Keprta, K. L., Singerling, S. A., Brenker, F. E., Timms, N. E., Rickard, W. D. A., Barnes, J. J., Libourel, G., Ray, S., Corrigan, C. M., Haenecour, P., Gainsforth, Z., Dominguez, G., King, A. J., Keller, L. P., Thompson, M. S., Sandford, S. A., … Lauretta, D. S. (2025). An evaporite sequence from ancient brine recorded in Bennu samples. *Nature*, *637*(8048), 1072–1077. https://doi.org/10.1038/s41586-024-08495-6

McEwen, A. S., Dundas, C. M., Mattson, S. S., Toigo, A. D., Ojha, L., Wray, J. J., Chojnacki, M., Byrne, S., Murchie, S. L., & Thomas, N. (2014). Recurring slope lineae in equatorial regions of Mars. *Nature Geoscience*, *7*(1), 53–58. https://doi.org/10.1038/ngeo2014

McEwen, A. S., Eliason, E. M., Bergstrom, J. W., Bridges, N. T., Hansen, C. J., Delamere, W. A., Grant, J. A., Gulick, V. C., Herkenhoff, K. E., Keszthelyi, L., Kirk, R. L., Mellon, M. T., Squyres, S. W., Thomas, N., & Weitz, C. M. (2007). Mars Reconnaissance Orbiter's High Resolution Imaging Science Experiment (HiRISE). *Journal of Geophysical Research: Planets*, *112*(E5). https://doi.org/10.1029/2005JE002605

McEwen, A. S., Ojha, L., Dundas, C. M., Mattson, S. S., Byrne, S., Wray, J. J., Cull, S. C., Murchie, S. L., Thomas, N., & Gulick, V. C. (2011). Seasonal Flows on Warm Martian Slopes. *Science*, *333*(6043), 740–743. https://doi.org/10.1126/science.1204816

McEwen, A. S., Schaefer, E. I., Dundas, C. M., Sutton, S. S., Tamppari, L. K., & Chojnacki, M. (2021). Mars: Abundant Recurring Slope Lineae (RSL) Following the Planet-Encircling Dust Event (PEDE) of 2018. *Journal of Geophysical Research: Planets*, *126*(4), e2020JE006575. https://doi.org/10.1029/2020JE006575

McSween, H. Y., & Keil, K. (2000). Mixing relationships in the Martian regolith and the composition of globally homogeneous dust. *Geochimica et Cosmochimica Acta*, *64*(12), 2155–2166. https://doi.org/10.1016/S0016-7037(99)00401-9

Meisner, A., Snoek, B. L., Nesme, J., Dent, E., Jacquiod, S., Classen, A. T., & Priemé, A. (2021). Soil microbial legacies differ following drying-rewetting and freezing-thawing cycles. *The ISME Journal*, *15*(4), 1207–1221. https://doi.org/10.1038/s41396-020-00844-3

Meslin, P.-Y., Gasnault, O., Forni, O., Schröder, S., Cousin, A., Berger, G., Clegg, S. M., Lasue, J., Maurice, S., Sautter, V., Le Mouélic, S., Wiens, R. C., Fabre, C., Goetz, W., Bish, D., Mangold, N., Ehlmann, B., Lanza, N., Harri, A.-M., … Berger, J. (2013). Soil

Diversity and Hydration as Observed by ChemCam at Gale Crater, Mars. *Science*, *341*(6153), 1238670. https://doi.org/10.1126/science.1238670

Ming, D. W., Archer, P. D., Glavin, D. P., Eigenbrode, J. L., Franz, H. B., Sutter, B., Brunner, A. E., Stern, J. C., Freissinet, C., McAdam, A. C., Mahaffy, P. R., Cabane, M., Coll, P., Campbell, J. L., Atreya, S. K., Niles, P. B., Bell, J. F., Bish, D. L., Brinckerhoff, W. B., … Moores, J. E. (2014). Volatile and Organic Compositions of Sedimentary Rocks in Yellowknife Bay, Gale Crater, Mars. *Science*, *343*(6169), 1245267. https://doi.org/10.1126/science.1245267

Minitti, M. E., Kah, L. C., Yingst, R. A., Edgett, K. S., Anderson, R. C., Beegle, L. W., Carsten, J. L., Deen, R. G., Goetz, W., Hardgrove, C., Harker, D. E., Herkenhoff, K. E., Hurowitz, J. A., Jandura, L., Kennedy, M. R., Kocurek, G., Krezoski, G. M., Kuhn, S. R., Limonadi, D., … Van Beek, T. (2013). MAHLI at the Rocknest sand shadow: Science and science-enabling activities. *Journal of Geophysical Research: Planets*, *118*(11), 2338–2360. https://doi.org/10.1002/2013JE004426

Moeller, R. C., Jandura, L., Rosette, K., Robinson, M., Samuels, J., Silverman, M., Brown, K., Duffy, E., Yazzie, A., Jens, E., Brockie, I., White, L., Goreva, Y., Zorn, T., Okon, A., Lin, J., Frost, M., Collins, C., Williams, J. B., … Biesiadecki, J. (2020). The Sampling and Caching Subsystem (SCS) for the Scientific Exploration of Jezero Crater by the Mars 2020 Perseverance Rover. *Space Science Reviews*, *217*(1), 5. https://doi.org/10.1007/s11214-020-00783-7

Möhlmann, D. (2004). Water in the upper martian surface at mid- and low-latitudes: Presence, state, and consequences. *Icarus*, *168*(2), 318–323. https://doi.org/10.1016/j.icarus.2003.11.008

Möhlmann, D. (2005). Adsorption Water-Related Potential Chemical and Biological Processes in the Upper Martian Surface. *Astrobiology*, *5*(6), 770–777. https://doi.org/10.1089/ast.2005.5.770

Moore, H. J., Bickler, D. B., Crisp, J. A., Eisen, H. J., Gensler, J. A., Haldemann, A. F. C., Matijevic, J. R., Reid, L. K., & Pavlics, F. (1999). Soil-like deposits observed by Sojourner, the Pathfinder rover. *Journal of Geophysical Research: Planets*, *104*(E4), 8729–8746. https://doi.org/10.1029/1998JE900005

Moreland, E. L., Siebach, K. L., Costin, G., Tice, M. M., Hurowitz, J. A., Treiman, A. H., Simon, J. I., Liu, Y., Jiang, Y., Udry, A., & Dehouck, E. (submitted). Mineral Identifications in PIXL XRF Data from the First 1100 Sols of the Mars 2020 Mission Using the MIST Algorithm. *Journal of Geophysical Research: Planets*.

Morris, R. V., Ming, D. W., Gellert, R., Vaniman, D. T., Bish, D. L., Blake, D. F., Chipera, S. J., Morrison, S. M., Downs, R. T., Rampe, E. B., Treiman, A. H., Yen, A. S., Achilles, C. N., Archer, P. D., Bristow, T. F., Cavanaugh, P., Fenrdrich, K., Crisp, J. A., Des Marais, D. J., … Morookian, J. M. (2015, March 16). *Update on the Chemical Composition Of Crystalline, Smectite, and Amorphous Components for Rocknest Soil and John Klein and Cumberland Mudstone Drill Fines at Gale Crater, Mars*. Lunar and Planetary Science Conference, The Woodlands, TX. https://ntrs.nasa.gov/citations/20150001942

Navarro-González, R., Vargas, E., de la Rosa, J., Raga, A. C., & McKay, C. P. (2010). Reanalysis of the Viking results suggests perchlorate and organics at midlatitudes on Mars. *Journal of Geophysical Research: Planets*, *115*(E12). https://doi.org/10.1029/2010JE003599

Nemere, P., Barber, T., Galvin, A., Fedell, S. M., Stonebraker, R., Wright, A. P., & Davidoff, S. (2024). *PIXLISE* [Computer software]. https://www.pixlise.org/

Newman, C. E., Lewis, S. R., Read, P. L., & Forget, F. (2002). Modeling the Martian dust cycle, 1. Representations of dust transport processes. *Journal of Geophysical Research: Planets*, *107*(E12), 6-1-6–18. https://doi.org/10.1029/2002JE001910

Nikolakakos, G., & Whiteway, J. A. (2015). Laboratory investigation of perchlorate deliquescence at the surface of Mars with a Raman scattering lidar. *Geophysical Research Letters*, *42*(19), 7899–7906. https://doi.org/10.1002/2015GL065434

Nimmo, F., & Tanaka, K. (2005). EARLY CRUSTAL EVOLUTION OF MARS1. *Annual Review of Earth and Planetary Sciences*, *33*(Volume 33, 2005), 133–161. https://doi.org/10.1146/annurev.earth.33.092203.122637

Niziński, P., Błażewicz, A., Kończyk, J., & Michalski, R. (2021). Perchlorate – properties, toxicity and human health effects: An updated review. *Reviews on Environmental Health*, *36*(2), 199–222. https://doi.org/10.1515/reveh-2020-0006

Nuding, D. L., Davis, R. D., Gough, R. V., & Tolbert, M. A. (2015). The aqueous stability of a Mars salt analog: Instant Mars. *Journal of Geophysical Research: Planets*, *120*(3), 588–598. https://doi.org/10.1002/2014JE004722

Nuding, D. L., Rivera-Valentin, E. G., Davis, R. D., Gough, R. V., Chevrier, V. F., & Tolbert, M. A. (2014). Deliquescence and efflorescence of calcium perchlorate: An investigation of stable aqueous solutions relevant to Mars. *Icarus*, *243*, 420–428. https://doi.org/10.1016/j.icarus.2014.08.036

O'Connell-Cooper, C. D., Spray, J. G., Thompson, L. M., Gellert, R., Berger, J. A., Boyd, N. I., Desouza, E. D., Perrett, G. M., Schmidt, M., & VanBommel, S. J. (2017). APXS-derived chemistry of the Bagnold dune sands: Comparisons with Gale Crater soils and the global Martian average. *Journal of Geophysical Research: Planets*, *122*(12), 2623–2643. https://doi.org/10.1002/2017JE005268

O'Connell-Cooper, C. D., Thompson, L. M., Spray, J. G., Berger, J. A., VanBommel, S. J., Gellert, R., Boyd, N. I., & DeSouza, E. (2018). Chemical Diversity of Sands Within the Linear and Barchan Dunes of the Bagnold Dunes, Gale Crater, as Revealed by APXS Onboard Curiosity. *Geophysical Research Letters*, *45*(18), 9460–9470. https://doi.org/10.1029/2018GL079026

Ojha, L., Lewis, K., Karunatillake, S., & Schmidt, M. (2018). The Medusae Fossae Formation as the single largest source of dust on Mars. *Nature Communications*, *9*(1), 2867. https://doi.org/10.1038/s41467-018-05291-5

Ojha, L., McEwen, A., Dundas, C., Byrne, S., Mattson, S., Wray, J., Masse, M., & Schaefer, E. (2014). HiRISE observations of Recurring Slope Lineae (RSL) during southern summer on Mars. *Icarus*, *231*, 365–376. https://doi.org/10.1016/j.icarus.2013.12.021

Ojha, L., Wilhelm, M. B., Murchie, S. L., McEwen, A. S., Wray, J. J., Hanley, J., Massé, M., & Chojnacki, M. (2015). Spectral evidence for hydrated salts in recurring slope lineae on Mars. *Nature Geoscience*, *8*(11), 829–832. https://doi.org/10.1038/ngeo2546

Orenstein, B. J., Jones, M. W. M., Flannery, D. T., Wright, A. P., Davidoff, S., Tice, M. M., Nothdurft, L., & Allwood, A. C. (2024). In-situ mapping of monocrystalline regions on Mars. *Icarus*, *420*, 116202. https://doi.org/10.1016/j.icarus.2024.116202

Origins, Worlds, and Life: A Decadal Strategy for Planetary Science and Astrobiology 2023-2032 (with Committee on the Planetary Science and Astrobiology Decadal Survey, Space Studies Board, Division on Engineering and Physical Sciences, & National Academies of Sciences, Engineering, and Medicine). (2023). National Academies Press. https://doi.org/10.17226/26522

Pedregosa, F., Varoquaux, G., Gramfort, A., Michel, V., Thirion, B., Grisel, O., Blondel, M., Prettenhofer, P., Weiss, R., Dubourg, V., Vanderplas, J., Passos, A., Cournapeau, D., Brucher, M., Perrot, M., & Duchesnay, É. (2011). Scikit-learn: Machine Learning in Python. *Journal of Machine Learning Research*, *12*(85), 2825–2830.

Pestova, O. N., Myund, L. A., Khripun, M. K., & Prigaro, A. V. (2005). Polythermal Study of the Systems M(ClO4)2-H2O (M2+ = Mg2+, Ca2+, Sr2+, Ba2+). *Russian Journal of Applied Chemistry*, *78*(3), 409–413. https://doi.org/10.1007/s11167-005-0306-z

Peters, G. H., Abbey, W., Bearman, G. H., Mungas, G. S., Smith, J. A., Anderson, R. C., Douglas, S., & Beegle, L. W. (2008). Mojave Mars simulant—Characterization of a new geologic Mars analog. *Icarus*, *197*(2), 470–479. https://doi.org/10.1016/j.icarus.2008.05.004

Phua, Y. Y., Ehlmann, B. L., Siljeström, S., Czaja, A. D., Beck, P., Connell, S., Wiens, R. C., Jakubek, R. S., Williams, R. M. E., Zorzano, M.-P., Minitti, M. E., Pascuzzo, A. C., Hand, K. P., Bhartia, R., Kah, L. C., Mandon, L., Razzell Hollis, J., Scheller, E. L., Sharma, S., … Yanchilina, A. G. (2024). Characterizing Hydrated Sulfates and Altered Phases in Jezero Crater Fan and Floor Geologic Units With SHERLOC on Mars 2020. *Journal of Geophysical Research: Planets*, *129*(7), e2023JE008251. https://doi.org/10.1029/2023JE008251

Polkko, J., Hieta, M., Harri, A.-M., Tamppari, L., Martínez, G., Viúdez-Moreiras, D., Savijärvi, H., Conrad, P., Zorzano Mier, M. P., De La Torre Juarez, M., Hueso, R., Munguira, A., Leino, J., Gómez, F., Jaakonaho, I., Fischer, E., Genzer, M., Apestigue, V., Arruego, I., … Team, M. (2023). Initial Results of the Relative Humidity Observations by MEDA Instrument Onboard the Mars 2020 Perseverance Rover. *Journal of Geophysical Research: Planets*, *128*(2), e2022JE007447. https://doi.org/10.1029/2022JE007447

Pommerol, A., Schmitt, B., Beck, P., & Brissaud, O. (2009). Water sorption on martian regolith analogs: Thermodynamics and near-infrared reflectance spectroscopy. *Icarus*, *204*(1), 114–136. https://doi.org/10.1016/j.icarus.2009.06.013

Preston, S. L., Siebach, K. L., Lapôtre, M. G. A., & Banham, S. G. (2024). Grain Size Measurements of the Eolian Stimson Formation, Gale Crater, Mars and Implications for Sand Provenance and Paleoatmospheric Conditions. *Journal of Geophysical Research: Planets*, *129*(11), e2024JE008369. https://doi.org/10.1029/2024JE008369

Primm, K. M., Gough, R. V., Wong, J., Rivera-Valentin, E. G., Martinez, G. M., Hogancamp, J. V., Archer, P. D., Ming, D. W., & Tolbert, M. A. (2018). The Effect of Mars-Relevant Soil

Analogs on the Water Uptake of Magnesium Perchlorate and Implications for the Near-Surface of Mars. *Journal of Geophysical Research: Planets*, *123*(8), 2076–2088. https://doi.org/10.1029/2018JE005540

Rampe, E. B., Blake, D. F., Bristow, T. F., Ming, D. W., Vaniman, D. T., Morris, R. V., Achilles, C. N., Chipera, S. J., Morrison, S. M., Tu, V. M., Yen, A. S., Castle, N., Downs, G. W., Downs, R. T., Grotzinger, J. P., Hazen, R. M., Treiman, A. H., Peretyazhko, T. S., Des Marais, D. J., … Wiens, R. C. (2020). Mineralogy and geochemistry of sedimentary rocks and eolian sediments in Gale crater, Mars: A review after six Earth years of exploration with *Curiosity*. *Geochemistry*, *80*(2), 125605. https://doi.org/10.1016/j.chemer.2020.125605

Rampe, E. B., Lapotre, M. G. A., Bristow, T. F., Arvidson, R. E., Morris, R. V., Achilles, C. N., Weitz, C., Blake, D. F., Ming, D. W., Morrison, S. M., Vaniman, D. T., Chipera, S. J., Downs, R. T., Grotzinger, J. P., Hazen, R. M., Peretyazhko, T. S., Sutter, B., Tu, V., Yen, A. S., … Treiman, A. H. (2018). Sand Mineralogy Within the Bagnold Dunes, Gale Crater, as Observed In Situ and From Orbit. *Geophysical Research Letters*, *45*(18), 9488–9497. https://doi.org/10.1029/2018GL079073

Rard, J. A., & Platford, R. F. (1991). Experimental Methods: Isopiestic. In *Activity Coefficients in Electrolyte Solutions* (pp. 209–277). CRC Press.

Rice, M. S., Johnson, J. R., Million, C. C., St. Clair, M., Horgan, B. N., Vaughan, A., Núñez, J. I., Garczynski, B., Curtis, S., Kinch, K. B., Merusi, M., Hayes, A., Bell, J. F., Duflot, L., Lapo, K., Evans, A. A., Eng, A., Cloutis, E., Brown, A., & Annex, A. M. (2023). Spectral Variability of Rocks and Soils on the Jezero Crater Floor: A Summary of Multispectral

Observations From Perseverance's Mastcam-Z Instrument. *Journal of Geophysical Research: Planets*, *128*(10), e2022JE007548. https://doi.org/10.1029/2022JE007548

Rivera-Valentín, E. G., Chevrier, V. F., Soto, A., & Martínez, G. (2020). Distribution and habitability of (meta)stable brines on present-day Mars. *Nature Astronomy*, *4*(8), 756–761. https://doi.org/10.1038/s41550-020-1080-9

Rodriguez-Manfredi, J. A., de la Torre Juárez, M., Alonso, A., Apéstigue, V., Arruego, I., Atienza, T., Banfield, D., Boland, J., Carrera, M. A., Castañer, L., Ceballos, J., Chen-Chen, H., Cobos, A., Conrad, P. G., Cordoba, E., del Río-Gaztelurrutia, T., de Vicente-Retortillo, A., Domínguez-Pumar, M., Espejo, S., … The MEDA team. (2021). The Mars Environmental Dynamics Analyzer, MEDA. A Suite of Environmental Sensors for the Mars 2020 Mission. *Space Science Reviews*, *217*(3), 48. https://doi.org/10.1007/s11214-021-00816-9

Royer, C., Poulet, F., Wiens, R. C., Montmessin, F., Beck, P., Beyssac, O., Clavé, É., Dehouck, E., Fouchet, T., Johnson, J. R., Mandon, L., Bernard, S., Caravaca, G., Le Mouélic, S., Pilorget, C., Quantin-Nataf, C., Maurice, S., & Cousin, A. (2025). The mineralogical composition of Jezero Crater Western Fan: Multigaussian modeling of Perseverance/SuperCam near-infrared observations and overview of major units. *Icarus*, *434*, 116538. https://doi.org/10.1016/j.icarus.2025.116538

Rummel, J. D., Beaty, D. W., Jones, M. A., Bakermans, C., Barlow, N. G., Boston, P. J., Chevrier, V. F., Clark, B. C., de Vera, J.-P. P., Gough, R. V., Hallsworth, J. E., Head, J. W., Hipkin, V. J., Kieft, T. L., McEwen, A. S., Mellon, M. T., Mikucki, J. A., Nicholson, W. L., Omelon, C. R., … Wray, J. J. (2014). A New Analysis of Mars "Special Regions":

Findings of the Second MEPAG Special Regions Science Analysis Group (SR-SAG2). *Astrobiology*, *14*(11), 887–968. https://doi.org/10.1089/ast.2014.1227

Savijärvi, H. I., & Harri, A.-M. (2021). Water vapor adsorption on Mars. *Icarus*, *357*, 114270. https://doi.org/10.1016/j.icarus.2020.114270

Scheller, E. L., Razzell Hollis, J., Cardarelli, E. L., Steele, A., Beegle, L. W., Bhartia, R., Conrad, P., Uckert, K., Sharma, S., Ehlmann, B. L., Abbey, W. J., Asher, S. A., Benison, K. C., Berger, E. L., Beyssac, O., Bleefeld, B. L., Bosak, T., Brown, A. J., Burton, A. S., … Zorzano, M.-P. (2022). Aqueous alteration processes in Jezero crater, Mars—Implications for organic geochemistry. *Science*, *378*(6624), 1105–1110. https://doi.org/10.1126/science.abo5204

Schmidt, M. E., Allwood, A., Cable, M. L., Clark, B. C., Hausrath, E. M., Henneke, J., Hurowitz, J. A., Kizovski, T. V., Klevang, D. A., Shumway, A., Tice, M., VanBommel, S., Bedford, C. C., & Brown, A. (2024). *Volcanic Plume Origin for Widespread, Indurated Surface Coatings in Jezero Crater*. *3040*, 1954. https://ui.adsabs.harvard.edu/abs/2024LPICo3040.1954S

Schmidt, M. E., Kizovski, T. V., Liu, Y., Hernandez-Montenegro, J. D., Tice, M. M., Treiman, A. H., Hurowitz, J. A., Klevang, D. A., Knight, A. L., Labrie, J., Tosca, N. J., VanBommel, S. J., Benaroya, S., Crumpler, L. S., Horgan, B. H. N., Morris, R. V., Simon, J. I., Udry, A., Yanchilina, A., … Wadhwa, M. (2025). Diverse and highly differentiated lava suite in Jezero crater, Mars: Constraints on intracrustal magmatism revealed by Mars 2020 PIXL. *Science Advances*, *11*(4), eadr2613. https://doi.org/10.1126/sciadv.adr2613

Schmidt, M. E., Perrett, G. M., Bray, S. L., Bradley, N. J., Lee, R. E., Berger, J. A., Campbell, J. L., Ly, C., Squyres, S. W., & Tesselaar, D. (2018). Dusty Rocks in Gale Crater: Assessing Areal Coverage and Separating Dust and Rock Contributions in APXS Analyses. *Journal of Geophysical Research: Planets*, *123*(7), 1649–1673. https://doi.org/10.1029/2018JE005553

Sherman, J. (1955). The theoretical derivation of fluorescent X-ray intensities from mixtures. *Spectrochimica Acta*, *7*, 283–306. https://doi.org/10.1016/0371-1951(55)80041-0

Shumway, A. O., Catling, D. C., & Toner, J. D. (2023a). Regolith Inhibits Salt and Ice Crystallization in Mg(ClO4)2 Brine, Implying More Persistent and Potentially Habitable Brines on Mars. *The Planetary Science Journal*, *4*(8), 143. https://doi.org/10.3847/PSJ/ace891

Shumway, A. O., Catling, D. C., & Toner, J. D. (2023b). *Regolith Inhibits Salt Crystallization in Magnesium Perchlorate Brine, Suggesting More Persistent and Habitable Brines on Mars*. *2806*, 2478. https://ui.adsabs.harvard.edu/abs/2023LPICo2806.2478S

Siebach, K. L., Moreland, E. L., Costin, G., & Jiang. (submitted). Mineral Identification by Stoichiometry (MIST) Algorithm. *Computers and Geoscience*.

Siljeström, S., Czaja, A. D., Corpolongo, A., Berger, E. L., Li, A. Y., Cardarelli, E., Abbey, W., Asher, S. A., Beegle, L. W., Benison, K. C., Bhartia, R., Bleefeld, B. L., Burton, A. S., Bykov, S. V., Clark, B., DeFlores, L., Ehlmann, B. L., Fornaro, T., Fox, A., … Zorzano, M.-P. (2024). Evidence of Sulfate-Rich Fluid Alteration in Jezero Crater Floor, Mars.

Journal of Geophysical Research: Planets, *129*(1), e2023JE007989. https://doi.org/10.1029/2023JE007989

Slank, R. A., Rivera-Valentín, E. G., & Chevrier, V. F. (2022). Experimental Constraints on Deliquescence of Calcium Perchlorate Mixed with a Mars Regolith Analog. *The Planetary Science Journal*, *3*(7), 154. https://doi.org/10.3847/PSJ/ac75c4

Squyres, S. W. (1984). The History of Water on Mars. *Annual Review of Earth and Planetary Sciences*, *12*(Volume 12, 1984), 83–106. https://doi.org/10.1146/annurev.ea.12.050184.000503

Squyres, S. W., Knoll, A. H., Arvidson, R. E., Clark, B. C., Grotzinger, J. P., Jolliff, B. L., McLennan, S. M., Tosca, N., Bell, J. F., Calvin, W. M., Farrand, W. H., Glotch, T. D., Golombek, M. P., Herkenhoff, K. E., Johnson, J. R., Klingelhöfer, G., McSween, H. Y., & Yen, A. S. (2006). Two Years at Meridiani Planum: Results from the Opportunity Rover. *Science*, *313*(5792), 1403–1407. https://doi.org/10.1126/science.1130890

Stack, K. M., Ives, L. R. W., Gupta, S., Lamb, M. P., Tebolt, M., Caravaca, G., Grotzinger, J. P., Russell, P., Shuster, D. L., Williams, A. J., Amundsen, H., Alwmark, S., Annex, A. M., Barnes, R., Bell III, J., Beyssac, O., Bosak, T., Crumpler, L. S., Dehouck, E., … Wiens, R. C. (2024). Sedimentology and Stratigraphy of the Shenandoah Formation, Western Fan, Jezero Crater, Mars. *Journal of Geophysical Research: Planets*, *129*(2), e2023JE008187. https://doi.org/10.1029/2023JE008187

Stevenson, A., Hamill, P. G., O’Kane, C. J., Kminek, G., Rummel, J. D., Voytek, M. A., Dijksterhuis, J., & Hallsworth, J. E. (2017). Aspergillus penicillioides differentiation and cell division at 0.585 water activity. *Environmental Microbiology*, *19*(2), 687–697. https://doi.org/10.1111/1462-2920.13597

Stillman, D. E., Bue, B. D., Wagstaff, K. L., Primm, K. M., Michaels, T. I., & Grimm, R. E. (2020). Evaluation of wet and dry recurring slope lineae (RSL) formation mechanisms based on quantitative mapping of RSL in Garni Crater, Valles Marineris, Mars. *Icarus*, *335*, 113420. https://doi.org/10.1016/j.icarus.2019.113420

Stillman, D. E., & Grimm, R. E. (2011). Dielectric signatures of adsorbed and salty liquid water at the Phoenix landing site, Mars. *Journal of Geophysical Research: Planets*, *116*(E9). https://doi.org/10.1029/2011JE003838

Stillman, D. E., & Grimm, R. E. (2018). Two pulses of seasonal activity in martian southern mid-latitude recurring slope lineae (RSL). *Icarus*, *302*, 126–133. https://doi.org/10.1016/j.icarus.2017.10.026

Stillman, D. E., Grimm, R. E., & Dec, S. F. (2010). Low-Frequency Electrical Properties of Ice−Silicate Mixtures. *The Journal of Physical Chemistry B*, *114*(18), 6065–6073. https://doi.org/10.1021/jp9070778

Stillman, D. E., Michaels, T. I., & Grimm, R. E. (2017). Characteristics of the numerous and widespread recurring slope lineae (RSL) in Valles Marineris, Mars. *Icarus*, *285*, 195–210. https://doi.org/10.1016/j.icarus.2016.10.025

Stillman, D. E., Michaels, T. I., Grimm, R. E., & Hanley, J. (2016). Observations and modeling of northern mid-latitude recurring slope lineae (RSL) suggest recharge by a present-day martian briny aquifer. *Icarus*, *265*, 125–138. https://doi.org/10.1016/j.icarus.2015.10.007

Stillman, D. E., Michaels, T. I., Grimm, R. E., & Harrison, K. P. (2014). New observations of martian southern mid-latitude recurring slope lineae (RSL) imply formation by freshwater subsurface flows. *Icarus*, *233*, 328–341. https://doi.org/10.1016/j.icarus.2014.01.017

Sullivan, R., Anderson, R., Biesiadecki, J., Bond, T., & Stewart, H. (2011). Cohesions, friction angles, and other physical properties of Martian regolith from Mars Exploration Rover wheel trenches and wheel scuffs. *Journal of Geophysical Research: Planets*, *116*(E2). https://doi.org/10.1029/2010JE003625

Sutter, B., Quinn, R. C., Archer, P. D., Glavin, D. P., Glotch, T. D., Kounaves, S. P., Osterloo, M. M., Rampe, E. B., & Ming, D. W. (2017). Measurements of Oxychlorine species on Mars. *International Journal of Astrobiology*, *16*(3), 203–217. https://doi.org/10.1017/S1473550416000057

Taylor, S. R., & McLennan, S. (2009). *Planetary Crusts: Their Composition, Origin and Evolution*. Cambridge University Press.

Tebolt, M., Levy, J., Goudge, T., & Schorghofer, N. (2020). Slope, elevation, and thermal inertia trends of martian recurring slope lineae initiation and termination points: Multiple possible processes occurring on coarse, sandy slopes. *Icarus*, *338*, 113536. https://doi.org/10.1016/j.icarus.2019.113536

Tice, M. M., Hurowitz, J. A., Allwood, A. C., Jones, M. W. M., Orenstein, B. J., Davidoff, S., Wright, A. P., Pedersen, D. A. K., Henneke, J., Tosca, N. J., Moore, K. R., Clark, B. C., McLennan, S. M., Flannery, D. T., Steele, A., Brown, A. J., Zorzano, M.-P., Hickman-Lewis, K., Liu, Y., … THE PIXL TEAM. (2022). Alteration history of Séítah formation rocks inferred by PIXL x-ray fluorescence, x-ray diffraction, and multispectral imaging on Mars. *Science Advances*, *8*(47), eabp9084. https://doi.org/10.1126/sciadv.abp9084

Tice, M. M., O'Neil, L. P., Clark, B. C., Ganly, B. P., Jones, M. W. M., Orenstein, B. J., Flannery, D. A., VanBommel, S. J., Schmidt, M. E., Nemere, P., Davidoff, S., Galvin, A., Heirwegh, C., Elam, W. T., Wade, L., Allwood, A. C., & Hurowitz, J. A. (2023). *PIXL on Perseverance as a Complete X-ray Spectroscopic Instrument: Analyzing X-ray Fluorescence, Scattering, and Diffraction in Martian Rocks*. *2806*, 2659. https://ui.adsabs.harvard.edu/abs/2023LPICo2806.2659T

Toner, J. D., & Catling, D. C. (2016). Water activities of NaClO4, Ca(ClO4)2, and Mg(ClO4)2 brines from experimental heat capacities: Water activity >0.6 below 200K. *Geochimica et Cosmochimica Acta*, *181*, 164–174. https://doi.org/10.1016/j.gca.2016.03.005

Toner, J. D., & Catling, D. C. (2018). Chlorate brines on Mars: Implications for the occurrence of liquid water and deliquescence. *Earth and Planetary Science Letters*, *497*, 161–168. https://doi.org/10.1016/j.epsl.2018.06.011

Toner, J. D., Catling, D. C., & Light, B. (2014a). Soluble salts at the Phoenix Lander site, Mars: A reanalysis of the Wet Chemistry Laboratory data. *Geochimica et Cosmochimica Acta*, *136*, 142–168. https://doi.org/10.1016/j.gca.2014.03.030

Toner, J. D., Catling, D. C., & Light, B. (2014b). The formation of supercooled brines, viscous liquids, and low-temperature perchlorate glasses in aqueous solutions relevant to Mars. *Icarus*, *233*, 36–47. https://doi.org/10.1016/j.icarus.2014.01.018

Toner, J. D., Catling, D. C., & Light, B. (2015a). A revised Pitzer model for low-temperature soluble salt assemblages at the Phoenix site, Mars. *Geochimica et Cosmochimica Acta*, *166*, 327–343. https://doi.org/10.1016/j.gca.2015.06.011

Toner, J. D., Catling, D. C., & Light, B. (2015b). Modeling salt precipitation from brines on Mars: Evaporation versus freezing origin for soil salts. *Icarus*, *250*, 451–461. https://doi.org/10.1016/j.icarus.2014.12.013

Toner, J. D., Sletten, R. S., Liu, L., Catling, D. C., Ming, D. W., Mushkin, A., & Lin, P.-C. (2022). Wet streaks in the McMurdo Dry Valleys, Antarctica: Implications for Recurring Slope Lineae on Mars. *Earth and Planetary Science Letters*, *589*, 117582. https://doi.org/10.1016/j.epsl.2022.117582

Tosca, N. J., Agee, C. B., Cockell, C. S., Glavin, D. P., Hutzler, A., Marty, B., McCubbin, F. M., Regberg, A. B., Velbel, M. A., Kminek, G., Meyer, M. A., Beaty, D. W., Carrier, B. L., Haltigin, T., Hays, L. E., Busemann, H., Cavalazzi, B., Debaille, V., Grady, M. M., … Zorzano, M.-P. (2022). Time-Sensitive Aspects of Mars Sample Return (MSR) Science. *Astrobiology*, *22*(S1), S-81. https://doi.org/10.1089/ast.2021.0115

Tosca, N. J., Tice, M. M., Hurowitz, J. A., Pedersen, D. A. K., Henneke, J., Mandon, L., McCubbin, F. M., Schmidt, M. E., Kizovski, T. V., Liu, Y., & Li, A. Y. (in review). In-situ Evidence for Serpentinization Within the Maaz Formation, Jezero Crater, Mars. *Science Advances*.

Udry, A., Ostwald, A., Sautter, V., Cousin, A., Beyssac, O., Forni, O., Dromart, G., Benzerara, K., Nachon, M., Horgan, B., Mandon, L., Clavé, E., Dehouck, E., Gibbons, E., Alwmark, S., Ravanis, E., Wiens, R. C., Legett, C., Anderson, R., … Team, the S.

(2023). A Mars 2020 Perseverance SuperCam Perspective on the Igneous Nature of the Máaz Formation at Jezero Crater and Link With Séítah, Mars. *Journal of Geophysical Research: Planets*, *128*(7), e2022JE007440. https://doi.org/10.1029/2022JE007440

van Es, H. (2017). A New Definition of Soil. *CSA News*, *62*(10), 20–21. https://doi.org/10.2134/csa2017.62.1016

VanBommel, S. J. (2024). *X-Ray Interrogation Effects in APXS and PIXL Data*. 10th International Conference on Mars, Pasadena, CA. https://www.hou.usra.edu/meetings/tenthmars2024/pdf/3044.pdf

VanBommel, S. J., Berger, J. A., Gellert, R., O'Connell-Cooper, C. D., McCraig, M. A., Thompson, L. M., Fedo, C. M., Des Marais, D. J., Fey, D. M., Yen, A. S., Clark, B. C., Treiman, A. H., & Boyd, N. I. (2023). Elemental composition of manganese- and phosphorus-rich nodules in the Knockfarril Hill member, Gale crater, Mars. *Icarus*, *392*, 115372. https://doi.org/10.1016/j.icarus.2022.115372

VanBommel, S. J., Gellert, R., Berger, J. A., McCraig, M. A., O'Connell-Cooper, C. D., Thompson, L. M., Yen, A. S., Boyd, N. I., & Knight, A. L. (2022). *High-Throughput Modeling of Surface Coatings and Layering Effects in Mars X-Ray Fluorescence Data*. *2678*, 1587. https://ui.adsabs.harvard.edu/abs/2022LPICo2678.1587V

VanBommel, S. J., Knight, A. L., Hurowitz, J. A., Lanza, N. L., & Ollila, A. M. (2023). *Laboratory Measurements of Surface Layers and Coatings with PIXL*. *2806*, 1215. https://ui.adsabs.harvard.edu/abs/2023LPICo2806.1215V

VanBommel, S. J., Knight, A. L., Schmidt, M. E., Yingst, R. A., Henneke, J., Klevang, D., Allwood, A. C., Tice, M. M., Cable, M. L., Heirwegh, C. M., Elam, W. T., Colosimo, P., Christian, J. R., Liu, Y., Jones, M., Flannery, D., Clark, B. C., Das, A., & Ganly, B. (2024). *COMPOSITIONAL AND VOLUMETRIC ANALYSES OF DUST ON THE PIXL CALIBRATION TARGET.*

VanBommel, S. J., Sharma, S., Kizovski, T. V., Heirwegh, C. M., Christian, J. R., Knight, A. L., Ganly, B., Allwood, A. C., Hurowitz, J. A., Tice, M. M., Cable, M. L., Elam, W. T., Jones, M. W. M., Clark, B. C., Treiman, A. H., Schmidt, M. E., Liu, Y., & Das, A. (2025). Rare earth element assessment in Jezero crater using the Planetary Instrument for X-ray Lithochemistry on the Mars 2020 rover Perseverance: A case study of cerium. *Icarus*, *425*, 116355. https://doi.org/10.1016/j.icarus.2024.116355

Vaughan, A., Minitti, M. E., Cardarelli, E. L., Johnson, J. R., Kah, L. C., Pilleri, P., Rice, M. S., Sephton, M., Horgan, B. H. N., Wiens, R. C., Yingst, R. A., Zorzano Mier, M.-P., Anderson, R., Bell III, J. F., Brown, A. J., Cloutis, E. A., Cousin, A., Herkenhoff, K. E., Hausrath, E. M., … St. Clair, M. (2023). Regolith of the Crater Floor Units, Jezero Crater, Mars: Textures, Composition, and Implications for Provenance. *Journal of Geophysical Research: Planets*, *128*(3), e2022JE007437. https://doi.org/10.1029/2022JE007437

Wang, A., Ling, Z., Yan, Y., McEwen, A. S., Mellon, M. T., Smith, M. D., Jolliff, B. L., & Head, J. (2019). Subsurface Cl-bearing salts as potential contributors to recurring slope lineae (RSL) on Mars. *Icarus*, *333*, 464–480. https://doi.org/10.1016/j.icarus.2019.06.024

Wang, L., Liu, J., Yu, X., Wang, T., & Feng, R. (2021). A Simplified Model for the Phase Composition Curve of Saline Soils Considering the Second Phase Transition. *Water Resources Research*, *57*(1), e2020WR028556. https://doi.org/10.1029/2020WR028556

Werner, S. C. (2008). The early martian evolution—Constraints from basin formation ages. *Icarus*, *195*(1), 45–60. https://doi.org/10.1016/j.icarus.2007.12.008

Wiens, R. C., Clavé, E., Beck, P., Royer, C., Bedford, C., Beyssac, O., Quantin, C., Udry, A., Mangold, N., Dehouck, E., Maurice, S., Cousin, A., Forni, O., Caravaca, G., Brown, A., Johnson, J. R., Clegg, S. M., Ollila, A. M., Anderson, R. B., … Poblacion, I. (2024). *Chemistry and Mineralogy of the Margin Unit, Jezero Crater, Mars, Observed by M2020 / SuperCam*. https://www.hou.usra.edu/meetings/lpsc2024/pdf/1329.pdf

Wiens, R. C., Maurice, S., Robinson, S. H., Nelson, A. E., Cais, P., Bernardi, P., Newell, R. T., Clegg, S., Sharma, S. K., Storms, S., Deming, J., Beckman, D., Ollila, A. M., Gasnault, O., Anderson, R. B., André, Y., Michael Angel, S., Arana, G., Auden, E., … Willis, P. (2020). The SuperCam Instrument Suite on the NASA Mars 2020 Rover: Body Unit and Combined System Tests. *Space Science Reviews*, *217*(1), 4. https://doi.org/10.1007/s11214-020-00777-5

Wiens, R. C., Udry, A., Beyssac, O., Quantin-Nataf, C., Mangold, N., Cousin, A., Mandon, L., Bosak, T., Forni, O., McLennan, S. M., Sautter, V., Brown, A., Benzerara, K., Johnson, J. R., Mayhew, L., Maurice, S., Anderson, R. B., Clegg, S. M., Crumpler, L., … The SuperCam Team. (2022). Compositionally and density stratified igneous terrain in

Jezero crater, Mars. *Science Advances*, *8*(34), eabo3399. https://doi.org/10.1126/sciadv.abo3399

Williams, A. (2021). *Mars Life Explorer Mission Concept Study*.

Wordsworth, R. D. (2016). The Climate of Early Mars. *Annual Review of Earth and Planetary Sciences*, *44*(Volume 44, 2016), 381–408. https://doi.org/10.1146/annurev-earth-060115-012355

Wray, J. J. (2021). Contemporary Liquid Water on Mars? *Annual Review of Earth and Planetary Sciences*, *49*(1), 141–171. https://doi.org/10.1146/annurev-earth-072420-071823

Wright, A. P., Nemere, P., Galvin, A., Chau, D. H., & Davidoff, S. (2023). Lessons from the Development of an Anomaly Detection Interface on the Mars Perseverance Rover using the ISHMAP Framework. *Proceedings of the 28th International Conference on Intelligent User Interfaces*, 91–105. https://doi.org/10.1145/3581641.3584036

Yen, A. S., Gellert, R., Schröder, C., Morris, R. V., Bell, J. F., Knudson, A. T., Clark, B. C., Ming, D. W., Crisp, J. A., Arvidson, R. E., Blaney, D., Brückner, J., Christensen, P. R., DesMarais, D. J., de Souza, P. A., Economou, T. E., Ghosh, A., Hahn, B. C., Herkenhoff, K. E., … Zipfel, J. (2005). An integrated view of the chemistry and mineralogy of martian soils. *Nature*, *436*(7047), 49–54. https://doi.org/10.1038/nature03637

Appendix A. Supplementary Information for Chapter 4

A.1 Dust Layer Model

Identifying regolith mineralogy is complicated by the presence of dust, which affects PIXL's measurements of reflectance, diffraction, and composition. XRF measurements on a dusty surface result in a convolution of signals from the substrate and dust, which varies non-linearly with X-ray energy (e.g., atomic number; Berger et al., 2016; Knight et al., 2024; VanBommel et al., 2023). Instead, potential compositions of dust-free regolith were inferred through layering and deconvolution analyses on various likely substrates (VanBommel et al., 2022; 2023). Error bars are large and solutions are non-unique, but this method provides reasonable results when considered holistically alongside analysis of mixing trends, diffraction data, and reflectance results.

A.2 K-means Clustering Algorithm

In order to delineate the various regolith components, individual PIXL measurements were sorted into categories based on similar composition and diffraction properties using a K-means clustering algorithm that was adapted from the Python package Scikit-Learn (Pedregosa et al., 2011). A K-means algorithm sorts data into "clusters" based on their proximity to iteratively-generated cluster centers in N-dimensional feature space. PIXL regolith data were clustered according to their elemental composition (wt. %) and whether or not diffraction peaks were identified at that point. For each element, compositional data were scaled to zero mean and a standard deviation of one, a typical data processing technique to ensure each feature (i.e., element or oxide) is evenly weighted in the clustering routine. This rescaling allows the algorithm to identify trends in minor elements (e.g., Cr) instead of being dominated by the most abundant elements. Diffraction data were binary (i.e., detected = 1, not detected = 0) and therefore did not need to be normalized.

The algorithm defined the clusters based on the *Marmot Bay* map dataset (sol 601), which was selected for its high density of measurements and diversity of compositions encountered (Fig. 4-5). The number of clusters was determined by repeatedly running the algorithm with two to nine clusters, then comparing the resulting clusters to MCC spectral data (Fig. 4-4) and RGB composition and diffraction maps (Fig. 4-5). The results best agreed with visible and compositional trends when the algorithm was set to identify six clusters. The first cluster is characterized by consistent diffraction peaks and a Fe,Mg-silicate composition. This cluster is populated by the ~1 mm, rounded, gray-ish grains in Fig. 4-4. The second cluster is notable for a lack of diffraction peaks, and a low-Fe, high-Si composition; the larger, angular, lighter-toned grains in Fig. 4 are sorted into this cluster. A third cluster groups points with no diffraction peaks and very high levels of Fe and Mg, with low levels of Si; two grains are sorted into this cluster. The fourth cluster identified a few small grains that are highly enriched in Cr and/or Ti. The fifth cluster groups most of the finer-grained material (grain size < 0.5 mm), which share a similar composition. The final cluster groups points with high levels of S, Cl, and P.

Next, we used the clustering routine based on the *Marmot Bay* map dataset to sort data from the remaining regolith scans into the six defined clusters. There are some limitations to this method, since every point will be sorted into the nearest cluster, even if the point represents a new composition not present in the original training dataset. When new grain types were present, we identified the outliers manually by inspecting their composition on binary and ternary diagrams. Overall, this method performed quite well at classifying regolith components across scans. For example, at *Topographers Peak*, which is mostly composed of finer-grained regolith, 96.7% of points (n = 1626) were classified in the same cluster as the fines at *Marmot Bay*. At *Ursus Cove*, the rounded gray grains that appear visibly and chemically similar to grains at *Marmot Bay* were reliably sorted into the same cluster.

A.3 Chlorine Quantification

The quantification of Cl introduces an additional analytical burden in PIXL analyses due to spectral overlap between the Cl K_{α} line and backscattered Rh L lines (from the anode of PIXL's excitation source), which could lead to an overestimation of Cl. The contribution of backscattered X-rays from PIXL's Rh anode is considered during analysis and subsequent quantification by PIQUANT (Heirwegh et al., 2022), however small uncertainties in these line shapes can induce significant deviations in Cl attribution, especially at low wt. % Cl. PIQUANT's model of the fines spectrum produces a good match for the observed data, however, due to notable deviations from prior measurements, we do not rule out as-of-yet unknown potential errors that could result in PIXL over-quantifying Cl.

A.4 Pyroxene

Across all three targets, PIXL measured a few points with compositions that follow a mixing trend towards an endmember that may be consistent with a pyroxene. However, due to small sample size (at most, three contiguous points with this composition) and compositional mixing with the surrounding fines, we cannot conclusively identify the mineral. Pyroxene could plausibly have been present, as it was detected in regolith across Jezero crater by the MastCam-Z and SuperCam instruments (Cousin et al., 2025; Vaughan et al., 2023), and may have been present in the fines at *Observation Mountain* (Hausrath et al., 2025). SuperCam observations across the rover's traverse indicate that pyroxene was less common in regolith on the fan front than on the crater floor (Cousin et al., 2025), which could explain why PIXL data did not contain strong evidence of pyroxene.

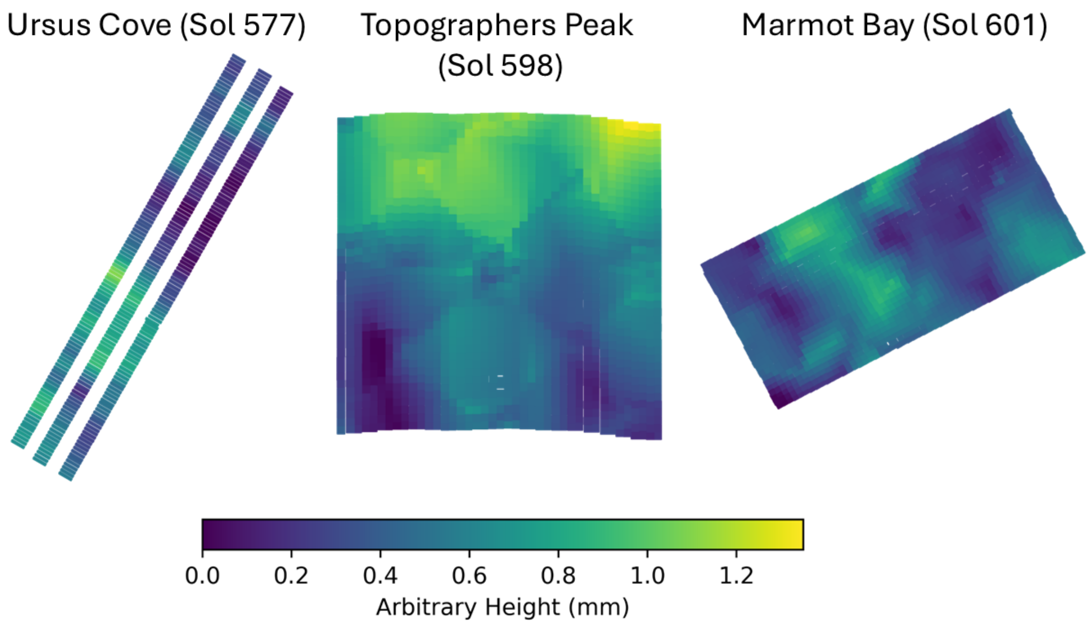

Figure A-1. Topography maps of the regolith targets, based on the Z-location reported by PIXL. The lowest height value in each scan is rescaled to zero. The same color scale is used across all scans.

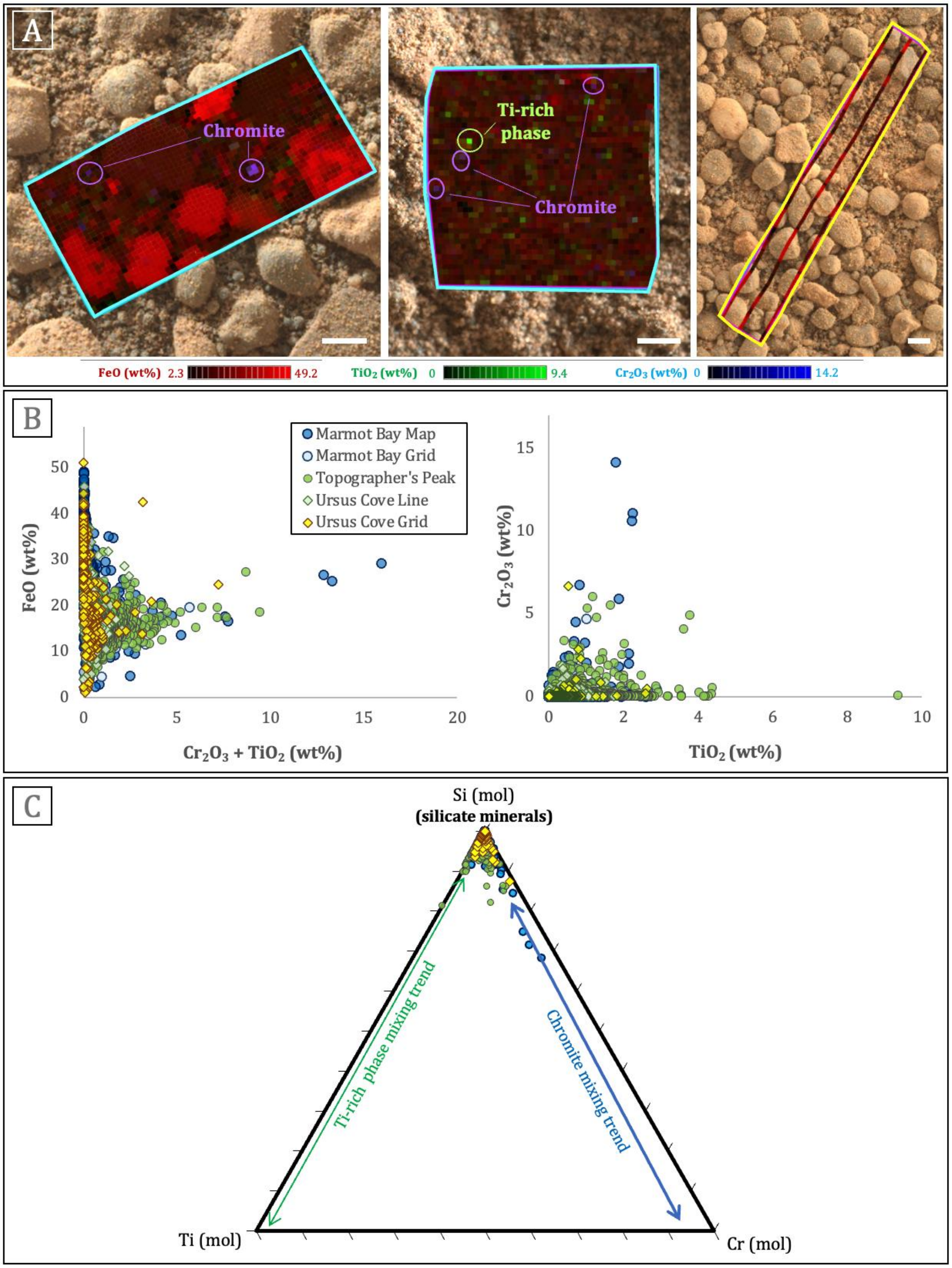

Figure A-2. Chromite compositions. A) Color maps showing the abundance of FeO_T (red), TiO_2 (green), and Cr_2O_3 (blue), overlaid on WATSON images of the Marmot Bay, Topographers Peak, and Ursus Cove targets, respectively. White scale bar shows 1 mm. B) Plots of FeO_T vs.

$Cr_2O_3 + TiO_2$ (wt. %) and Cr_2O_3 vs. TiO_2 (wt. %). Color and shape indicate which scan the data come from. C) Ternary plot of Si, Cr, and Ti (mol). Arrows show mixing trends towards pure chromite and an unidentified Ti-rich spinel phase. We identify spinels in seven points in *Marmot Bay*, four in *Topographers Peak*, and one in *Ursus Cove*.

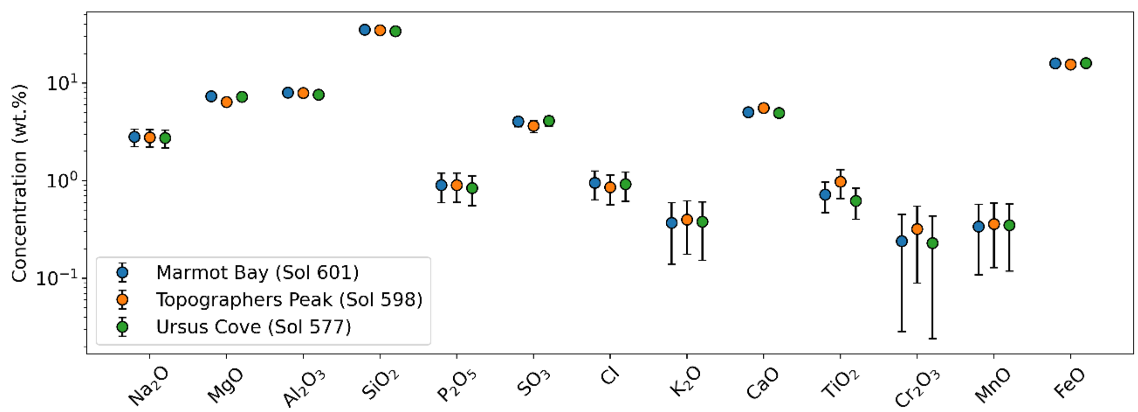

Figure A-3. Comparison of finer-grained regolith fraction (i.e., soils) across three PIXL regolith targets. Soils at all three targets are geochemically uniform for all major elements, within uncertainties. Values and uncertainties are also reported in Table A-3.

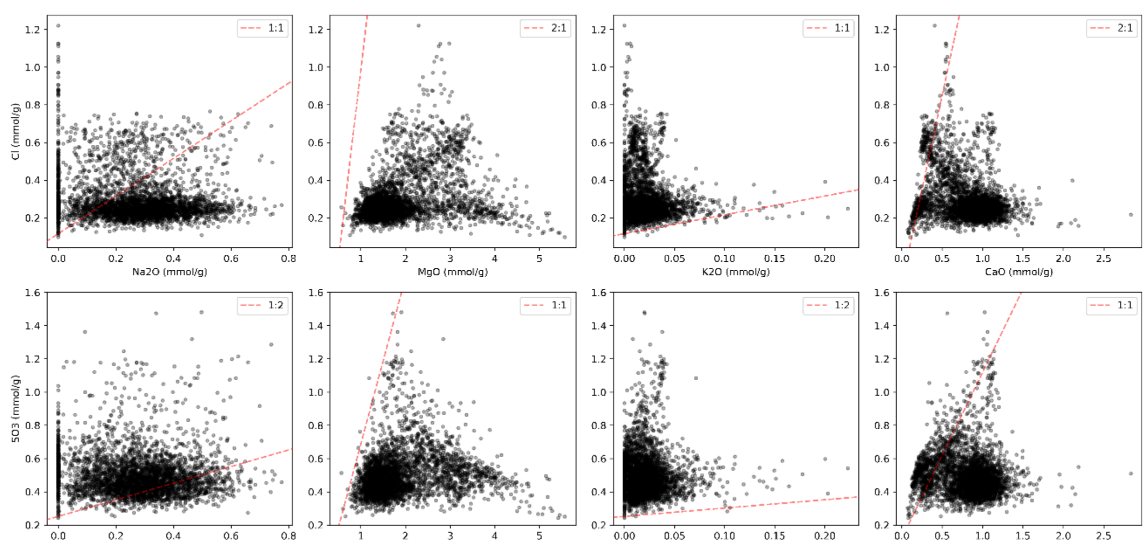

Figure A-4. Scatter plots of all PIXL regolith measurements show correlations between various potential cations and SO_3 and Cl. Red dashed lines represent stoichiometric ratios of salts that would form from the two components (e.g., 1:2 for $CaCl_2$, or 1:1 for $MgSO_4$). Some high SO_3 points follow a 1:1 trend with Ca, suggesting calcium sulfates are plausible. This is consistent with previous interpretations of Ca-sulfate present in dust (Knight et al., 2024). Ca sulfate may also have been contributed from nearby *Yori Pass* style bedrock, which had veins of gypsum and anhydrite (Jones et al., 2025). Similarly, some high-Cl points follow a 2:1 molar trend with Ca, which is consistent with $CaCl_2$ and/or $Ca(ClO_4)_2$ (other oxychlorine phases are also possible). Both S and Cl correlate with K_2O at high K abundances, which is consistent with potassium chloride and/or perchlorate, as well as potassium sulfate. However, all K_2O abundances are < 0.25 mmol/g, so these would be minor phases. Neither S nor Cl correlate strongly with Na.

Table A-1. (Uploaded separately to NASA's Planetary Data System Geosciences node; https://pds-geosciences.wustl.edu/m2020/; doi:10.17189/esjs-6z59) Oxide abundances for individual PIXL measurements across five regolith scans. Abundances have been corrected for effects caused by diffraction, topography, and roughness following the methodology described in Schmidt, et al. (2025). "PMC" stands for PIXL Motion Counter and is a unique integer assigned to each measurement within a scan. PMCs may be categorized into one of several regions of interest (ROIs) based on similar chemistry and diffraction properties (see section 3 of main text). ROIs were not assigned for the two grid scans (*Ursus Cove* sol 589 and Marmot *Bay* sol 600) because of low density of measurements and few spots on any single grain complicated identification of grain type. Uncertainties are reported from the PIQUANT software (Heirweigh et al., 2022).

Figure number	Target Name (Informal)	Instrument	Image ID
4-2A	*Ursus Cove*	Front Hazcam	FLF_0588_0719153024_565RAS_N0290000 FHAZ00206_0A0295J01
4-2B	*Ursus Cove*	Mastcam-Z	ZLF_0566_0717178520_553RAS_N0290000 ZCAM08587_0340LMJ01

4-2C	*Ursus Cove*	WATSON	SIF_0589_0719234796_609FDR_N0290000 SRLC00451_0000LMJ01
4-3A	*Observation Mountain*	Front Hazcam	FLF_0599_0720116670_012RAS_ N0300000FHAZ00206_0A0295J01
4-3B	*Observation Mountain*	Front Hazcam	FLF_0593_0719593428_996RAS_ N0300000FHAZ02008_0A0095J01
4-3C	*Topographers Peak*	Mastcam-Z	SI1_0598_0720049360_660FDR_N0300000 SRLC00071_000090J01
4-3D	*Topographers Peak*	WATSON	SI1_0598_0720049360_660FDR_N0300000 SRLC00071_000090J01
4-3E	*Marmot Bay*	WATSON	SIF_0598_0720040845_183RAS_N0300000 SRLC02504_0000LMJ01
4-3F	*Marmot Bay*	WATSON	SIF_0598_0720040987_687RAS_N0300000 SRLC00604_0000LMJ01

Table A-2. Image files used. Figure numbers correspond to figures in the main text.

Table A-3. (Uploaded separately to NASA's Planetary Data System Geosciences node; https://pds-geosciences.wustl.edu/m2020/; doi:10.17189/esjs-6z59) Bulk sum oxide abundances for each region of interest (ROI).

Appendix B. Curriculum Vitae

Andrew O. Shumway

EDUCATION

2025 Ph.D. in Earth & Space Sciences and Astrobiology (dual-title)
"Soil, Salt, and Water: The Formation and Stability of Brines in Martian Regolith"
University of Washington, Seattle, WA; Advisor: Prof. David Catling

2018 B.S. in Physics, *with Highest Honors.* Minor in Spanish.
Georgia Institute of Technology, Atlanta, GA

EXPERIENCE

2023, Summer **Visiting Researcher** - Hot Environments Lab
NASA Goddard Space Flight Center, Greenbelt, MD

- Studied hot, dense CO_2-rich atmospheres via laboratory FTIR spectroscopy experiments, with applications to upcoming Venus missions and modeling of exoplanet atmospheres.

2022 - Present **Science Payload Uplink/Downlink Lead** - *Perseverance* rover, PIXL team
Jet Propulsion Laboratory, Pasadena, CA

- Conducting *in situ* geological and astrobiological investigations of Martian rocks and regolith using micro-scale X-ray spectroscopy.
- Remotely operating rover instrumentation to optimize scientific return within operational constraints (i.e., time, power, and data volume).

2018 - 2025 **Graduate Research Assistant**
Department of Earth & Space Sciences, University of Washington

- Investigating the geochemistry and habitability of Mars' surface via analog laboratory experiments and modeling of salty, wet soils.

2016 - 2018 **Undergraduate Research Assistant**
School of Earth & Atmospheric Sciences, Georgia Tech

- Analyzed satellite imagery (visible and ultraviolet) to document low altitude, water-ice clouds in Valles Marineris, which revealed a seasonal correlation with surface "slump" features.

PUBLICATIONS

In prep. **Shumway, A. O.**, King, S., Catling, D. C., and Toner, J. D. (*in prep.)* "Seasonal Loss of Adsorbed Water as a Formation Mechanism for Recurring Slope Lineae on Mars."

In review **Shumway, A. O.**, Kizovski, T. V., Catling, D. C., et al. (*in review*) "Mineralogically Diverse

	and Salt-rich Regolith in Jezero Crater Characterized using X-ray Spectroscopy." *Journal for Geophysical Review: Planets*.
Accepted	Kizovski, T. V., Schmidt, M. E., O'Neil, L.O., et al., (including **Shumway, A. O.**) (*accepted*) "Fe-phosphates in Jezero Crater as Evidence for an Ancient Habitable Environment on Mars" *Nature Communications*.
2025	Jones, M. W. M., Flannery, D. T., Hurowitz, J. A., et al. (including **Shumway, A. O.**) "In situ crystallographic mapping constrains sulfate precipitation and timing in Jezero crater, Mars." *Science Advances, 11*(16), eadt3048. https://doi.org/10.1126/sciadv.adt3048
2025	Hausrath, E. M., Sullivan, R., Goreva, Y., Zorzano, M.P., Vaughan, A., Cousin, A., Siljeström, S., Sharma, S., **Shumway, A. O.**, et al. (2025) "Collection and In Situ Analyses of Regolith Samples by the Mars 2020 Rover: Implications for Their Formation and Alteration History." *Journal for Geophysical Review: Planets*.
2023	**Shumway, A. O.**, Catling, D. C., & Toner, J. D. (2023). "Regolith Inhibits Salt and Ice Crystallization in $Mg(ClO_4)_2$ Brine, Implying More Persistent and Potentially Habitable Brines on Mars." *The Planetary Science Journal*, *4*(8), 143. https://doi.org/10.3847/PSJ/ace891
2017	Ojha, L., Chojnacki, M., McDonald, G. D., **Shumway, A.,** Wolff, M. J., Smith, M. D., McEwen, A. S., Ferrier, K., Huber, C., Wray, J. J., & Toigo, A. (2017). "Seasonal Slumps in Juventae Chasma, Mars." *Journal of Geophysical Research: Planets*, *122*(10), 2193–2214. https://doi.org/10.1002/2017JE005375

Non-Refereed

2023	Hausrath, E. M., Farley, K. A., Sullivan, R., Goreva, Y., Kizovski, T. V., **Shumway, A. O.**, et al. "Initial Report: M2020-634-20 Atmo Mountain." In Farley, K., & Stack, K. *Mars 2020 Initial Reports Volume 2*. DOI: 10.17189/49zd-2k55. (non-refereed technical report)

SKILLS

- Software: Python, Matlab, Mathematica, PHREEQC, LaTeX, AutoCAD
- Instruments and techniques: X-ray spectroscopy, differential scanning calorimetry, Fourier transform infrared (FTIR) spectroscopy, multispectral analysis, high-vacuum systems, high temperature and pressure cells, wet chemistry techniques, gas cylinders, 3D printing, soldering
- Languages: English (fluent), Spanish (proficient)

OTHER EDUCATION & WORKSHOPS

2024, April	Connecting Community Scientific Hypotheses to Mars Sample Science MEPAG/ExMAG Workshop, Washington, D.C.

2023, Summer — Planetary Science Summer School

Jet Propulsion Laboratory, Pasadena, CA

- Formulated a New Frontiers-class mission concept: *Nautilus*, an multi-flyby investigation of Neptune's icy moon, Triton.

TEACHING EXPERIENCE

University of Washington:

2021	Instructor of record, *Communicating Science to the Public Effectively* (C ENV 500)
2020	Head Teaching Assistant, *Space and Space Travel* (ESS 102)
2019	Teaching Assistant, *Introduction to Astrobiology* (ASTBIO 115, two quarters)
2018, 2025	Teaching Assistant, *Introduction to Geology* (ESS 101)

Georgia Institute of Technology:

2018	Teaching Assistant, *Introductory Physics II* (PHYS 2212, two semesters)
2017	Teaching Assistant, *Introductory Physics I* (PHYS 2211)

SERVICE & OUTREACH

2024 — Search for Life Mission Concept Science Analysis Group, Mars Exploration Program

- Working with a team of planetary scientists and astrobiologists to refine science objectives and technical requirements to enable a life detection mission on Mars

2024 — Co-organizer, Mission Ideation Factory Workshop, NASA Astrobiology Program

- Designed a workshop for early career astrobiologists that simulated two life detection missions on Mars; created synthetic datasets for several instruments, which participants analyzed for evidence of extant life.

2021-2023 — Awards Committee, Earth & Space Sciences Dept., University of Washington

- Reviewed grant proposals and fellowship applications to allocate over $350,000 each year to graduate and undergraduate researchers.

2020-Present — Director, *Engage* science communication organization

- Developing curriculum, organizing public events, and teaching science communication skills to graduate students in STEM.

2018-Present — Volunteer, *Rockin' Out* Geosciences outreach program

- Leading Earth and Planetary Science lessons for K-12 students

2018-2022 — Executive Senator, Graduate & Professional Student Senate at UW

- Represented graduate student peers in determining university policy.

2017 — Audio director, *Inside the Black Box* radio program

- Managed weekly live broadcasting of STEM-communication radio show on WREK Atlanta, 91.1 FM

2016-2018	Physics Representative, Student Gov. Assoc. at Georgia Tech	

2016-2018 Physics Representative, Student Gov. Assoc. at Georgia Tech

- Interpreted financial policy to allocate funds to student organizations; represented constituents in guiding university policies

2015-2016 President, Society of Physics Students at Georgia Tech

- Presided over weekly meetings and organized visiting speakers, educational activities, and outreach programs for a club of ~50 undergraduate students.

FUNDING, SCHOLARSHIPS, AND HONORS

Total funding secured: $75,250

2024	David A. Johnston Award for Excellence in Research ($5,000)
2024	Inquisitive Graduate Student Award ($3,000)
2024	Distinguished Scholar Fellowship ($15,000)
2024	Best Use of Graphics, UW Earth & Space Science Research Gala ($150)
2024	Astrobiology Science Conference Student Travel Grant ($1,000)
2024	Lunar and Planetary Institute Career Development Award ($1,000)
2022	Best Space & Planetary Science talk, UW Earth & Space Science Research Gala ($250)
2021	Best Astrobiology talk, UW Earth & Space Science Research Gala ($350)
2019, 2020	Howard & Leila Coombs Endowed Fellowship ($15,000 x2)
2018-2021	ARCS Fellowship ($17,500)
2018	Sigma Pi Sigma inductee (physics honors society)
2016	George International Study Abroad Scholarship ($2,000)
2014-2018	Zell Miller Scholarship (full tuition scholarship) - *Georgia Tech*
2014-2018	Dean's List - *Georgia Tech*

INVITED TALKS

2024, Oct. "Searching for Water in Mars' Salty Soil." Rose City Astronomers. Oregon Museum of Science and Industry, Portland, OR.

2023, Nov. "Salt and Pebbles: How Regolith Could Form More Persistent Brines on Mars' Surface." SoftRock Seminar. UT Austin, Austin, TX. (virtual)

CONFERENCE PROCEEDINGS

Presenting Author

2024 **Shumway A. O.,** et al. "Regolith Composition on the Jezero Delta Front Revealed with PIXL: Implications for Brine-Forming Salts" *Tenth International Conference on Mars.* (poster)

2024 **Shumway A. O.,** et al. "Experimental Infrared Spectroscopy of CO_2 at Venus-relevant

Temperatures and Pressures" *Astrobiology Science Conference.* (poster)

2024 **Shumway A. O.**, et al. "Novel Micro-XRF Measurements of Regolith in Jezero Crater, Mars." *Lunar and Planetary Science Conference*. (poster)

2023 **Shumway A. O.**, Catling, D. C., and Toner, J. D. "Regolith Inhibits Salt Crystallization in Magnesium Perchlorate Brine, Suggesting More Persistent and Habitable Brines on Mars." *54th Lunar and Planetary Science Conference.* (oral)

2022 **Shumway A. O.**, Catling, D. C., and Toner, J. D.. "Predicting Water Content and Habitability of Perchlorate-rich Martian Soils." *Astrobiology Science Conference.* (oral)

2021 **Shumway A. O.**, Catling, D. C., and Toner, J. D. "Soils Increase the Stability of Magnesium Perchlorate Brines on Mars." *Brines Across the Solar System: Modern Brines.* (oral)

2021 **Shumway A. O.** "Water desorption could trigger seasonal grain flows on Martian slopes." *University of Washington, Earth & Space Science Research Gala.* (oral)

2020 **Shumway A. O.** and Toner, J. D.. "Water Desorption as a Mechanism for Recurring Slope Lineae Formation." *American Geophys. Union.* (poster)

2020[1] **Shumway A. O.**, Toner, J. D., and King, S. C. "Seasonal slope hydration cycles could explain the formation of recurring slope lineae." *Lunar and Planetary Science Conference.* (oral)

2019 **Shumway A. O**. and Toner, J. D. "Unfreezable briny water in Martian soils." *Astrobiology Science Conference.* (oral)

2018 **Shumway A. O.**, Ojha, L., and Wolff, M. J. "Seasonal Atmospheric Obscuration in Valles Marineris, Mars" *49th Lunar and Planetary Science Conference*. (poster)

Co-Authored

2024 Knight, A. L., et al., (including **Shumway, A. O.**) "Dust Accumulation on the PIXL Calibration Target: Phosphorus Enrichment and Role of Electrostatic Effects." *Tenth International Conference on Mars. 3007*, 3393. (poster)

2024 Kohler, E., **Shumway, A. O.**, et al. "A Multi-method Approach to Observing and Characterizing the Venusian Atmosphere." *Lunar and Planetary Science Conference. 2510* (oral)

2024 Schmidt, M. E., et al. (including **Shumway, A. O.**) "Volcanic Plume Origin for Widespread, Indurated Surface Coatings in Jezero Crater." *Lunar and Planetary Science Conference*. *3040*, 1954. (poster)

2024 Steckler, A., et al. (including **Shumway, A. O.**) "The Science Case for Nautilus: A Multi-Flyby Mission Concept To Triton" *Lunar and Planetary Science Conference* (poster)

[1] Conference canceled after acceptance of abstract, due to onset of the COVID-19 pandemic.

2023 Hausrath, E. M., et al. (including **Shumway, A. O.**) "The First Regolith Samples from Mars.", *Lunar and Planetary Science Conference, 2806*, 2379. (poster)

2023 Bravenec, A. D., **Shumway A. O.,** et al. "Supercooling, Vitrification, and Freeze Concentration in Oxychlorine Brines: Relevance to Mars and Icy Worlds." *LPI Contributions* 2689: 2021.

2023 Horvath, T., et al. (including **Shumway, A. O.**) "The Architecture of Nautilus: A Multi-flyby Mission Concept to Triton" *American Geophysical Union.* (poster)

2023 Steckler, A., et al. (including **Shumway, A. O.**) "The Science Case for Nautilus: A Multi-Flyby Mission Concept to Triton." *American Geophysical Union*. (poster)